THE PRODUCT AND PROCESS OF HEME DEGRADATION IN *STAPHYLOCOCCUS AUREUS*

By

Michelle Lynne Reniere

Dissertation

Submitted to the Faculty of the

Graduate School of Vanderbilt University

in partial fulfillment of the requirements

for the degree of

DOCTOR OF PHILOSOPHY

In

Microbiology and Immunology

May, 2010

Nashville, Tennessee

Approved:

Sebastian Joyce

Brian O. Bachmann

Paul E. Bock

Timothy L. Cover

Dana Borden Lacy

Eric P. Skaar

To Dad,

you’re the greatest.

Thanks for everything.

ACKNOWLEDGEMENTS

I am extremely grateful to my mentor Eric Skaar for all that he has taught me and for his friendship. He is a great scientist, an excellent writer, and a fantastic teacher. I have learned so much from him and had a lot of fun in the process. I could not have asked for a better mentor or a better working environment. Everyone in the Skaar Laboratory has contributed to my graduate education. In particular, I have learned a lot from Victor Torres, Devin Stauff, and Gleb Pishchany. No matter what they were doing, they were always willing to stop and help, which I greatly appreciate. I would also like to thank current lab members Amanda McCoy, Indriati "Margie" Hood, Neal Hammer, Kathryn Haley, and Laura Anzaldi, as well as previous lab members Danielle Bagaley, Keith Adams, and Jeff Mason. I really appreciate your friendship and your collaborative attitudes that make the Skaar lab a really fun place to work.

I am also thankful for the collaborators that have contributed to this work. Michael Murphy at the University of British Columbia and his trainees Georgia Ukpabi and Woo Cheol Lee contributed several crystal structures to this project. Susan Opalenik in the Vanderbilt Molecular Genetics Core assisted with the quantitative PCR experiments described in Chapter II. I am particularly indebted to Donald Stec in the NMR Small Molecule Facility at Vanderbilt for performing some of the NMR experiments (Chapter IV). Additionally, S. Reese Harry in David W. Wright's laboratory helped with the initial staphylobilin purification (Chapter IV).

I acknowledge my thesis committee: Sebastian Joyce, Brian Bachmann, Paul Bock, Timothy Cover, and D. Borden Lacy. Thank you for your support and advice. I am particularly grateful for the help I received from Brian Bachmann who contributed greatly to the staphylobilin project and was very patient in teaching me NMR.

Thank you to the department of Microbiology and Immunology, Jacek Hawiger, and all of the administrative staff. I also thank Dr. Richard Hoover for his support. I was supported by the NIH Training Grant in Mechanisms of Vascular Disease, 5 T32 HL07751. My work was supported by the United States Public Health Service Grant AI69233 from the National Institute of Allergy and Infectious Diseases.

Finally, thank you to my family who is a constant source of support, advice, and laughter. I could not have gotten this far without you.

TABLE OF CONTENTS

LIST OF TABLES

LIST OF FIGURES

LIST OF ABBREVIATIONS

CFU	Colony forming units
CO	Carbon monoxide
COSY	Homonuclear correlation spectroscopy
Dip	2,2'-Dipyridyl
DMEM	Dulbecco's Modified Eagle's Medium
EM	Electron microscopy
Fur	Ferric uptake regulator
HMBC	Heteronuclear multiple bond coherence
HO-1	Human heme oxygenase-1
HOs	Heme oxygenases (general)
ICP-MS	Inductively-coupled plasma mass spectrometry
Isd	Iron-regulated surface determinant
IVIS	*In vivo* bioluminescence imaging
MRSA	Methicillin-resistant *Staphylococcus aureus*
NOESY	Nuclear Overhauser effect spectroscopy
PMSF	Phenylmethylsulphonyl fluoride
PPIX	Protoporphyrin IX
TBS	Tris-buffered saline
TFA	Trifluoroacetic acid
TSB	Tryptic soy broth

CHAPTER I

INTRODUCTION

Staphylococcus aureus

Staphylococcus aureus is a Gram positive bacterium that was discovered in 1880 when Sir Alexander Ogsten observed that injecting pus from infected patients into mice produced similar abscesses (49). *S. aureus* harmlessly colonizes the squamous epithelium of the anterior nares of approximately thirty percent of the human population (50). However, upon breakage of host protective barriers, *S. aureus* is capable of invading and colonizing almost every organ in the human body, causing a diverse array of serious infections. The most common invasive diseases caused by *S. aureus* include bacteremia, pneumonia, osteomyelitis, endocarditis, and septic shock (48, 50). *S. aureus* infections are an escalating problem in developed countries, as the incidence of drug-resistant strains is rapidly increasing. In fact, as of 2005 invasive methicillin-resistant *S. aureus* (MRSA) infections were responsible for more deaths annually in the United States than AIDS (9, 48). Particularly alarming is the emergence of vancomycin-resistant strains, which suggests that complete antibiotic resistance of this bacterium is inevitable.

S. aureus is an extremely successful pathogen due to its arsenal of effectors capable of opposing the various assaults of the host immune system. The initial response of the innate immune system to infection includes phagocyte activation and mobilization, opsonization to promote phagocytocis, and direct killing by antimicrobial peptides and reactive oxygen species (27). Virulence factors produced by *S. aureus* allow the bacteria to evade these host responses. For example, formyl peptides synthesized by bacteria activate neutrophils. *S. aureus* counters this immune activation

by secreting the chemotaxis inhibitory protein of staphylococci (CHIPS), which binds to the neutrophil formyl peptide receptor to block chemotaxis. Secretion of the extracellular adherence protein (Eap) also interferes with neutrophil chemotaxis by preventing leukocyte adhesion and extravasation (27). *S. aureus* also has several mechanisms for evading opsonization. The first defense is a capsular polysaccharide that coats the bacterium and limits neutrophil access to cell-surface molecules. Secondly, cell wall-anchored protein A binds the Fc region of antibodies, effectively covering the bacterium in antibodies arranged in an orientation that is incompatible with neutrophil Fc receptor recognition. Moreover, *S. aureus* is able to oppose the complement system by secreting the staphylococcal complement inhibitor (SCIN), which prevents complement deposition on the bacterial surface (83). The cell wall-anchored protein IsdH is also capable of binding a component of the complement system (C3) in a way that hinders opsonization (113).

If the host is able to overcome these evasion tactics and engulf staphylococci, the bacteria are capable of surviving in phagosomes in a semi-dormant state referred to as small colony variants (114). Modifications of wall teichoic acids and lipoteichoic acids naturally reduce the affinity of phagosomal cationic peptides to the bacterial surface. Additionally, secreted proteins such as staphylokinase and aureolysin inactivate antimicrobial peptides in the phagosome (27). *S. aureus* combats the neutrophil oxidative burst through expression of superoxide dismutases (SODs) and the yellow carotenoid pigment staphyloxanthin, which scavenges free radicals (99). Moreover, *S. aureus* can directly kill host cells by secreting toxins that damage host membranes, leading to cell lysis.

In addition to the innate immune defenses mentioned above, the host actively starves invading pathogens of essential nutrients, a strategy referred to as “nutritional immunity” (117). The most important nutrient in the battle between host and pathogen is

iron, which is required for the growth of most bacteria but is unavailable in the mammalian host (8). Just as *S. aureus* has developed methods for combating the host innate immune system, it has also developed sophisticated mechanisms for iron acquisition during infection.

Iron and Infection

"In the resolution of the contest between invader and host, iron may be the critical determinant" (117).

During infection bacteria encounter an environment in which greater than 90% of iron is intracellular, and therefore inaccessible (21). Vertebrates go to great lengths to sequester serum iron within proteins, rendering this vital metal inaccessible to invading pathogens. During infection, production of the extracellular iron-binding proteins lactoferrin and transferrin is increased. The intracellular iron-binding protein ferritin is also increased to efficiently sequester intracellular iron. These infection-induced alterations in iron-binding protein levels are mediated by the short peptide hepcidin, the master regulator of iron metabolism (34).

At the initiation of a microbial infection the host-derived cytokine interleukin-6 signals hepatocytes to elevate production and secretion of hepcidin. Hepcidin reduces extracellular iron levels by suppressing the secretion of dietary iron into the blood and stimulating macrophages to retain iron from recycled hemoglobin (34). Additionally, the synthesis and secretion of lactoferrin from neutrophil secondary granules is increased in the acute phase of infection (45). The macrophage transferrin receptor is down-regulated, limiting the amount of transferrin-iron incorporated into the cells (35). Simultaneously, production of ferritin is increased to bind intracellular iron stores. The combined effect of these alterations is to decrease available iron inside the cells in order to withhold iron from intracellular invaders. The efficiency of this iron-withholding system

is exemplified by the disorder known as “anemia of chronic infection”. Decreased iron availability causes a reduction in red blood cell production, leading to anemia after prolonged infection (45, 127).

The importance of iron sequestration techniques for combating infection is evident by the increased susceptibility to infection of individuals with iron overload diseases. For example, iron overload in macrophages (such as in African siderosis) causes an increased risk of tuberculosis, a bacterial infection which flourishes in iron-loaded alveolar macrophages (116). Additionally, the administration of iron sucrose to hemodialysis patients is known to lead to an accumulation of non-transferrin-bound iron in the serum, which enhances the growth of *S. aureus* and the risk of developing sepsis (4, 41). Furthermore, in a murine model of *Vibrio vulnificus* infection, injection of excess iron into the mice reduced the LD_{50} from 6,000,000 to a single bacterium (124).

Pathogens have evolved diverse sophisticated mechanisms to capture iron from many host iron-binding proteins. The majority of non-heme iron within vertebrates is bound by ferritin, lactoferrin, or transferrin. Ferritin, the intracellular iron storage protein, is unlikely to be used as an iron source by extracellular bacteria such as *S. aureus*. In contrast, lactoferrin is found in many bodily fluids, including saliva, tears, and nasal secretions (8). However, rather than promoting growth by providing the bacterium with iron, lactoferrin exhibits a bacteriostatic effect on *S. aureus in vitro*. This growth inhibition is attributed to both its iron-chelating properties and serine protease activity (1, 15). Alternatively, transferrin-iron is found in the serum and is a viable iron source to extracellular pathogens. Iron acquisition from transferrin is mediated primarily by siderophores in *S. aureus* (56, 70). Siderophores are low molecular weight iron chelators that have an extraordinarily high affinity for iron. After removing iron from transferrin, the siderophore-iron complex is recognized by bacterial receptors and internalized.

The vast majority of iron in the human body (approximately 80%) is found as a component of heme (21). Heme, or iron-protoporphyrin IX, is an essential cofactor in many proteins due to its robust redox potential. However, its reactivity also makes it a potentially dangerous molecule, as it catalyzes peroxidase and oxidase reactions which can result in damage to proteins and DNA. Vertebrates therefore sequester heme in hemoproteins to prevent oxidative damage. Hemoglobin, the major oxygen transport protein contained within erythrocytes, is the most abundant hemoprotein in mammals (19). Hemoglobin that is released into the serum upon erythrocyte lysis is quickly bound by circulating haptoglobin, which then traffics to the liver for degradation. In addition to hemoglobin, heme-iron is also bound by myoglobin, the oxygen storage protein in vertebrates. *In vitro, S. aureus* preferentially imports heme-iron when other iron sources are concurrently available, indicating that heme is most likely the primary source of iron during infection (97). *S. aureus* is able to utilize myoglobin as a heme-iron source *in vitro*; however, the mechanism by which this occurs and its relevance to pathogenesis are unknown (108).

To acquire heme-iron from hemoglobin, *S. aureus* must first liberate hemoglobin from within host erythrocytes. To this end, *S. aureus* secretes several hemolysins which form pores in host cell membranes, causing lysis and release of cellular contents (60). Upon erythrocyte lysis, *S. aureus* binds the liberated hemoglobin and hemoglobin-haptoglobin complexes via proteins of the iron-regulated surface determinant (Isd) system (98). The Isd system is comprised of nine iron-regulated proteins (IsdA-I) that act in concert to bind host hemoproteins, transport heme into the bacterial cytoplasm, and degrade heme to release nutrient iron (Figure 1). To date, the Isd system is the most extensively characterized heme-uptake system in Gram positive bacteria and homologues have been found in *Bacillus anthracis, Listeria monocytogenes,* and *Clostridium tetani* (98).

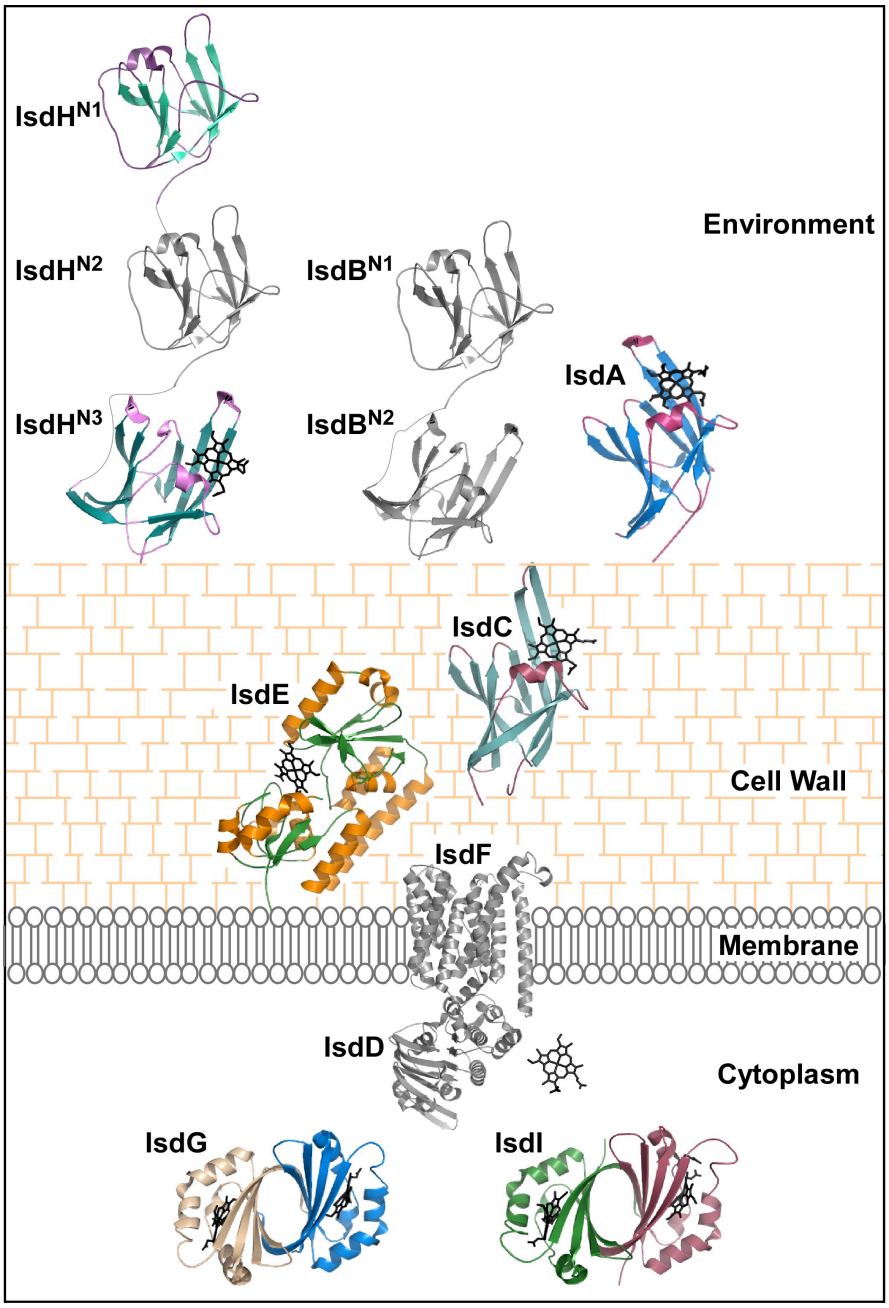

Figure 1. Model of Isd heme acquisition in *S. aureus*. The model for heme transport predicts that once heme is removed from hemoglobin by IsdB or IsdH it is transferred in the following order: IsdA → IsdC → IsdE → IsdDF →IsdGI. PDB codes are as follows: $IsdH^{N1}$ (2H3K), $IsdH^{N3}$-heme complex (2Z6F), IsdA NEAT domain complexed with heme (2ITF), IsdC-heme complex (2O6P), IsdE-heme complex (2Q8Q), IsdG-N7A complexed with heme (2ZDO), IsdI complexed with cobalt protoporphyrin IX (2ZDP). Protein domains in gray are based on sequence similarity to proteins with a published structure. $IsdH^{N1}$ shares 59% sequence identity with $IsdH^{N2}$ and 46% sequence identity with $IsdB^{N1}$. $IsdH^{N3}$ shares 56% sequence identity with $IsdB^{N2}$. IsdD and IsdF belong to the vitamin B12 ABC transporter family, the prototype of which is BtuCD from *Escherichia coli* (2QI9).

The iron-regulated surface determinant (Isd) system of *S. aureus*

The first obstacle in heme-iron acquisition during staphylococcal infection is the capture of host hemoproteins and the removal of heme. To this end, the hemoprotein receptors IsdB and IsdH (also called HarA) bind hemoglobin and hemoglobin-haptoglobin complexes (22, 59, 73, 128). IsdH is the only staphylococcal haptoglobin-binding protein, while both IsdB and IsdH exhibit hemoglobin binding activities. Although IsdH is capable of binding hemoglobin *in vitro*, inactivation of *isdH* does not alter the ability of *S. aureus* to utilize hemoglobin as an iron source. However, *isdB* mutants are impaired in their ability to use hemoglobin as a sole iron source, indicating that in *S. aureus* IsdB is the primary hemoglobin receptor (108). After binding the hemoprotein, the heme cofactor is removed via an as-yet undefined mechanism.

Heme acquired from host hemoproteins must next be transported across the thick Gram positive cell wall, a process mediated by IsdA and IsdC (Figure 1). These cell-wall anchored proteins bind heme with modest affinity and traffic it across the dense layers of peptidoglycan (94, 112). IsdA is one of the most abundant proteins expressed on the surface of iron-starved *S. aureus* and it has been shown to bind a diverse array of host ligands. In addition to heme, IsdA has been reported to bind lactoferrin and the extracellular matrix proteins fibrinogen and fibronectin (15, 16). The biological ramifications of this broad binding specificity have not been established, but presumably IsdA-mediated ligand binding promotes the ability of *S. aureus* to adapt to its environment and colonize its host. IsdC is believed to function as the central heme channel from the outer cell wall to the cytoplasmic membrane due to its unique sortase B-catalyzed anchoring that positions it within the cell wall rather than exposed to the surface (57).

From IsdC heme is transferred to IsdE, the lipoprotein component of the ATP-binding cassette (ABC) transporter (38, 65). IsdD and IsdF are putative ABC transporter

components, in which IsdD is a membrane-associated ATP-binding protein and IsdF is a membrane-spanning permease (59). It is thought that the IsdE-heme complex will transfer heme through IsdF into the cytoplasm using energy generated by IsdD (81).

Once heme enters the cytoplasm, we propose that *S. aureus* can utilize heme in one of two ways: as a nutrient iron source or as a cofactor for bacterial hemoproteins (81). As well as being a valuable source of nutrient iron, heme is potentially useful to *S. aureus* in its intact form. Intact heme is required as a cofactor in numerous enzymes, many of which are found in the cytoplasmic membrane, such as cytochromes (106). It is possible that when iron is not a limiting nutrient, *S. aureus* will acquire low levels of heme for use in bacterial hemoproteins, as scavenging heme requires less energy than synthesizing heme *de novo* (72). This "molecular hijacking" hypothesis is supported by evidence that exogenous heme is preferentially acquired and segregated intact to the membrane when non-heme iron sources are concurrently available (97). More research is necessary to elucidate the fate of exogenously acquired intact heme and its role in bacterial hemoproteins (Chapter V).

In order to utilize heme as an iron source the porphyrin ring must be cleaved to release the coordinated iron atom. Heme oxygenases are a ubiquitous family of enzymes that catabolize heme to carbon monoxide, α-biliverdin, and free iron (Figure 2). The Isd system includes two heme oxygenases dedicated to this task, IsdG and IsdI (96).

Heme oxygenases

The first bacterial heme oxygenase described was HmuO from *Corynebacterium diphtheriae*, which was identified based on its homology to human heme oxygenase 1 (HO-1) (87). Since that initial report, numerous additional HO-1-like enzymes have been identified in bacteria (Table 1). Despite sharing little sequence identity, members of the

HO-1 family exhibit significant structural similarity. The HO-1 enzymes are monomeric α-helical proteins, each with a single active site and GXXXG catalytic motif (Figure 2A) (90). Heme catabolism by the HO-1 family of enzymes has been studied extensively in both bacteria and vertebrates and the mechanism of heme degradation is believed to proceed similarly across most heme oxygenases (109). The canonical heme degradation reaction proceeds through a ferric hydroperoxo intermediate which self-hydroxylates exclusively at the α-*meso* carbon of the porphyrin ring, ultimately resulting in the formation of α-biliverdin with concomitant release of carbon monoxide (CO) and free iron (Figure 2B) (111). In mammals biliverdin is further reduced to bilirubin by biliverdin reductase; however, the ultimate fate of biliverdin in bacteria is unknown as homologues of biliverdin reductase have not been discovered in bacteria.

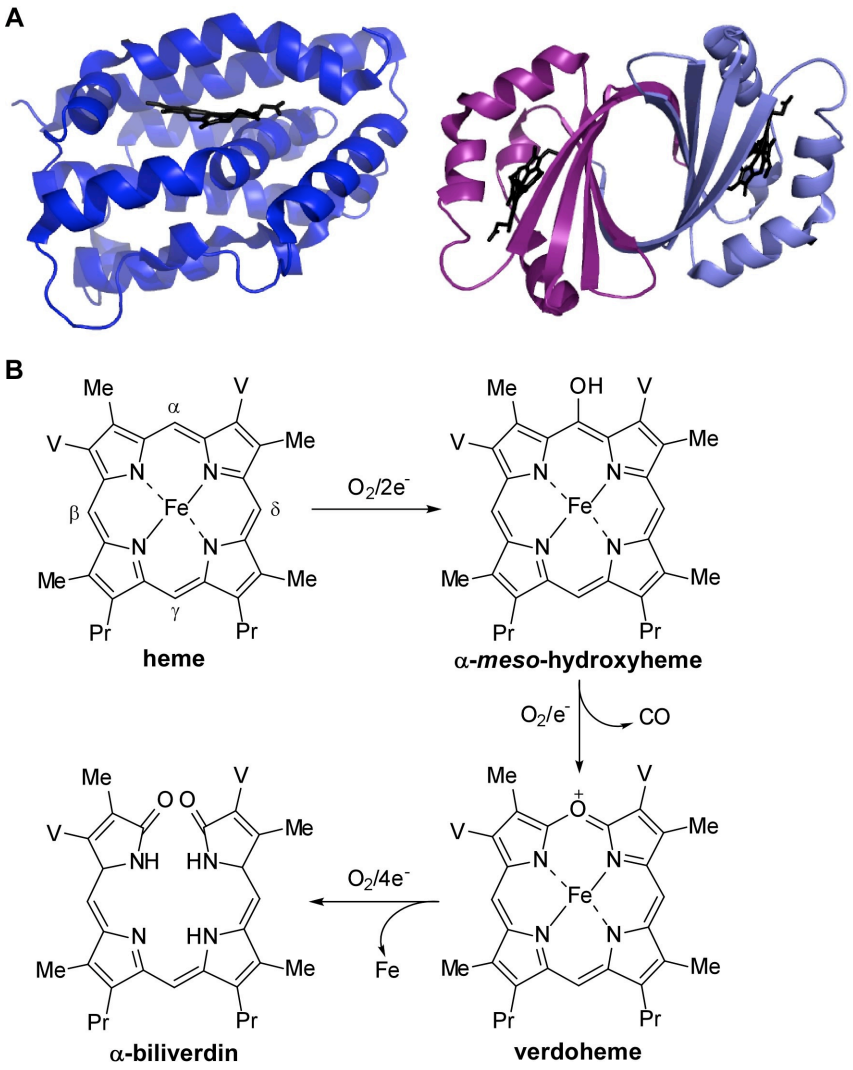

Figure 2. Heme oxygenases of the HO-1 family degrade heme to α-biliverdin. A. Human HO-1 bound to heme (left panel, PDB 1N45) is compared to IsdG N7A mutant bound to heme (right panel, PDB 2DZO). The two monomers of IsdG are colored in different shades of purple. **B.** The canonical heme degradation pathway requires seven electrons and three moles of oxygen. Heme degradation results in carbon monoxide (CO), free iron, and α-biliverdin. Abbreviations are as follows: Me, methyl ($-CH_3$); V, vinyl ($-CH_2-CH_3$); Pr, propionate ($-CH_2-CH_2-COOH$). The heme *meso*-carbons are labeled α, β γ, δ.

In addition to its role in heme catabolism, human HO-1 is essential for protecting against oxidative damage incurred during inflammation by generating antioxidants (14, 47). In 1987, bilirubin, the end product of mammalian heme degradation, was found to be one of the most powerful serum antioxidants due to its extended system of conjugated double bonds and reactive hydrogen atoms (101). Heme degradation also produces equimolar concentrations of CO, a molecule with diverse functions *in vivo*. In humans >85% of endogenous CO results from heme catabolism. Although toxic at high concentrations, physiological levels of CO exert a multitude of beneficial effects, including vasodilatory, anti-inflammatory, and immunomodulatory (47). Moreover, the free iron that is liberated during heme catabolism up-regulates ferritin, another powerful cellular antioxidant (47). In addition, the intermediate biliverdin has been attributed antiviral activities (63). Considering the essential functions of biliverdin, bilirubin, CO, and iron within vertebrate cells, it is likely that heme catabolites also have important physiological roles in bacteria.

Although the vast majority of HO-1-family enzymes produce α-biliverdin, a few exceptions have been observed. One example is *pa*-HO (PigA) from *Pseudomonas aeruginosa* which differs in its regiospecificity, producing a mixture of β- and δ-biliverdin (79). In addition, the blood-sucking insect *Rhodnius prolixus* degrades heme to dicysteinly-γ-biliverdin (69). In this heme degradation pathway heme is first modified by addition of two cysteinylglycine dipeptides, followed by oxidative cleavage of the porphyrin ring. The biological significance of these unconventional biliverdin molecules is not yet understood.

The IsdG-family of heme oxygenases, first identified in *S. aureus*, is structurally distinct from the HO-1 family (Figure 2A). *S. aureus* expresses two paralagous heme oxygenases, IsdG and IsdI (96). Orthologues have been identified in other staphylococci and several pathogenic species of *Bacillus* and *Listeria,* as well as *Mycobacterium*

tuberculosis and the plant symbiont *Bradyrhizobium japonicum* (Table 1). IsdG-family members form homodimeric β-barrel structures with two separate active sites, each containing three residues (Asn, Trp, His) that are required for activity (125). Initial reports demonstrated IsdG-catalyzed cleavage of the macrocyclic ring with concomitant release of free iron, although the precise mechanism of heme degradation by this class of heme oxygenases has not yet been delineated (96). We have observed that *in vitro* heme degradation catalyzed by recombinant IsdG results in the formation of a yellow reaction product distinct from the blue-green biliverdin chromophore. Taken together, these structural and biochemical observations suggest that members of the IsdG-family of heme oxygenases degrade heme by a unique mechanism, resulting in the formation of a product that is distinct from biliverdin. The purification and structural determination of the products of IsdG- and IsdI-catalyzed heme degradation is described in Chapter IV.

Table 1. Bacterial heme oxygenases

Species	Heme Oxygenase(s)	Reference
HO-1 family		
Corynebacterium diphtheriae	HmuO	(87)
Pseudomonas aeruginosa	PigA, BphO	(79)
Neisseria spp.	HemO	(131)
IsdG family		
Bacillus anthracis	IsdG	(95)
Bradyrhizobium japonicum	HmuD, HmuQ	(76)
Listeria monocytogenes	IsdG	(96)
Mycobacterium tuberculosis	MhuD	(13)
Staphylococcus aureus	IsdG, IsdI	(96)
Other*		
Campylobacter jejuni	ChuZ	(82)
Escherichia coli 0157:H7	ChuS	(104)
Helicobacter pylori	HugZ	(39)
Leptospira interrogans	HemO	(64)

* The ChuS structure is unlike that of the HO-1 family or IsdG family. ChuZ, HugZ, and *L. interrogans* HemO have not yet been structurally characterized.

Research objectives and significance

Herein I elucidate the genetic regulation of *isdG* and *isdI* and assess the contribution of heme degradation to staphylococcal pathogenesis. I found that although IsdG and IsdI share 64% sequence identity, they are differentially regulated according to the microenvironment experienced by the bacterium (Chapter II). This may represent a strategy by which *S. aureus* fine-tunes the expression of heme oxygenase activity during infection, as I found that bacteria lacking *isdG* and/or *isdI* exhibit differential virulence defects (Chapter II). In addition, I have identified a post-transcriptional regulatory mechanism in which IsdG is specifically stabilized in the presence of the substrate heme. Studies into the mechanism of this heme-dependent stability have identified two residues that are absolutely required for IsdG degradation in the absence of heme (Chapter III). Current experiments are aimed at identifying the protease(s) responsible for IsdG degradation (Chapter VI). Finally, we have determined the structure of the IsdG- and IsdI-catalyzed heme degradation products and shown that this new family of heme oxygenases degrade heme to a novel chromophore which we have named staphylobilin (Chapter IV).

Collectively, my studies have significantly advanced our understanding of heme catabolism in *S. aureus*, a process that I have shown is required for staphylococcal pathogenesis. Additionally, I have identified a regulatory mechanism in which two similar proteins are differentially degraded, a potentially useful system for investigating mechanisms of substrate recognition by staphylococcal intracellular proteases. Moreover, the unique structure and mechanism of the IsdG-family of heme oxygenases indicates that these enzymes may be viable therapeutic targets. Future studies will build upon these foundational discoveries to determine the intracellular fate and function of staphylobilin and determine the functional relevance of IsdG degradation *in vivo*.

CHAPTER II

STAPHYLOCOCCUS AUREUS HEME OXYGENASES ARE DIFFERENTIALLY REGULATED BY IRON AND HEME

Introduction

Staphylococcus aureus is able to obtain iron from heme during infection via the iron-regulated surface determinant (Isd) system. The nine proteins of the Isd system work in concert to bind host hemoproteins, remove the heme cofactor, and passage heme into the cytoplasm (59, 81). Once heme enters the cytoplasm it has been proposed that IsdG and IsdI, two paralogous heme oxygenases, degrade heme to release free iron for use as a nutrient source (98). In support of this model, IsdG and IsdI have been shown to catalytically degrade heme *in vitro* in a reaction that requires oxygen (53, 96). Further, *S. aureus isdI* expressed *in trans* is able to complement the heme utilization defect of a *Corynebacterium ulcerans* heme oxygenase mutant, indicating a role for IsdI in heme-iron utilization *in vivo* (96).

In accordance with their role in iron acquisition, the cell wall-anchored and membrane transport proteins of the Isd system are regulated by the ferric uptake regulator (Fur), such that maximal expression occurs in iron-deplete environments (59). Fur is a ubiquitous bacterial transcription factor that binds consensus DNA sequences and inhibits transcription when iron is abundant (25). Many genes encoding bacterial heme oxygenases are also regulated in an iron-dependent manner, including: *hmuO* in *Corynebacterium diphtheriae, hugZ* in *Helicobacter pylori, chuZ* in *Campylobacter jejuni, pigA* in *Pseudomonas aeruginosa,* and *hemO* in *Neisseria spp.* (39, 67, 82, 85, 93). In addition to iron, *hmuO* is regulated by heme via two signal transduction systems.

Maximal *hmuO* promoter activity is observed in iron-deplete environments that contain heme or hemoglobin (5)

Despite the accumulating data supporting a role for IsdG and IsdI in heme degradation during infection, the importance of IsdG and IsdI to staphylococcal biology is not yet known. Furthermore, regulatory networks governing the expression of these enzymes have not been explored. Additionally, a mechanistic explanation for why *S. aureus* encodes two paralogous enzymes that appear to be functionally redundant has not been provided. Finally, the contribution of heme degradation to pathogenesis has not been evaluated. This latter point is surprising in light of the fact that heme degrading enzymes have been described in twelve distinct genera of pathogenic bacteria (Table 1).

I sought to address each of these missing links by defining the role of heme oxygenases in staphylococcal biology and pathogenesis. Specifically, I demonstrate that IsdG and IsdI are each required for *S. aureus* heme utilization, as both are required for optimal growth on heme as a sole iron source. Investigation into the regulation of these enzymes reveals that IsdG and IsdI are differentially regulated by local iron and heme environments, providing a functional distinction between these two paralogous enzymes. Specifically, *isdG* and *isdI* are both transcriptionally regulated by iron in a Fur-dependent manner, while IsdG is also regulated post-transcriptionally by heme. Moreover, *in vivo* bioluminescence imaging indicates that *isdI* is expressed in infected tissues, primarily at the sites of abscess formation. Finally, I demonstrate that IsdG and IsdI are each required for full *S. aureus* virulence. Taken together, these results establish a role for heme degradation in bacterial pathogenesis and identify a complex regulatory system responsible for ensuring efficient heme catabolism during infection.

Methods

Bacterial strains and growth conditions. *S. aureus* clinical isolate Newman was used in all experiments (24). Isogenic variants lacking *fur*, *isdC, isdD, isdE, isdF, srtB, isdG* have been previously described (59). Mutations in *isdI* were made by allelic replacement of the coding sequence with *tetM* (3). The double heme oxygenase knockout strain (Δ*isdGI*) was made by transducing the Δ*isdI::tetM* allele into Δ*isdG* using the transducing phage Φ-85 as has been described previously (96). Bacteria were grown overnight (for stationary phase cultures) in tryptic soy broth (TSB) at 37°C with shaking at 180 rpm unless otherwise stated.

For complementation studies, *S. aureus* strains Newman Δ*isdG* and Δ*isdGI* were transformed with a plasmid encoding a full length copy of *isdG* under control of the *S. aureus* lipoprotein diacylglycerol transferase (*lgt*) constitutive promoter in the pOS1-derived vector (7, 88). *isdG* coding sequence was PCR amplified from Newman genomic DNA and cloned into pCR2.1 (Invitrogen). Successful transformants were screened and those with the correct insert were subcloned into pOS1p*lgt*, making p*isdG*.

Heme nutrition plate assay. *S. aureus* strains Newman wild type, Δ*isdG*, Δ*isdI*, and Δ*isdGI* were passaged for 2 days in iron-deplete media (TSB + 1 mM 2,2'-dipyridyl [dip]) followed by a 4 hour subculture (1:100) in iron-deplete media. The cultures were then normalized by optical density and sedimented. The pellets were resuspended in TSB + 6 mM dip and 60 µL was spotted in triplicate on TSA plates containing 6 mM dip and various concentrations of heme (Sigma). The iron-deplete, heme-containing plates were incubated at 37°C in the dark for 2-3 days and the diameter of each colony was measured using the AlphaImager (Alpha Innotech) software.

Fractionation of staphylococci. Overnight cultures of *S. aureus* were normalized by optical density and sedimented. The bacteria were washed with Tris-buffered saline

(TBS, 50 mM Tris pH 7.5, 150 mM NaCl), resuspended in TSM buffer (100 mM Tris pH 7.0, 500 mM sucrose, 10 mM $MgCl_2$) and incubated in the presence of 30 µg lysostaphin at 37°C for 30 minutes. The samples were then pelleted and the supernatants (cell wall fraction) were collected and analyzed by 12% SDS-PAGE followed by immunoblotting. For analysis of membrane and cytoplasmic proteins, the protoplasts were resuspended in BugBuster Protein Extraction Reagent (Novagen) with proteinase inhibitor and sonicated for 10 seconds. The whole protoplast fractions were normalized by total protein concentration, separated by 15% SDS-PAGE, and analyzed by immunoblotting.

Immunoblot Protein Quantification. Immunoblotting was performed in quadruplicate as described above. The intensities of the protein bands were quantified using the Odyssey System software by LI-COR, Inc. and were normalized by the intensities of the cross-reacting protein A bands.

RNA Isolation. Overnight cultures of wild type *S. aureus* were subcultured (1:100) in triplicate into TSB alone, TSB supplemented with dip (1 mM), or TSB supplemented with dip and heme (5 µM). Mid-log phase cultures (OD_{600} = 0.25) were mixed with an equal volume of ice-cold ethanol-acetone and stored at -80°C. For RNA isolation, samples were thawed on ice and pelleted. Pellets were resuspended in RLT buffer and transferred to Lysing Matrix B tubes (MP Bio). Cells were lysed by processing in a FastPrep Instrument (MP Bio) two times for 20 sec each, followed by centrifugation. The supernatant was used for RNA isolation using RNeasy Mini kit according to manufacturer's recommendations (QIAGEN). Contaminating DNA was removed by adding 10 units DNase I (Amersham Biosciences) to RNA samples and incubating in RQ1 buffer (Promega) at 37°C for 30 min. Following DNase treatment the samples were re-purified using the RNeasy Mini kit according to manufacturer's protocol for RNA clean-up (QIAGEN). RNA concentration and purity were measured by optical density at 260 nm and 280 nm, respectively.

Real time RT-PCR. For cDNA synthesis, 2 µg total cellular RNA was reverse transcribed with M-MLV reverse transcriptase according to manufacturer's recommendations (Promega). 10 ng cDNA was amplified using Platinum Quantitative PCR SuperMix-UDG and SYBR Green I Nucleic Acid Stain (Invitrogen) in an iCycler iQ (Bio-Rad). The quantification of each sample was carried out relative to 16S rRNA and each PCR reaction was measured in quadruplicate. Relative quantification was performed using the comparative C_T method according to User Bulletin #2: ABI Prism 7700 Sequence Detection System, Applied Biosystems, 2001.

Pulse-Chase and Immunoprecipitation. Mid-log cultures of *S. aureus* Δ*isdG* p*isdG* grown in iron-deplete medium or iron-deplete medium supplemented with 10 µM heme were pelleted and washed three times in Dulbecco's Modified Eagle's Medium (DMEM) lacking methionine (Cellgro). Bacteria were then resuspended in DMEM lacking methionine and supplemented with iron sulfate (10 µM) or dip (1 mM), with or without heme (10 µM). Cells were then pulsed with ^{35}S-methionine (110 µCi) for two minutes at 37°C. Time zero samples were taken and added to an equal volume of 10% trichloroacetic acid (TCA) on ice. Subsequently, the chase solution (casamino acids, methionine, and cysteine) was added and samples were taken at the indicated time points and mixed with an equal volume of TCA on ice. Bacteria were then pelleted and washed with acetone. To remove the cell wall, bacteria were treated with lysostaphin (40 µg) in TSM buffer for 30 minutes at 37°C and then pelleted and washed with acetone. Protoplasts were lysed by boiling in 0.5 M Tris, pH 7.5, 4% SDS. After pelleting, supernatants were removed and mixed with IsdG antisera diluted 1:500 in RIPA buffer for 1.5 hours. Subsequently 50 µL of protein A-sepharose slurry was added and incubated for 1 hour. Protein A beads were then washed and the bound antibody-protein complexes were removed by boiling in reducing SDS-PAGE sample buffer. Samples were separated by electrophoresis, dried, and analyzed using a PhosphorImager.

Murine model of infection. Six to eight week old BALB/c mice (Jackson Laboratories) were infected with 4 x 10^6 colony forming units (CFU) of wild-type *S. aureus* Newman, Δ*isdG,* Δ*isdI,* or Δ*isdGI* mutant strains suspended in PBS by retroorbital injection. Four days post-infection mice were euthanized with CO_2 and hearts and kidneys were removed and homogenized in sterile PBS. Colonization of each organ was determined by enumerating CFU on tryptic soy agar.

Bioluminescence imaging. The promoterless vector p*Xen* coding for the *luxABCDE* operon of *Photorhabdus luminescens*, and modified for Gram positive bacteria, was obtained from Xenogen (28). The promoter region of DNA for *isdI* was cloned into p*Xen* to make p*isdI.Xen*. The promoterless vector was used as a control for background luminescence in all experiments. Luminescence *in vitro* and *in vivo* was measured using the Xenogen IVIS 200 and LiveImage 2.0 software.

For *in vivo* bioluminescence imaging, six to eight week old BALB/c mice (Jackson Laboratories) were infected with 3 x 10^7 CFU of wild type Newman carrying either p*Xen* or p*isdI.Xen* suspended in PBS by retroorbital injection. Beginning 24 hours prior to infection, and continuing throughout the infection, mice were given chloramphenicol (0.5 mg/mL) in their drinking water in order to select for bacteria carrying the plasmid. Four days post-infection the mice were euthanized with CO_2 and organs were removed and imaged *ex vivo.* After imaging, the organs were homogenized in PBS and colonization was determined by enumerating colony forming units on tryptic soy agar in order to ensure the bacterial load in each organ was consistent between strains.

Results

S. aureus IsdG and IsdI are required for growth on heme as a sole iron source.

IsdG and IsdI have been shown to catalytically degrade heme *in vitro* (96), however their contribution to staphylococcal heme-iron utilization has not been evaluated. To assess the role of IsdG and IsdI *in vivo*, we inactivated *isdG* and *isdI*, individually and in combination, in *S. aureus* strain Newman. We hypothesized that mutants lacking IsdG and/or IsdI would not be able to grow when heme is the only available iron source. Due to the lack of sensitivity of liquid growth assays, we sought to test our hypothesis by comparing the growth of *S. aureus* wild type, Δ*isdG*, Δ*isdI*, and Δ*isdGI* strains on solid media in which heme is the sole iron source. We observed that *S. aureus* lacking *isdG*, *isdI* or *isdGI* exhibit significantly impaired growth on heme as a sole iron source when compared to wild type (Figure 3). In contrast, all four strains show similar growth kinetics when grown on iron-rich or iron-depleted medium (data not shown). Interestingly, inactivation of *isdG* and *isdI* in combination does not enhance the heme utilization defect over that of either individual mutant strain. It is possible that this observation may be the result of the heme utilization defect reaching the limit of detection of the assay. Alternatively, this may be due to each enzyme having distinct functions in *S. aureus*. Importantly, the observation that both enzymes are required for efficient heme utilization strongly suggests that IsdG and IsdI have distinct contributions to heme catabolism.

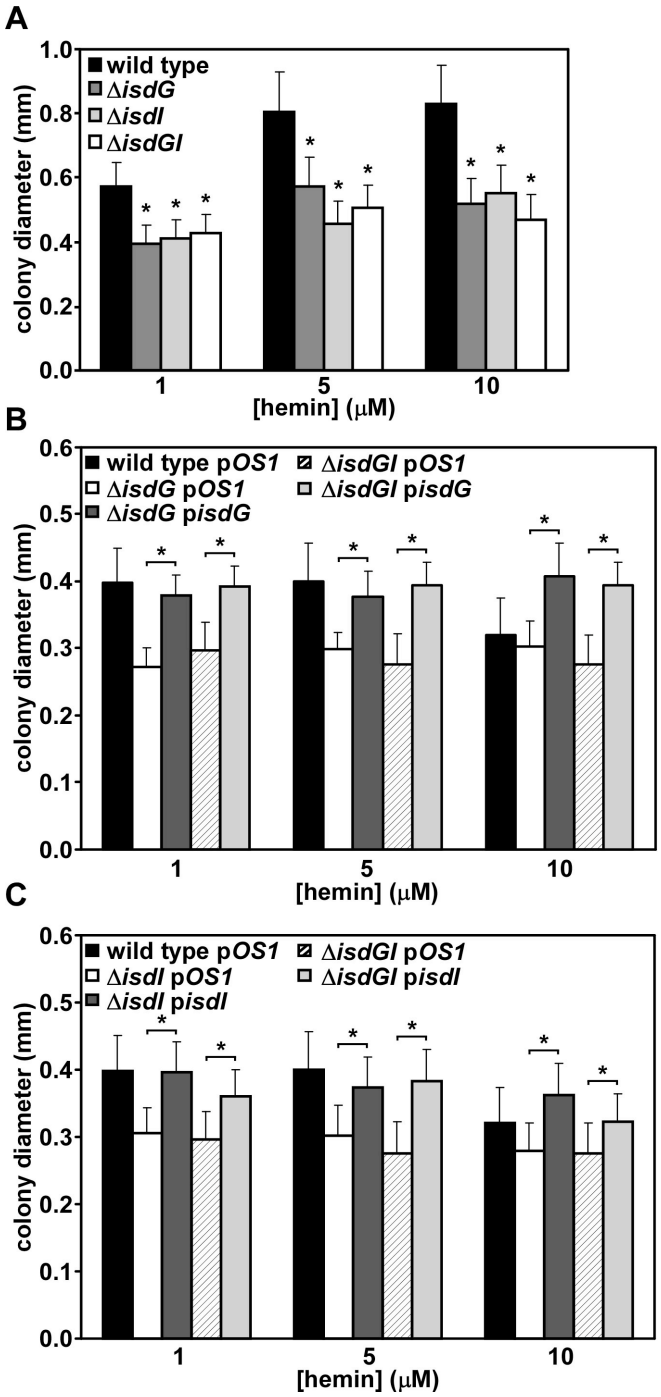

Figure 3. Growth of *S. aureus* heme oxygenase mutants on heme as a sole iron source. A. The colony diameter of *S. aureus* wild type Δ*isdG*, Δ*isdI*, and Δ*isdGI* was measured after growth on solid media containing an iron chelator and various concentrations of heme. **B and C.** Strains listed in *A* were transformed with an empty vector (p*OS1*) or a vector expressing *isdG* or *isdI* from a constitutive promoter (p*isdG*, p*isdI*) and colony diameter was measured as in *A*. Asterisks denote statistical significance between wild type and mutant strains (panel *A*) or mutant strains and complemented strains (panel *B* and *C*), as measured by Student's *t* test ($p < 0.0001$).

To ensure that the absence of *isdG* and *isdI* is responsible for the observed defect in heme utilization, I performed complementation analyses. To this end, I provided a full-length copy of either *isdG* or *isdI in trans* in an effort to reverse the observed growth defects of the various mutant strains. I found that constitutive expression of *isdG* or *isdI* restores the growth of Δ*isdG* and Δ*isdI* respectively, confirming that the observed heme utilization defect of the mutants is due to the absence of heme oxygenase (Figure 3B and C). Surprisingly, over-expression of either *isdG* or *isdI* restores the growth of the double mutant to wild-type levels when heme is the sole iron source (Figure 3B and C), indicating that over-expression of IsdG or IsdI is able to compensate for the lack of both heme oxygenases. These results suggest that *S. aureus* may encode for two heme-degrading enzymes as a mechanism to fine-tune the abundance of heme oxygenase in the cell.

IsdG and IsdI are differentially regulated by iron and heme.

IsdG and IsdI are not functionally redundant given that deletion of either *isdG* or *isdI* individually decreases the ability of *S. aureus* to grow on heme as a sole iron source. Moreover, over-expression of either IsdG or IsdI complements the loss of both enzymes, suggesting that the efficiency of heme utilization is impacted by the abundance of IsdG and IsdI. Based on these findings, we reasoned that *isdG* and *isdI* may be differentially regulated in *S. aureus*.

Due to the location of putative Fur-binding sequences upstream of the transcription start sites for *isdG* and *isdI* (59, 96), we hypothesized that these enzymes are regulated by iron availability in a Fur-dependent manner. To test this hypothesis I employed immunoblotting to examine the expression of IsdG and IsdI following growth of *S. aureus* in media containing the iron chelator 2,2'-dipyridyl (dip). I observed an increase in the expression of both IsdG and IsdI as the concentration of iron chelator

was increased (Figure 4A). This iron-dependent increase was much more pronounced for IsdI as compared to IsdG. As a demonstration that this iron-dependent regulation of IsdG and IsdI is mediated by Fur, I found that a *S. aureus* strain inactivated for *fur* expresses IsdG and IsdI at levels comparable to those observed in maximally iron-starved *S. aureus* (Figure 4A). These results demonstrate that IsdG and IsdI are regulated by iron in a Fur-dependent manner.

As IsdG and IsdI are heme-degrading enzymes that are required for heme utilization (Figure 3), I next sought to investigate the effect of heme exposure on IsdG and IsdI expression. In an attempt to represent the predicted nutrient environment encountered during infection, I performed these experiments on iron-starved *S. aureus*. These experiments revealed that IsdI expression is not affected by exposing iron-starved *S. aureus* to heme (Figure 4B). In contrast, the abundance of IsdG is enhanced upon exposure to exogenous heme (Figure 4B). This heme-dependent increase in IsdG only occurs when *S. aureus* has been starved for iron, as IsdG was not detected when *S. aureus* was grown in iron-replete media supplemented with exogenous heme (data not shown). Although minor differences in absolute protein concentrations were observed between gels, the effect of heme and iron on IsdG and IsdI abundance was consistent across all experiments.

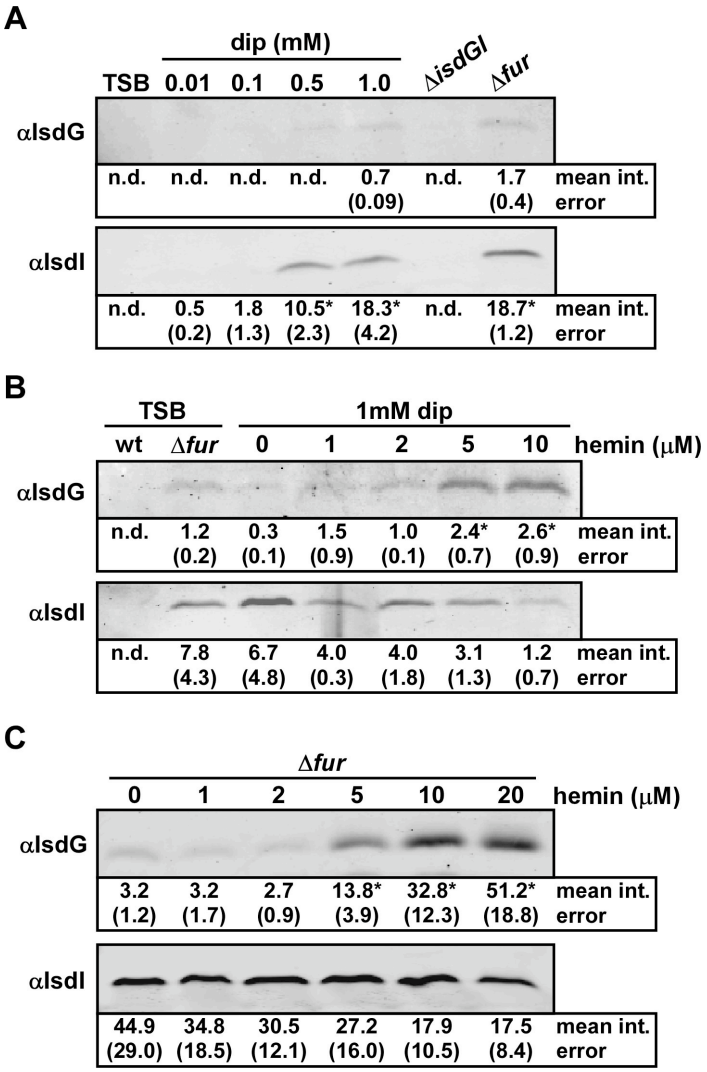

Figure 4. Regulation of IsdG and IsdI by iron and heme. The mean intensity of each band, as determined by densitometric analyses, is presented under the blots in arbitrary units, with corresponding standard error. Bands that were not detected for quantification are reported as not determined (n.d.). Statistical significance was determined using the Student's *t* test. Results are representative of at least four independent experiments. **A.** The effect of iron chelation by 2,2'-dipyridyl (dip) on expression of IsdG and IsdI was analyzed by immunoblot. Asterisks denote statistically significant increases, as compared with 0.01 mM dip ($p < 0.0001$). **B.** The effect of exogenous heme on expression of IsdG and IsdI in iron-deplete media (dip) was analyzed by immunoblot. Asterisks denote statistically significant increases, as compared with 0 μM heme ($p < 0.03$). The slight decrease in IsdI abundance in 10 μM heme compared with 0 μM heme is not statistically significant ($p > 0.06$). **C.** The effect of exogenous heme on expression of IsdG and IsdI in an isogenic Δ*fur* strain was analyzed by immunoblot. Asterisks denote statistically significant increases, as compared with 0 μM heme ($p < 0.0002$). The slight decrease in IsdI abundance in 20 μM heme compared with 0 μM heme is not statistically significant ($p > 0.1$).

To determine if Fur contributes to the heme-dependent increase in IsdG expression, I monitored IsdG expression in *S. aureus* Δ*fur* exposed to heme. In these experiments, a similar increase in the abundance of IsdG upon heme exposure was observed compared to wild type, indicating that Fur is not responsible for the heme-dependent regulation of IsdG (Figure 4C). Taken together, these experiments show that IsdG and IsdI are differentially regulated by iron and heme. More specifically, IsdI is robustly expressed upon iron starvation whereas IsdG abundance is maximal in iron-depleted medium containing heme.

Proteins encoded within the Isd operon are differentially regulated by heme.

isdG is the terminal gene in the Isd operon (59, 96). In keeping with this genomic assignment, *isdG* is predicted to be co-transcribed with the upstream genes *isdCDEFsrtB* (Figure 5A). To test this, I analyzed the expression of IsdG in a *S. aureus* strain in which *isdC* has been inactivated by the insertion of an antimicrobial resistance cassette, which leads to transcriptional termination of the operon (Δ*isdC*) (59). Expression of IsdG in the Δ*isdC* mutant was abolished regardless of the growth conditions under study (data not shown), supporting the model that *isdC* and *isdG* are encoded within the same transcriptional unit.

Based on the assignment of *isdG* as the terminal gene in the Isd operon, we reasoned that all of the proteins encoded within this operon would be up-regulated when iron-starved *S. aureus* encounters heme. To test this, a series of strains inactivated for various components of the Isd operon were examined for protein expression in iron-depleted media containing heme. As a negative control in these experiments, I analyzed the abundance of IsdI, as its expression is not affected by heme. As expected, IsdC, IsdD, IsdE, and SrtB were expressed in *S. aureus* Δ*fur*. Surprisingly, IsdG is the only protein expressed from the *isdCDEFsrtBisdG* operon with enhanced expression in the

presence of heme (Figure 5B, wt dip+heme vs Δ*fur*). Moreover, transcriptional termination at any gene upstream of *isdG* in the *isdCDEFsrtBisdG* operon abolishes expression of all downstream genes, further confirming that these genes are transcribed as a single unit. Taken together, these data suggest that the heme-dependent increase in IsdG expression occurs post-transcriptionally.

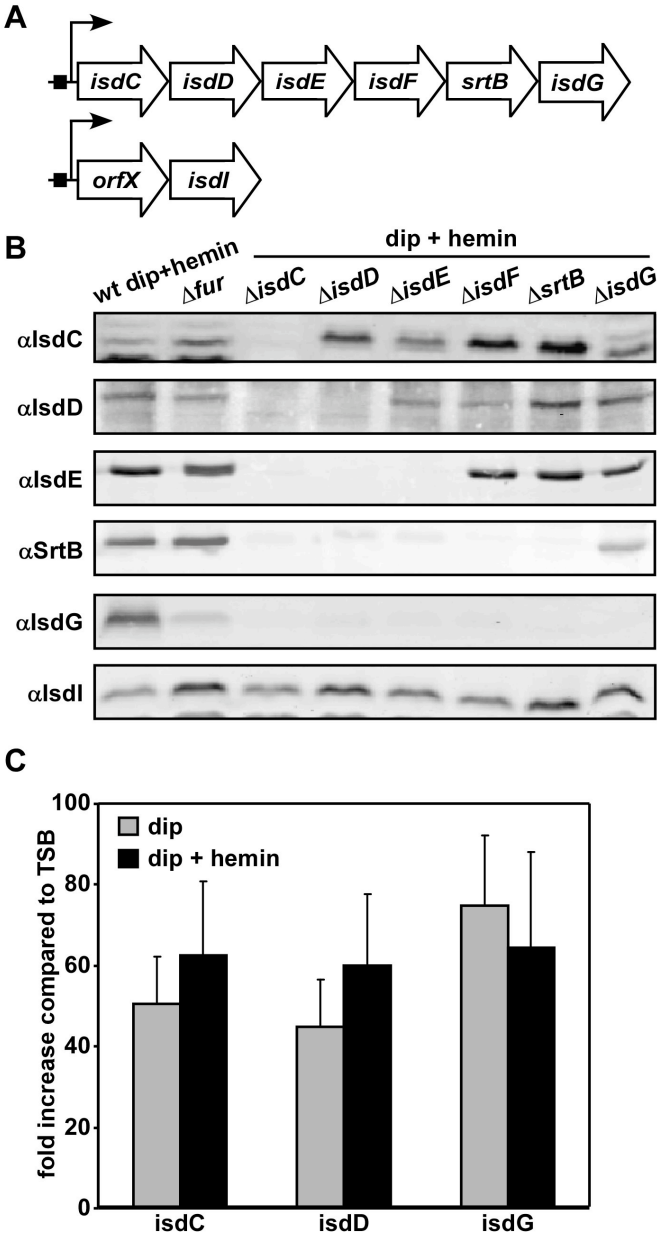

Figure 5. The role of transcription in the heme-dependent increase in IsdG. A. Schematic representation of the *isd* locus. The putative Fur-binding sites are denoted by black boxes upstream of putative transcription start sites (black arrows). *orfX* is an uncharacterized open reading frame upstream of *isdI*, and these genes are co-transcribed. **B.** Immunoblot analysis of Isd proteins in *S. aureus* wild type grown in iron-deplete medium containing heme (wt dip + heme) compared with isogenic strains lacking individual genes of the *isd* locus in identical growth media. All results are representative of at least three independent experiments. **C.** Transcript levels of *isdC*, *isdD* and *isdG* were analyzed by quantitative RT-PCR and normalized to 16S rRNA. *S. aureus* wild type was grown in iron-deplete media (dip, grey bars) and iron-deplete media containing 5 μM heme (dip + heme, black bars) and transcript levels were compared with those grown in TSB. Error bars represent the average range of triplicate experiments.

IsdG is regulated by heme via a post-transcriptional mechanism.

To investigate the mechanism responsible for the observed heme-dependent regulation of IsdG, I analyzed transcript levels of several *isd* genes in iron-rich medium, iron-deplete medium, and iron-deplete medium containing heme. I observed that transcript levels of *isdC*, *isdD*, and *isdG* are increased 40-70-fold upon iron starvation independent of heme, consistent with the Fur-regulation of this operon (Figure 5C). However, the transcript levels of *isdC*, *isdD*, or *isdG* from iron-starved *S. aureus* were not affected by heme exposure (Figure 5C). This is in stark contrast to the immunoblot analyses which showed an abundant increase of IsdG upon addition of heme to iron-depleted medium (Figure 4). These experiments confirm that the heme-dependent up-regulation of IsdG is occurring post-transcriptionally.

To determine if the post-transcriptional regulation of IsdG requires *cis*-acting sequences in the 5' untranslated region of *isdG*, I analyzed the effect of heme on IsdG expression when *isdG* transcription is driven by a constitutive promoter. The Δ*isdG* p*isdG* strain was utilized for this assay, as the coding sequence of *isdG* is cloned directly downstream of the constitutive *lgt* promoter, which is not affected by heme (7, 100). This vector does not contain any of the sequences typically present in the genomic context surrounding *isdG*, and hence, expression can be monitored independently of potential regulatory sequences surrounding *isdG*. I observed a 2.3-fold increase in the abundance of IsdG when Δ*isdG* p*isdG* was grown on heme as the only iron source (data not shown, $p < 0.015$), indicating that the *isdG* coding sequence is sufficient for the heme-dependent regulation of IsdG.

IsdG protein stability is enhanced by heme.

The heme-dependent increase in IsdG abundance in iron-deplete medium (Figure 4) is not a result of increased isdG transcription in this environment (Figure 5C).

One possible explanation for this is that the presence of heme stabilizes the IsdG protein. To investigate the iron- and heme-dependent stability of IsdG I utilized the *S. aureus* Δ*isdG* p*isdG* strain that constitutively expresses *isdG*. Following a pulse with ^{35}S-methionine, the fate of labeled IsdG was followed by immunoprecipitation over time. I observed that IsdG turnover is much more rapid in medium lacking heme as compared to medium containing heme, independently of the iron status (Figure 6A and C). In the presence of heme over 60% of the labeled protein remains after 150 minutes, whereas only 20% of the labeled protein remains at the end of the time course in the absence of heme. To determine if this heme-dependent stabilization is specific for IsdG, I performed a similar pulse–chase experiment to monitor the iron- and heme-dependent stability of IsdI. For these experiments, I utilized a *S. aureus* Δ*isdI* p*isdI* strain that constitutively expresses *isdI*. These experiments revealed that IsdI stability is unaffected by heme or iron status (Figure 6B and D). Combined with data from the qPCR results described previously, these data lead us to conclude that IsdG is most abundant when iron-starved in the presence of heme. This is an environment that is potentially encountered during infection following erythrocyte lysis.

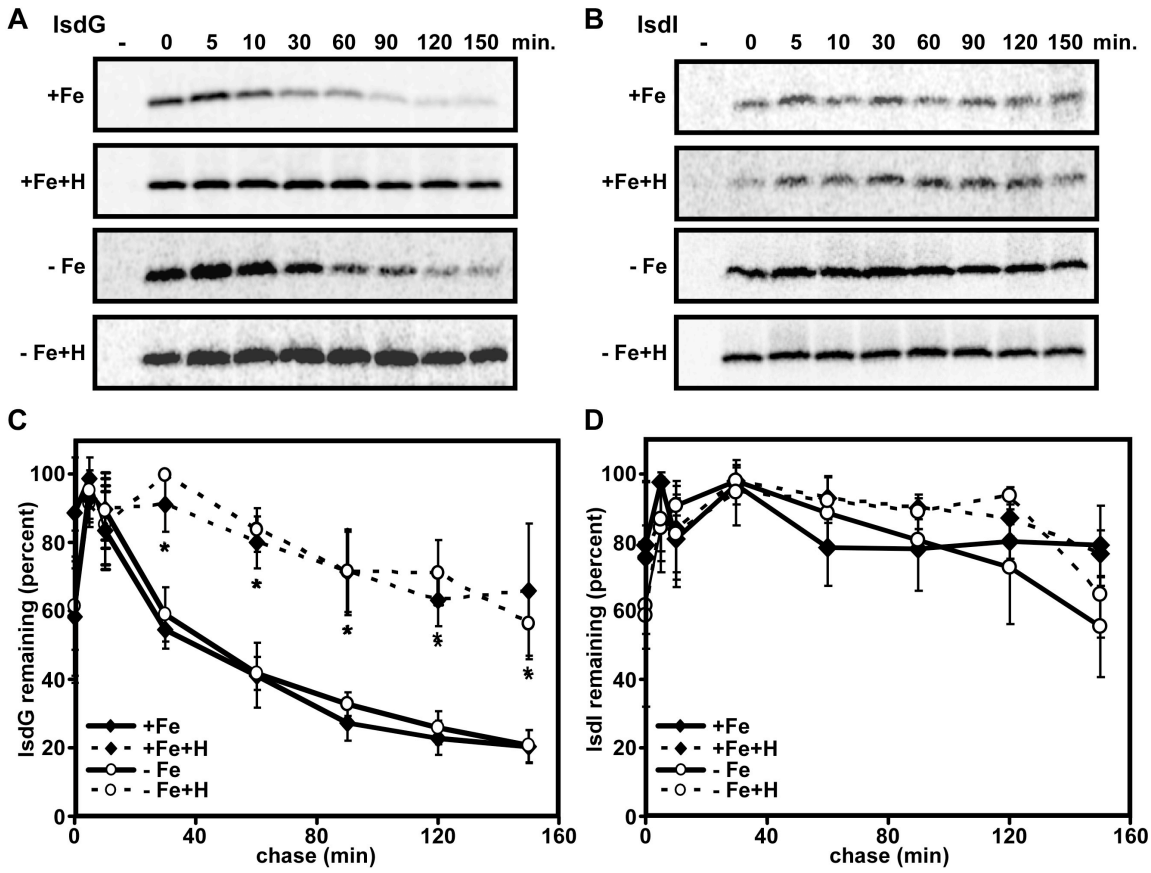

Figure 6. The role of heme in the stability of IsdG and IsdI. A and B. Phosphorimages of radiolabelled IsdG and IsdI immunoprecipitated from cells pulsed with ^{35}S-methionine, followed by a chase with unlabelled methionine for the time indicated. Pulse–chase analyses were carried out in media treated with iron sulfate (+Fe) or dip (−Fe) and 10 μM heme (+H). Dash indicates control cells in which primary antibody was omitted during immunoprecipitation. **C and D.** Quantification of IsdG and IsdI from quadruplicate experiments as described in *A* and *B.* Error bars represent standard deviation of data from at least three independent experiments. Asterisks denote statistical significance between conditions with and without heme irrespective of iron status, as measured by Student's *t* test ($p < 0.003$).

IsdG and IsdI are required for staphylococcal pathogenesis.

I have shown that IsdG and IsdI are required for staphylococcal growth when heme is the sole iron source (Figure 3). An abundance of available heme in an otherwise iron-free host is an environment likely encountered during the course of infection. Additionally, it has been shown that hemoglobin binding and heme acquisition systems are required for staphylococcal pathogenesis (97, 108). Therefore, I sought to test the pathological relevance of heme catabolism by investigating the requirement for IsdG and IsdI in *S. aureus* pathogenesis. To determine the contribution of IsdG- and IsdI-mediated heme-iron utilization to staphylococcal virulence, a mouse model of systemic abscess formation was employed. Mice were infected intravenously with wild type, Δ*isdG*, Δ*isdI*, or Δ*isdGI S. aureus*. Enumeration of bacteria in organs removed from mice four days after infection revealed a decrease in bacterial load of up to 2 logs for each mutant strain as compared to wild type in the hearts of infected animals (Figure 7A and B). Additionally, infection with the Δ*isdG* and Δ*isdGI* strains resulted in a 1-log decrease in bacterial load compared to wild type in the kidneys (Figure 7C and D). Taken together, these results demonstrate the importance of IsdG- and IsdI- mediated heme catabolism in staphylococcal virulence. The virulence decrease of Δ*isdG* and Δ*isdGI* observed in the kidneys suggests that heme degradation by IsdG is more significant than that mediated by IsdI when *S. aureus* colonizes this organ. The reason for this organ-specific requirement for IsdG is not known at this time. Importantly, this is the first demonstration that bacterial heme degrading enzymes contribute to virulence.

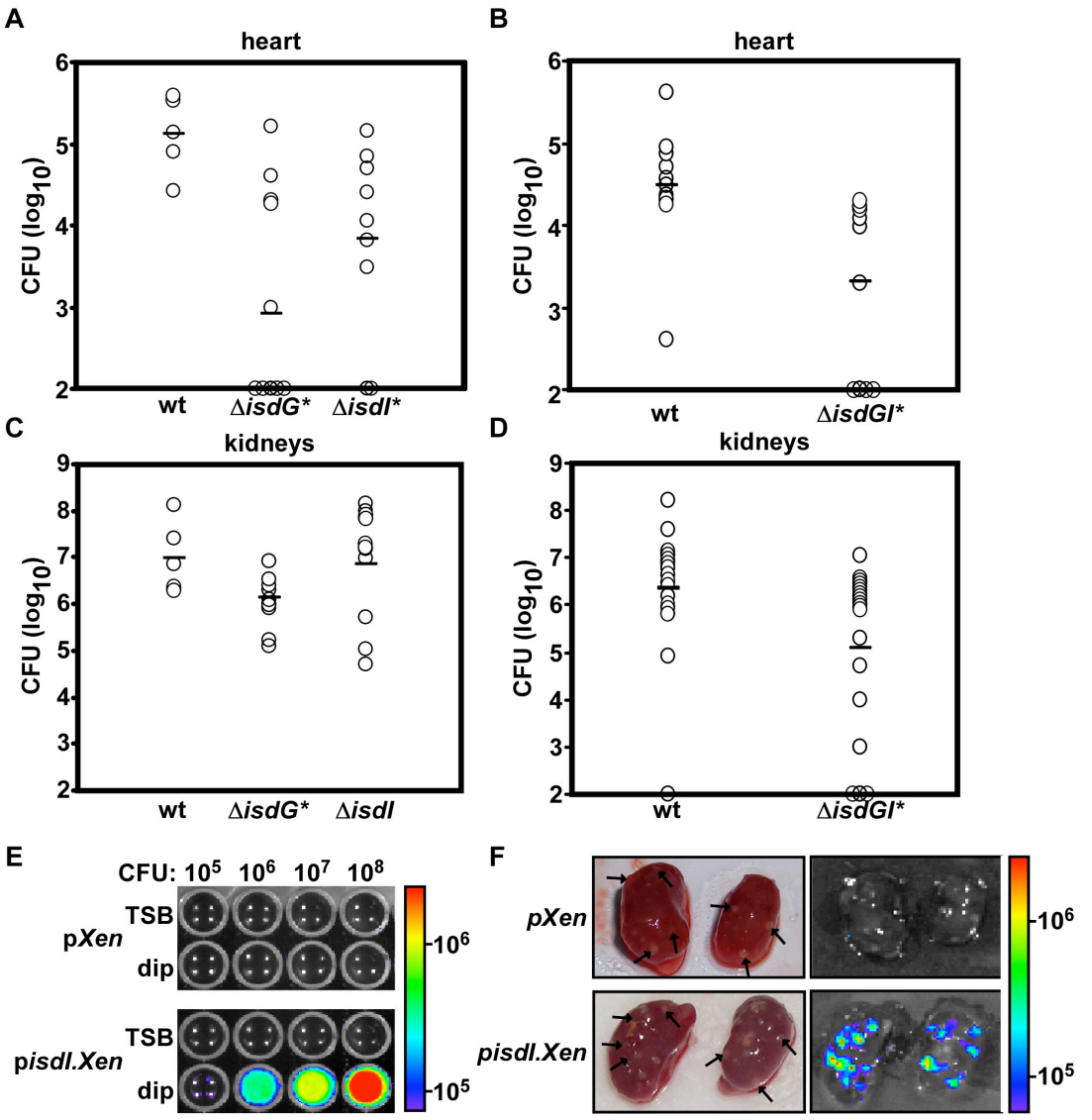

Figure 7. Contribution of IsdG and IsdI to *S. aureus* pathogenesis. *S. aureus* colonization of the hearts and kidneys of female Balb/c mice was analyzed 4 days post retroorbital infection. **A and C.** Colonization was compared between wild type, Δ*isdG* and Δ*isdI* strains. **B and D.** In a separate experiment, colonization of wild-type *S. aureus* was compared with the Δ*isdGI* strain. Each data point represents the CFU per organ in a single animal. The horizontal lines represent the mean CFU per organ. Asterisks denote statistical significance between wild type and the representative mutant strain as measured by Student's *t* test ($p < 0.04$). **E.** *S. aureus* harboring p*Xen* or p*isdI.Xen* was grown overnight in TSB or iron-deplete media (+dip). Serial dilutions were performed and luminescence was measured as described in the *Methods*. Luminescence scale is in p s^{-1} cm^{-2} $sr\Delta^{-1}$. **F.** At 4 days post infection kidneys were removed and imaged *ex vivo*. Pictured are kidneys from mice infected with *S. aureus* carrying p*Xen* or p*isdI.Xen* (left panels) and bioluminescent images of the same kidneys (right panels). Arrows indicate representative abscesses. Pictures and bioluminescent images are representative of at least five mice in each group. Bacterial load and number of abscesses were consistent between strains.

IsdI is expressed in tissue abscesses.

The decreased virulence of staphylococcal strains lacking *isdG* and *isdI* indicates that IsdG and IsdI are expressed and functional during infection. To investigate the expression of these enzymes in the context of infection I employed *in vivo* bioluminescence imaging (IVIS). This technique requires cloning the promoter of the gene of interest in front of the modified luciferase operon of *Photorhabdus luminescens* (28). When the promoter is activated the luciferase enzyme and its substrate are expressed and luminescence can be detected and quantified. The luminescent signal produced is of sufficient intensity to be detected through the tissues of an animal, thus enabling the detection of promoter activity *in vivo*. Because this technique monitors activation of a promoter, and our data indicate that IsdG is primarily regulated by a post-transcriptional mechanism, we were not able to investigate the *in vivo* expression of IsdG using this technology.

I first grew wild type *S. aureus* carrying either the p*Xen* vector (no promoter) or the p*isdI*.*Xen* vector in iron-rich medium or iron-deplete medium. As expected from the iron-dependent regulation of IsdI seen by protein analysis, the luminescent signal from bacteria harboring the p*isdI.Xen* vector is significantly increased in iron-deplete conditions (Figure 7E). Importantly, luminescence from the control vector is not above background levels from up to 10^8 bacteria, irrespective of the growth medium. To investigate the expression of IsdI in infected tissues, we infected Balb/c mice with wild type *S. aureus* harboring either p*Xen* or p*isdI.Xen*, using the same infection protocol described above. Four days post-infection the organs were harvested and imaged *ex vivo* via the IVIS imaging system. Luminescence was detected in the kidneys and livers of mice infected with bacteria carrying the p*isdI.Xen* plasmid (Figure 7F and data not shown). Notably, the luminescence co-localizes with sites of abscess formation in both organs and this trend was reproducible in every mouse analyzed (n = 5). Although the

number of bacteria and abscesses were similar in the organs from mice infected with bacteria harboring the control vector, no luminescence was detected in any mouse infected with this strain (n = 6). These results indicate that IsdI is expressed *in vivo* during infection. Considering that the total number of CFUs in the kidneys does not typically exceed 10^7, the significant luminescence observed in each individual abscess strongly suggests that *S. aureus* is starved for iron inside tissue abscesses.

Discussion

S. aureus heme-iron acquisition is vital for pathogenesis, but the intracellular components of this process have yet to be fully described (97, 108). IsdG and IsdI, two cytoplasmic proteins of the Isd heme-uptake machinery, are capable of degrading exogenously acquired heme to release free iron *in vitro* (96). I have shown that IsdG- and IsdI-catalyzed heme degradation is biologically significant, as IsdG and IsdI are each required for *S. aureus* growth on heme as a sole iron source (Figure 3). Additionally, I have provided a mechanistic explanation for the presence of two similar enzymes, in that they are differentially regulated according to the environment encountered by the bacteria. I have also demonstrated the importance of IsdG and IsdI in staphylococcal pathogenesis, as strains lacking these enzymes exhibit decreased virulence (Figure 7 A-D). Moreover, I have shown that IsdI is expressed at the site of infection coincident with the location of abscess formation (Figure 7F). These *in vivo* data suggest that abscesses are iron-starved microenvironments.

Although heme oxygenases have been described in over ten genera of pathogenic bacteria, very little is known about the regulatory mechanisms controlling expression of these enzymes. The exception to this is HmuO of *C. diphtheriae,* which is maximally expressed in low-iron high-heme (or hemoglobin) (5). However, unlike IsdG, HmuO is regulated at the level of transcription by the combined activity of the diphtheria toxin repressor protein (DtxR) and the response regulators ChrA and HrrA (5).

The observation that IsdG and IsdI are differentially regulated provides insight into the basis for two paralogous enzymes in *S. aureus* with seemingly identical functions. IsdG and IsdI are both regulated at the transcriptional level by Fur in response to iron availability (Figure 4 and 5). Additionally, IsdG abundance is regulated by heme availability via a post-transcriptional mechanism controlling protein stability (Figure 6).

P. aeruginosa is the only other pathogenic bacteria known to encode for two heme oxygenases (PigA and BphO). These have been shown to differ in their catalytic regiospecificity, in that they each produce a distinct isomer of biliverdin upon heme degradation (115). Although the regiospecificity of IsdG- and IsdI-catalyzed heme degradation is not yet known, it appears that in the case of *S. aureus*, the significance of encoding for two paralogous heme oxygenases is to fine-tune the expression of these enzymes according to the microenvironment encountered by the bacteria.

S. aureus is able to colonize and infect virtually every tissue of the vertebrate host. This diverse ecological range invariably requires significant flexibility in nutrient acquisition systems. It is tempting to speculate that, in the case of heme degradation, this flexibility is mediated by alterations in the abundance of IsdG and IsdI in response to heme and iron. The human body is virtually devoid of free iron due to the fact that the vast majority of iron is complexed as a component of heme (8). In healthy individuals, heme is bound to hemoglobin within erythrocytes and myoglobin within myocytes. During systemic infections, it is modeled that *S. aureus* can access this heme through the secretion of a number of potent hemolysins. Hemolysin expression is regulated in response to bacterial density by global virulence factors, which allow for controllable erythrocyte lysis at a time when colonization has been established and nutrient-iron needs are high (23, 44). In keeping with this model, it is possible that IsdI is expressed upon entry into the host to ensure that the low level of heme entering the staphylococcal cytoplasm is degraded and the iron is released. Following bacterial seeding of host organs, significant erythrocyte lysis is likely. Based on the efficiency of the Isd system for hemoglobin recognition and heme transport (59), this lysis would lead to a commensurate increase in heme transport into the staphylococcal cytoplasm. The intracellular amassing of heme would then stabilize IsdG, hence increasing its abundance. In effect, the simultaneous expression of both IsdG and IsdI would increase

the capacity of *S. aureus* to deal with a heme surplus. We predict that IsdG and IsdI abundance remains high until the nutrient iron needs of the organism have been satisfied. Considering that IsdI remains expressed inside abscesses four days following infection, it appears that *S. aureus* remains iron-starved during the course of infection in the animal model used in this work.

In support of this model, Cheng *et al.* recently reported that *isdA* and *isdB* mutants are defective in kidney abscess formation. In a wild type infection abscesses develop 2 – 5 days following infection, reinforcing the supposition that Isd-mediated heme uptake is required after bacterial seeding of host organs. Scanning electron microscopy also revealed the presence of red blood cells, a potential heme source, within staphylococcal communities at the center of abscesses. Based on these data, they propose a model in which heme-iron scavenging is required during abscess formation and maturation (12).

The presence of heme delays or prevents IsdG degradation, increasing the stability of the protein by 2.5-fold (Figure 6), representing a significant change in abundance for a catabolic enzyme. This regulatory strategy may be mediated by enzyme stabilization upon substrate binding. In keeping with this, it is possible that IsdG undergoes a conformational change or is partially unfolded in the absence of heme and is therefore targeted by proteases for degradation. Alternatively, heme could be stabilizing IsdG by binding outside the active site in a manner that hides or distorts possible protease target sites. Heme regulatory motifs (HRMs) have been described in eukaryotes and prokaryotes and are involved in heme-dependent transcription, translation, protein translocation, and protein stability (61, 77). HRMs are short sequence motifs containing an invariant cys-pro sequence. When heme binds an HRM it induces a conformational change, altering the function of the protein (61). This type of mechanism is unlikely in the case of IsdG, due to the lack of any cysteine or proline residues.

Additionally, the recent co-crystal structure of heme-bound IsdG reveals heme bound only in the active site (53). However, it is formally possible that heme can bind elsewhere on the protein under *in vivo* conditions, resulting in enhanced stabilization of IsdG.

In the present study, I demonstrate the role of IsdG and IsdI in staphylococcal heme-iron utilization and pathogenesis. Additionally, I reveal the mode of regulation to be a functional difference between these paralogous enzymes. Interestingly, IsdG and IsdI are 78% similar at the amino acid level, but only IsdG is post-translationally regulated by heme. Further experiments are necessary to provide a mechanistic explanation for the heme-dependent IsdG stabilization (Chapter III). The finding that IsdG and IsdI are required for full staphylococcal virulence establishes these enzymes as viable targets for the generation of novel antimicrobials to treat *S. aureus* infections. The potential to design small molecule inhibitors that specifically target bacterial heme oxygenases is further supported by the significant structural differences between this class of enzymes and the human heme oxygenases (91, 125). Considering the conservation of this enzyme family across *B. anthracis*, *L. monocytogenes*, *M. tuberculosis*, and the pathogenic *Staphylococci*, antimicrobials targeting the IsdG-family of heme oxygenases have the potential to be broadly applicable across a variety of infectious diseases.

CHAPTER III

ELUCIDATING THE MECHANISM OF IsdG DEGRADATION

Introduction

During infection of a vertebrate host *Staphylococcus aureus* encounters an environment in which greater than 80% of iron is found as a component of heme, the majority of which is bound to hemoglobin (8). In order to acquire iron for use as a nutrient source, *S. aureus* elaborates the iron-regulated surface determinant (Isd) system which binds host hemoglobin, removes the heme cofactor, and transports heme into the cytoplasm (98). The cytoplasmic components of this system are IsdG and IsdI, two paralagous heme oxygenases that degrade heme to release nutrient iron (96). IsdG and IsdI are each required for growth on heme as a sole iron source, an environment which is predicted to mimic conditions experienced by the bacterium during infection. Accordingly, each are required for staphylococcal pathogenesis in a murine model of systemic infection (80).

IsdG and IsdI degrade heme similarly, are 64% identical at the amino acid level and the three-dimensional structures can be superimposed with a root mean square deviation of less than 2 Å (53, 96). However, the observation that strains lacking either heme oxygenase are impaired for growth on heme indicates that IsdG and IsdI are not functionally redundant enzymes. In fact, IsdG and IsdI are differentially regulated by iron and heme depending on the microenvironment encountered by the bacteria (80). Under low iron conditions Fur-mediated transcriptional repression is released and *isdG* and *isdI* are transcribed. IsdG is also regulated at the post-transcriptional level such that IsdG is degraded in the absence of heme. Therefore, IsdI is most abundant in low iron

conditions, while IsdG levels are maximal in iron-deplete environments containing heme (80). We hypothesize that this differential regulation allows the bacteria to fine-tune the expression of heme oxygenase activity in order to adapt to the specific environment it encounters. However, the mechanism by which IsdG is specifically stabilized by heme has not yet been uncovered.

Bacteria are constantly monitoring proteins as a quality control measure to ensure that misfolded or damaged proteins do not accumulate and cause toxicity. Degradation of specific proteins may also allow the bacterium to rapidly adapt to changing environments when the activity of those proteins is no longer required. Protein turnover is accomplished through molecular chaperones that bind misfolded and aggregated proteins, and proteases that degrade nonnative proteins that cannot be salvaged (119). Bacterial proteases consist of an ATPase component, which recognizes and unfolds substrates in an ATP-dependent manner, and a proteolytic component responsible for protein destruction. Several ATPase subunits have also been shown to have chaperone activity independent of their role in protein degradation (42).

Protease substrate specificity is absolutely critical to prevent the uncontrolled degradation of normal cellular proteins. This fact is highlighted by the recent identification of a novel antibiotic that exerts its toxicity by binding an intracellular protease, rendering it constitutively active (6). The best characterized targeting mechanisms in bacteria are the N-end rule pathway and the SsrA tag. The N-end rule describes a universal system across Kingdoms in which the stability of a protein is dependent on its amino-terminal residue (2). The SsrA tag is an eleven amino acid peptide added to the carboxy-terminus of incomplete polypeptides upon ribosome stalling. Approximately 0.5% of *E. coli* proteins are SsrA-tagged during normal translation (66); however, the process of SsrA-tagging has not been investigated in *S. aureus*.

We sought to uncover the mechanism by which IsdG is specifically targeted for degradation in the absence of heme. The rate of IsdG degradation makes it an unlikely substrate for the N-end rule or the SsrA-tagging system, as both targeting mechanisms result in rapid degradation of substrates (54, 62, 80). Therefore, we hypothesized that IsdG is targeted for degradation by a novel mechanism. Here I show that IsdG catalytic activity is not required for heme-dependent IsdG stability. Furthermore, IsdG degradation is ATP-dependent, indicating that an ATP-dependent protease is responsible for IsdG degradation in the absence of heme. Finally, I demonstrate that the flexible loop region of IsdG, and specifically asparagine 84, is required for IsdG degradation. Combined, these results begin to elucidate the mechanism of heme-dependent IsdG stability. Moreover, these studies will lead to an increased understanding of targeted protein degradation in general, as the IsdG recognition sequence may be widely utilized in staphylococcal protein turnover.

Methods

Bacterial strains and growth conditions. *S. aureus* clinical isolate Newman was used in all experiments (24). The isogenic mutant lacking *isdG* has been described previously (80). Bacteria were grown in TSB at 37°C with shaking at 180 rpm unless otherwise stated.

IsdG mutagenesis. PFU mutagenesis was utilized to create point mutations in pET15b.*isdG* (118). All mutants were confirmed by sequencing (Vanderbilt University DNA sequencing facility). Plasmids were then transformed into *E. coli* BL21(DE3) pREL for expression and purification, as described previously (96). Heme binding was measured spectrophotometrically, as described previously (96). IsdG mutant coding sequences were excised using NdeI and BamHI and were inserted into p*OS1*p*lgt* (7). The p*isdG* mutant vectors were then transformed into the restriction negative strain RN4220, followed by transformation into Newman Δ*isdG*. The wild type p*isdG* complementation vector has been described previously (Chapter II).

Pulse-chase and immunoprecipitation. Pulse-chase analyses were performed as described in Chapter II.

Results

IsdG catalytic activity is dispensable for its heme-dependent stability.

In the presence of heme, IsdG degradation is markedly reduced (80). However, it is not known if IsdG is stabilized by heme or the product of heme degradation. To separate the catalytic activity and the heme-dependent stability of IsdG, I performed pulse-chase analyses on the IsdG N7A mutant, which binds heme but is not capable of degrading heme (53). It is expected that if the product of heme degradation is required for IsdG stability, the catalytically inactive N7A mutant will be degraded in both the presence and absence of heme. I observed a similar decrease in protein levels in the absence of heme for both the wild type and N7A mutant proteins (Figure 8). I hypothesize that the slight increase in IsdG N7A stability compared to wild type observed in the absence of heme is due to the irreversible binding of endogenous heme which stabilizes the inactive protein. Importantly, the stability of both proteins was increased similarly upon addition of heme (Figure 8). These results demonstrate that IsdG catalytic activity is dispensable for its stability. Therefore, the stability of IsdG is dependent upon the presence of substrate and not the product of heme degradation.

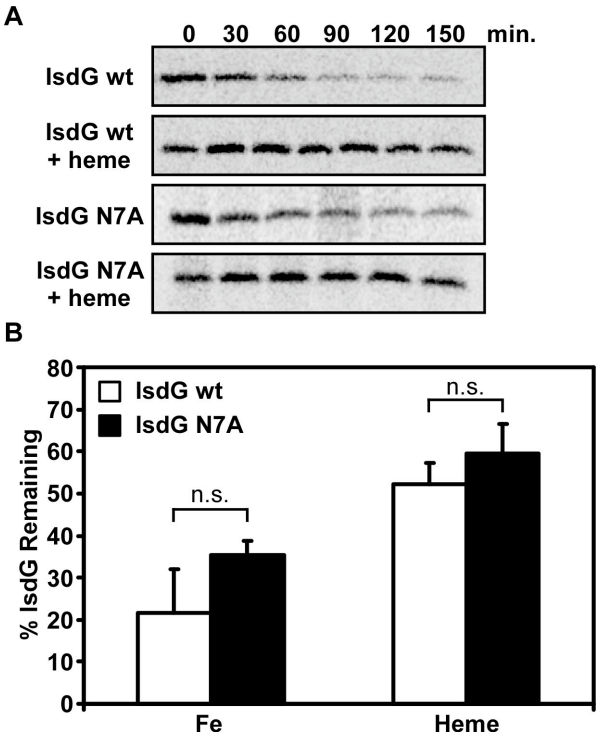

Figure 8. The role of heme degradation in IsdG stability. Pulse-chase analysis of *S. aureus* Δ*isdG* p*isdG* wild type and N7A point mutant which can bind heme but is catalytically inactive. **A.** Representative phosphorimages of immunoprecipitations over time in the presence and absence of heme. **B.** Percent IsdG remaining 150 minutes after addition of chase solution. Fe designates iron-replete samples lacking heme. Error bars represent the standard deviation of at least three independent experiments.

IsdG stability is increased by inhibiting ATPases.

IsdG stability is increased in the presence of exogenously added heme. We hypothesize that in the absence of substrate IsdG is specifically targeted for degradation by intracellular proteases. ATP-dependent intracellular proteases in *S. aureus* include: ClpCP, ClpXP, HslUV, and FtsH. The ATPase components of the Clp proteolytic complexes, ClpC and ClpX, also have chaperone activities independent of their role in proteolysis. Additionally, ClpX has been shown to have ATP-independent activities in *Bacillus subtilis* (40). Furthermore, ATP-independent cellular peptidases may play a role in protein turnover, although they have not been well described in *S. aureus* (89). The factor(s) required for IsdG turnover in the absence of heme are currently unknown.

To determine if IsdG degradation in the absence of heme is mediated by an ATP-dependent protease, we first analyzed the stability of IsdG in the presence of the respiratory poison sodium arsenate. Sodium arsenate structurally mimics inorganic phosphate, thereby inhibiting all cellular ATPases. A significant increase in IsdG stability is observed upon addition of sodium arsenate to the medium, an effect which occurs independently of heme (Figure 9). These results demonstrate that IsdG degradation in the absence of heme requires ATP, supporting the hypothesis that IsdG is specifically degraded by an ATP-dependent protease.

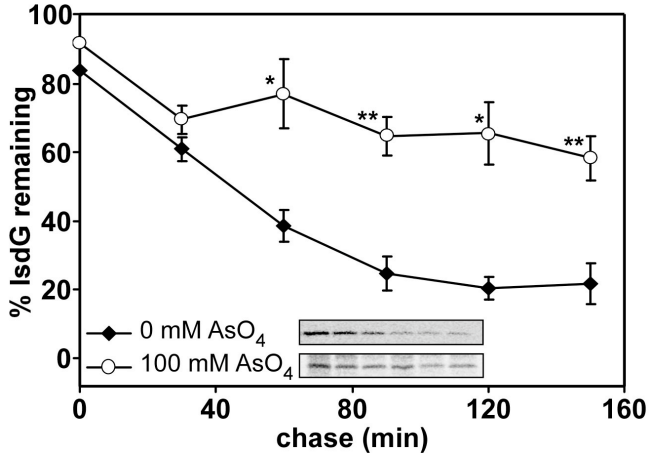

Figure 9. The role of ATP in IsdG stability. Pulse-chase analysis of *S. aureus* Δ*isdG* p*isdG* in the presence and absence of the respiratory poison sodium arsenate. Inset is a representative phosphorimage. Error bars represent the standard error of at least three experiments. Asterisks represent a statistically significant difference as compared to no additive (* $p < 0.03$, ** $p < 0.005$).

The flexible loop is required for IsdG degradation.

IsdG stability is ATP-dependent and requires the presence of exogenous heme. Therefore, we hypothesize that in the absence of substrate IsdG is specifically degraded by staphylococcal proteases. To that end, I sought to identify the region of IsdG that is recognized and targeted for degradation. We focused our search on α-helices and regions without secondary structure based on a recent proteome-wide analysis of proteolysis which found that β-strands are rarely tolerated in the cleavage sites of proteases (107). Additionally, the heme-dependent nature of IsdG degradation allows us to narrow our search to regions that undergo a conformational change upon heme binding. The differential regulation of IsdI, a paralagous protein which is 64% identical to IsdG but is not degraded, allows us to restrict our analysis further to regions that are dissimilar between the two enzymes (80, 96).

In silico analysis of IsdG and IsdI sequences indicated that amino acids 82-88 of IsdG comprise the region of highest divergence between the two proteins and is the most surface exposed region (Figure 10A). The apo-protein crystal structures reveal this region to be a disordered loop in both proteins that becomes ordered and more rigid upon porphyrin-binding (53, 125). Thus, amino acids 82-88 comprise the highest sequence divergence between IsdG and IsdI, is the region with the most drastic conformational change upon heme binding, and lacks secondary structure in the absence of heme. We hypothesized that this region may play a role in the difference in IsdG and IsdI stability. This hypothesis is supported by a recent report which concluded that the presence of a flexible loop is the critical component of an optimum protease cleavage site (107).

To test the role of the flexible loop in IsdG stability I constructed a chimeric IsdG protein that contains the IsdI loop amino acid sequence ($IsdG_{loop^*}$) and tested its stability by pulse-chase analysis (Figure 10A). $IsdG_{loop^*}$ is significantly more stable than wild type

protein in the absence of heme (Figure 10B). More than 50% of the labeled $IsdG_{loop*}$ protein remains after 150 minutes in comparison to 20% of wild type. In fact, $IsdG_{loop*}$ is equally stable in the absence of heme as wild type IsdG in the presence of heme, indicating that $IsdG_{loop*}$ stability is heme-independent. The $IsdG_{loop*}$ mutant in the presence of heme shows a trend towards greater stability than wild type, however this difference is not significant (Figure 10B). These results demonstrate that the IsdI loop sequence confers heme-independent stability upon IsdG and suggests that this region of IsdG may be recognized for degradation in the absence of heme.

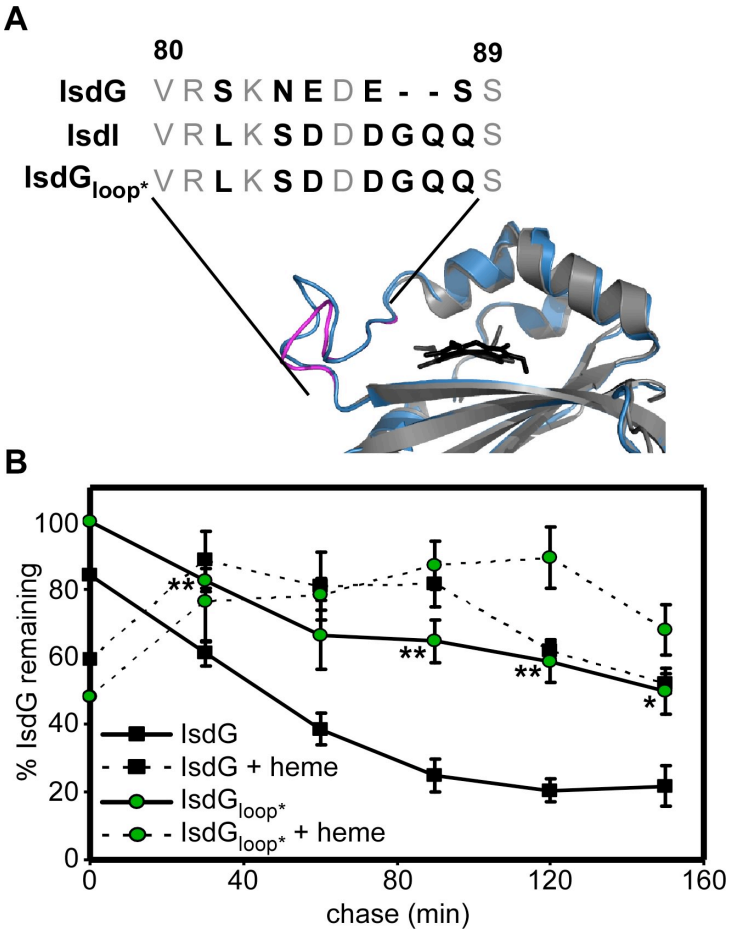

Figure 10. The role of the flexible loop in IsdG stability. A. Alignment of the flexible loop regions of IsdG and IsdI. IsdG$_{loop*}$ is an IsdG mutant with residues 82-88 mutated to the corresponding amino acid sequence of IsdI. The crystal structure of IsdI (blue) is superimposed with that of IsdG (gray) with heme depicted in a ball and stick model. The IsdG flexible loop is highlighted (magenta). **B.** Quantification of pulse-chase analyses of *S. aureus* Δ*isdG* p*isdG*$_{loop*}$. Asterisks indicate statistically significant differences as compared to IsdG wild type in the same growth medium (* $p < 0.03$, ** $p < 0.005$).

In order to more precisely define the sequence of IsdG required for its targeted degradation, a series of single point mutations in the flexible loop of IsdG were constructed. IsdG S82L is more stable than wild type in the absence of heme 30, 60, and 120 minutes following addition of the chase solution (Figure 11A). However, similarly to wild type, only 20% of the labeled S82L mutant protein remains after 150 minutes, suggesting that this mutation slows the degradation of IsdG, but does not inhibit degradation. IsdG N84S is significantly more stable than wild type in the absence of heme at all time points after 60 minutes (Figure 11B). Moreover, IsdG N84S stability is not significantly altered upon addition of heme, revealing that mutation of a single asparagine abolishes the heme-dependent stability of IsdG. Importantly, the difference in stability is not due to altered heme binding or degradation, as all IsdG mutants tested are able to bind and degrade heme similarly to wild type (data not shown).

IsdG 87[GQ]88, in which the flexible loop is elongated by two amino acids, is not altered in overall stability (Figure 11C). This was unexpected given that longer flexible loops are favorable for protease-mediated degradation (107). Thus, it is possible that the flexible loop is the recognition sequence, but not the site of protease cleavage. Combined, these results demonstrate that asparagine 84 is the critical component of the flexible loop in the degradation of IsdG.

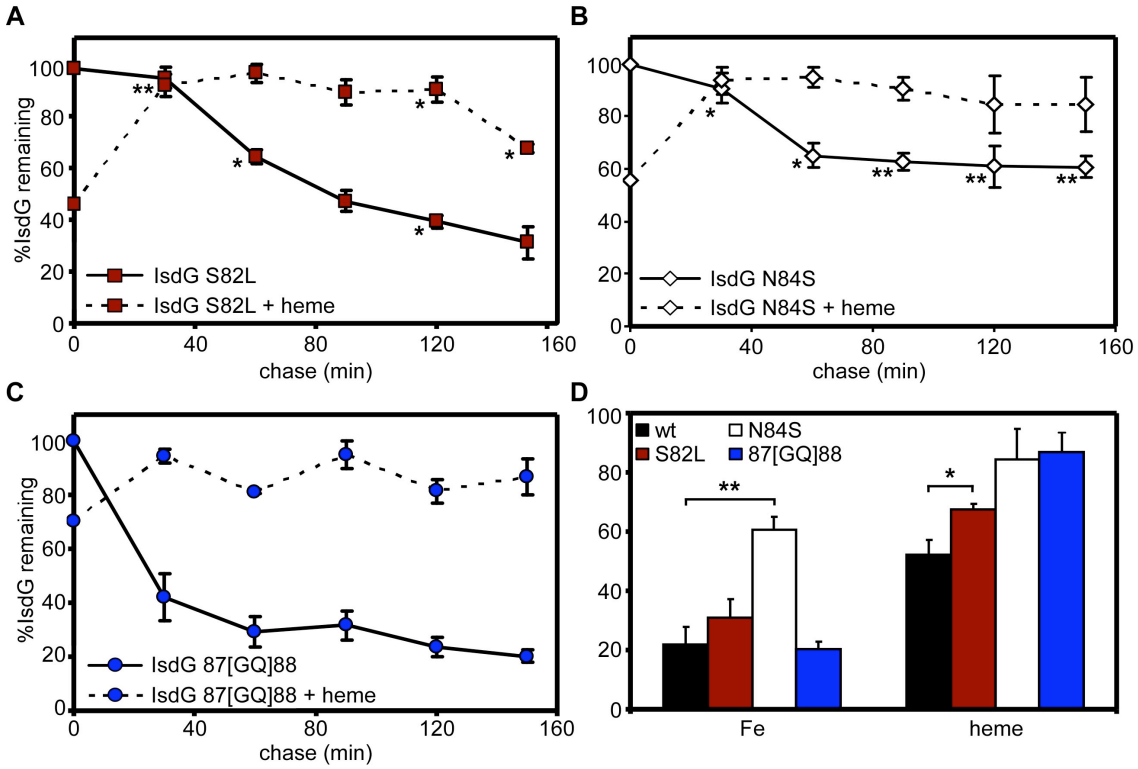

Figure 11. The stability of IsdG point mutants. A-C. Quantification of pulse-chase analyses of *S. aureus* Δ*isdG* p*isdG* loop mutants. **D.** Percent IsdG remaining 150 minutes after addition of chase solution. Error bars represent the standard error of at least three independent experiments. Asterisks indicate statistically significant differences as compared to IsdG wild type in the same growth medium (* $p < 0.03$, ** $p < 0.005$).

The flexible loop is not sufficient to target a protein for degradation.

We next sought to determine if the sequence of the IsdG flexible loop is sufficient to target a protein for degradation. To test this an IsdI chimera which encodes for the loop sequence of IsdG ($IsdI_{loop*}$) was constructed and analyzed for heme-dependent stability. I predicted that the $IsdI_{loop*}$ mutant would be degraded in the absence of heme. However, pulse-chase analyses showed that the $IsdI_{loop*}$ mutant protein stability is identical to that of wild type (data not shown). This result does not preclude the flexible loop being the target cleavage site or recognition sequence for IsdG. Proteases are not solely influenced by the amino acid sequence of the cleavage site. Rather, sequences surrounding the cleavage site are also known to play a role in the specificity of protease recognition. Additionally, secondary site interactions at surfaces distinct from the cleavage site may also be important for effective protease cleavage (107). Therefore, we conclude that the flexible loop is required for IsdG degradation in the absence of heme, although it is not a sufficient targeting sequence for proteolysis.

Discussion

S. aureus expresses two paralagous heme oxygenases that are differentially regulated depending upon the environment encountered by the bacterium. *isdG* and *isdI* are both transcribed under iron-limiting conditions while IsdG is additionally regulated post-transcriptionally by heme (Chapter II). The mechanism of the heme-dependent regulation of IsdG has not yet been investigated. Here I show that the catalytic activity of IsdG is dispensable for IsdG stability. This result demonstrates that the product of heme degradation is not required for IsdG stability. Furthermore, IsdG degradation is ATP-dependent, suggesting that an ATP-dependent protease degrades IsdG in the absence of heme. Finally, I establish that the flexible loop sequence, specifically asparagine 84, is required for IsdG degradation. Combined, these results begin to elucidate the mechanism of IsdG heme-dependent stability.

In iron-deplete environments *S. aureus* elaborates the Isd system in order to obtain heme-iron during infection (98). This system includes cell wall-anchored hemoprotein receptors, membrane heme transport proteins, and the cytoplasmic heme oxygenases IsdG and IsdI. We predict that upon encountering an iron-deplete environment without heme *S. aureus* adapts by decreasing heme oxygenase activity in the cell. This is accomplished through the specific proteolysis of IsdG. A precedence for substrate-dependent stability comes from the quorum-sensing regulator TraR in *Agrobacterium tumefaciens*. TraR requires its signal molecule, an autoinducing peptide (AAI), for proper folding and stability (129). It is postulated that the hydrophobic core of TraR is exposed to solvent in the absence of AAI, resulting in aggregation and proteolysis. However, in this system TraR that is synthesized in the absence of substrate is rapidly degraded with a half-life of 2 minutes. IsdG has a longer half-life in the absence of substrate (~67 minutes), suggesting that IsdG is properly folded in the

absence of heme, but is targeted for degradation at a step after translation and protein folding.

Post-translational regulation mediated by proteolysis must be a highly specific process to avoid degrading native proteins. Eukaryotes achieve specificity through a conserved tagging system that covalently attaches the small protein ubiquitin to lysine residues of the substrate. Enzymes that recognize ubiquitin-tagged proteins then present the substrate to the proteasome for degradation. An analogous system was recently identified in *M. tuberculosis* (71). The prokaryotic ubiquitin-like protein (Pup) is a small disordered protein that is covalently attached to the ε-amino groups of substrate lysines. The adaptor protein Mpa then unfolds the substrates and translocates them into the proteasome for degradation (11, 71). Although bacterial proteases such as ClpCP, ClpXP, and HslUV are structurally similar to the proteasome, a similar tagging system to ubiquitin and pupylation has not been identified in bacteria outside the Actinomycetes class (20).

Substrate recognition by bacterial proteases is multifaceted and requires precise structural presentation, cleavage site sequence and subsite specificity, and appropriate secondary site interactions (107). A recent study of the structural features of proteolytic substrates found that loop size and target sequence play critical roles in defining the susceptibility of protein substrates (18, 107). In fact, eukaryotic ubiquitin-tagged proteins are stable *in vitro* unless they also contain an unstructured region (89). Herein I have shown that the flexible loop sequence is required for IsdG degradation, although it is not sufficient. These results indicate that other factors, which may include subsite sequence specificity and secondary site recognition, play a role in IsdG stability. Ongoing experiments are aimed at elucidating the mechanism of IsdG degradation, particularly to identify the minimal region that is sufficient to target a staphylococcal protein for degradation (Chapter VI).

IsdG and IsdI are each required for *S. aureus* growth on heme as a sole iron source, an environment likely encountered during infection of a vertebrate host. Accordingly, IsdG and IsdI are both required for staphylococcal pathogenesis. Furthermore, a *S. aureus* mutant lacking *isdG* is more attenuated for virulence than the *isdI* mutant in both the hearts and kidneys of infected animals (Chapter II). This observation suggests that the differential regulation of IsdG and IsdI may be critical during pathogenesis. Moreover, a novel class of antibiotics was recently identified that exerts toxicity through the binding and constitutive activation of bacterial proteases (6). Combined, these facts suggest that elucidating the mechanism of IsdG degradation may lead to the identification of novel therapeutic targets. As *S. aureus* is increasingly becoming resistant to all available antibacterial agents, identifying novel therapeutic targets to combat this important pathogen is critical.

CHAPTER IV

THE IsdG-FAMILY OF HEME OXYGENASES DEGRADES HEME TO THE NOVEL CHROMOPHORE STAPHYLOBILIN

Introduction

During infection of a vertebrate host *Staphylococcus aureus* preferentially acquires iron from heme bound to host hemoglobin (97). In order to utilize heme as a nutrient iron source bacteria must cleave the tetrapyrrole ring to release the coordinated iron atom. This task is accomplished by heme oxygenases that catabolize heme to carbon monoxide, α-biliverdin, and free iron. The first bacterial heme oxygenase described was HmuO from *Corynebacterium diphtheriae*, which was identified based on its structural homology to human heme oxygenase 1 (HO-1) (86). Since that initial report, numerous additional HO-1-like heme oxygenases have been identified in both plant and mammalian pathogens (Table 1) (78, 122, 130). Extensive biochemical analyses of bacterial and vertebrate HO-1-like enzymes indicate that the mechanism of heme degradation is similar across all heme oxygenases, resulting in the production of biliverdin (110). In mammals biliverdin is further reduced to bilirubin by biliverdin reductase; however, the ultimate fate of biliverdin in bacteria is unknown as homologues of biliverdin reductase have not been discovered in bacteria.

The IsdG-family of heme oxygenases, first identified in *S. aureus*, is structurally distinct from the HO-1 family. Initial reports demonstrated IsdG-catalyzed cleavage of the macrocyclic ring with concomitant release of free iron, although the precise mechanism of heme degradation by this class of heme oxygenases has not yet been delineated (96). Recently it has been suggested that this family of enzymes degrade heme via a novel mechanism (81). Porphyrin-bound structures of IsdG-family enzymes

have revealed significant ruffling of the porphyrin ring in the active site. In fact, the porphyrin ring is distorted approximately 2 Å out of plane, far more than has been observed in any other heme-binding protein (53). Moreover, *in vitro* heme degradation catalyzed by recombinant IsdG results in the formation of a yellow reaction product distinct from the blue-green biliverdin chromophore (53, 81). Taken together, these structural and biochemical observations suggest that members of the IsdG-family of heme oxygenases degrade heme by a unique mechanism resulting in the formation of a product that is distinct from biliverdin. Herein we present the crystal structure of heme-bound IsdI and demonstrate that the IsdG-family of enzymes degrade heme to the oxo-bilirubin chromophore staphylobilin.

Methods

Protein purification. Recombinant IsdG and IsdI were purified from *Escherichia coli* BL21(DE3) as previously described (96). Purity was assessed by SDS-PAGE and concentrations were determined using a BCA protein assay.

Crystallography. Crystals of recombinant IsdI-heme were prepared by sitting drop vapour diffusion at 4°C. Protein (15 mg/ml in 20 mM Tris-HCl, 0.2 M NaCl) was mixed 1:1 with a reservoir of 25% polyethylene glycol 3350, 0.2 M $MgCl_2$, and 0.1 M Bis-Tris buffer pH 5.5. Prior to data collection crystals were looped from a cryoprotectant of 10% ethylene glycol in reservoir solution on ice and immersed in liquid nitrogen. Reduced crystals were obtained by soaking the ferric crystals in 50 mM sodium dithionite in cryoprotectant solution for 10 minutes before immersion in liquid nitrogen. Diffraction data sets were collected under a cryostream at 100 K on beamline 08ID-1 at the Canadian Light Source (Saskatoon, SK). The programs in the CCP4 suite (75) were used to solve and refine the structures. Data were processed and scaled with MOSFLM and SCALA (26), respectively. Initial phases were obtained with the program MolRep, using a search model of the protein moiety from the IsdI-CoPPIX structure (PDB ID: 2ZDP). Model building was carried out using COOT visualization software and the structure was refined with the program Refmac5. Final structure validation was done with the program PROCHECK and figures were prepared with the program PyMOL.

Heme degradation and product purification. Heme degradation reactions were performed in TBS at room temperature protected from light. IsdG or IsdI (50 μM) were incubated with equimolar hemin (Sigma) and catalase (from bovine liver, Sigma) at a 0.5:1 molar ratio of catalase:hemoprotein. We also performed the reactions in the presence of superoxide dismutase (20 units/mL) to test the role of superoxides in the heme degradation mechanism. Products and product distributions in reactions

performed in the presence of catalase and/or superoxide dismutase were unchanged. Ascorbic acid was added to a final concentration of 1 mM and spectral changes between 300-800 nm were monitored. After 2 hours the reactions were filtered through Centricon Plus spin filters (MWCO 5 kDa, Millipore) by centrifugation at 3,220 x g to remove buffer, salts, and non-degraded heme. The heme degradation product was eluted from the proteins by addition of water:acetonitrile (1:1) with 0.1% trifluoroacetic acid (TFA) followed by centrifugation. The eluate was lyophilized and resuspended in a minimum volume of water:acetonitrile (1:1) with 0.1% TFA, and further purified by reverse-phase chromatography on a Varian ProStar HPLC using a Microsorb-MV C-18 column. Biliverdin (MP Biomedicals) and bilirubin (Sigma) were dissolved in 0.1 M NaOH and diluted in water:acetonitrile (1:1) with 0.1% TFA for HPLC analysis.

HPLC analysis was performed using 95% water / 5% acetonitrile with 0.1% TFA as the mobile phase with a flow rate of 1 mL/min. After a 10 min equilibration period, a linear 40 min acetonitrile gradient (5%-80%) was employed and the final concentration was maintained for an additional 20 min. The eluant was monitored using a photodiode array detector from 200-900 nm and two peaks (λmax: 465nm) were individually collected and lyophilized for further analysis. The ratio of isomers was calculated by integration of the product peaks and averaged over ten experiments ($p < 0.0001$).

LC-MS/MS Analysis. Each lyophilized product was dissolved in acetonitrile:water (1:1) with 0.25% formic acid at a concentration of 80 ng/μL prior to injection. The LC-MS/MS analysis was performed on a Waters Acquity UPLC system (Waters, Milford, MA) integrated with a Thermo Finnigan LTQ linear ion trap mass spectrometer (Thermo Fisher Scientific, Waltham, MA) using a Thermo Hypersil Gold C18 column (1.9 μm, 2.1 x 150 mm). Prior to MS analysis, LC separation was performed using water:acetonitrile (95:5) with 0.25% formic acid as the mobile phase. After a 10 μl sample injection, a 20 minute linear acetonitrile gradient (5%-100%) was performed at a flow rate of 300 μl/min.

The following optimized parameters were used for the detection of analyte: N_2 sheath gas 36 psi; N_2 auxiliary gas 20 psi; capillary temperature 300^o C; source voltage 3.8 kV; source current 100 MA; skimmer offset 0.00 V; capillary offset -44.00 V; tube lens offset -103.30 V; activation time 30 ms (MS), 50 ms (MS2); isolation width 1 *m/z* (MS), 2 *m/z* (MS2). Data acquisition and quantitative spectral analyses were conducted using the Thermo-Finnigan Xcaliber software, version 2.0 Sur1.

NMR. NMR experiments were performed using a 14.0 T Bruker magnet equipped with a Bruker AV-III console operating at 600.13 MHz. All spectra with the exception of ^{13}C NMR were acquired in 3 mm NMR tubes using a Bruker 5 mm TCI cryogenically cooled NMR probe. Chemical shifts were referenced internally to DMSO-d_6 (2.49 ppm) which also served as the ^2H lock solvent. 1D ^{13}C NMR data were acquired using a 14.0 T Bruker magnet equipped with a Bruker AV-III console operating at 599.87 MHz using a Bruker 5 mm DCH cryogenically cooled NMR probe. For 1D ^1H NMR, typical experimental conditions included 32K data points, 20 ppm sweep width, a recycle delay of 1.5 seconds and 32-256 scans depending on sample concentration. For 2D ^1H-^1H COSY, experimental conditions included 2048 x 512 data matrix, 20 ppm sweep width, recycle delay of 1.5 seconds and 4 scans per increment. The data were processed using squared sinebell window function, symmetrized, and displayed in magnitude mode. For 2D ^1H-^1H nuclear Overhauser enhancement spectroscopy (NOESY), experimental conditions included a 2048 x 512 data matrix, a mixing time of 600 ms, 20 ppm sweep width, recycle delay of 1.5 seconds and 16 scans per increment. Multiplicity-edited HSQC experiments were acquired using a 1024 x 256 data matrix, a J(C-H) value of 145 Hz which resulted in a multiplicity selection delay of 34 ms, a recycle delay of 1.5 seconds and 16 scans per increment along with GARP decoupling on ^{13}C during the acquisition time (150 ms). The data were processed using a π/2 shifted squared sine window function and displayed with CH/CH_3 signals phased positive and CH_2 signals

phased negative. J_1(C-H) filtered HMBC experiments were acquired using a 2048 x 256 data matrix, a J(C-H) value of 9 Hz for detection of long range couplings resulting in an evolution delay of 55ms, J_1(C-H) filter delay of 145 Hz (34 ms) for the suppression of one-bond couplings, a recycle delay of 1.5 seconds and 128 scans per increment. The HMBC data was processed using a π/2 shifted squared sine window function and displayed in magnitude mode.

Results

The structure of heme-bound IsdI

We have previously determined the crystal structures of a catalytically inactive variant of IsdG bound to heme (FePPIX) as well as native IsdI bound to the heme analogue cobalt protoporphyrin IX (CoPPIX) (53). However, studies into the mechanism of heme degradation have been hindered by the fact that the crystal structure of a catalytically active IsdG-family member bound to the substrate heme has not been reported. To gain insight into the mechanism of heme catabolism by IsdG-family enzymes, we crystallized the catalytically active IsdI bound to heme by lowering the temperature to 4°C. The structure was solved to 1.5 Å resolution with one IsdI dimer in the asymmetric unit. The fold of the IsdI-heme complex is similar to that observed in the IsdI-CoPPIX structure and the heme porphyrin ring is also highly ruffled. We observe elongated density for a sixth iron ligand on the distal side of heme, best modeled as a coordinating dioxygen species (Figure 12A-C). The presence of an oxygen species implies that heme-iron was photoreduced to Fe(II) in the X-ray beam during data collection. Further reduction of the oxygen species is suggested by the elongated Fe-O bond length (2.05 Å) and decreases Fe-O-O angle (108º). Notably, dithionite reduced crystals yield a structure without a density for a sixth ligand (Figure 12D), likely due to the consumption of oxygen in the crystal by the reductant. No other significant differences are noted between the dithionite reduced and native structures.

In contrast to the HO-1 family of enzymes, the oxygen species in the IsdI heme-binding pocket is aligned with the imidazole plane of the coordinating histidine, which lies along the β,δ-axis of the porphyrin ring (Figure 12C). The orientation of the dioxygen is restricted by Phe22 and Asn6, which is also an H-bond donor to the oxygen species. In the HO-1 family, regiospecificity is also achieved by steric limitations of the dioxygen

ligand such that only the α-*meso* carbon is accessible for hydroxylation (110). In the two IsdI heme-binding pockets of the asymmetric unit, the oxygen species are in opposite orientations such that the β- or δ-*meso* carbons are aligned for hydroxylation, a regiospecificity distinct from that of the HO-1 family. The heme is bound predominantly in one orientation, suggesting that reaction at both *meso*-carbons is possible.

Due to the unique placement of the oxygen in the active site, we hypothesized that the product of heme degradation by IsdG-family enzymes exhibits unique regiospecificity compared to the canonical HO-1 like enzymes. We therefore sought to determine the structures of the products of IsdG- and IsdI-mediated heme degradation and add insight into the mechanism by which these enzymes degrade heme.

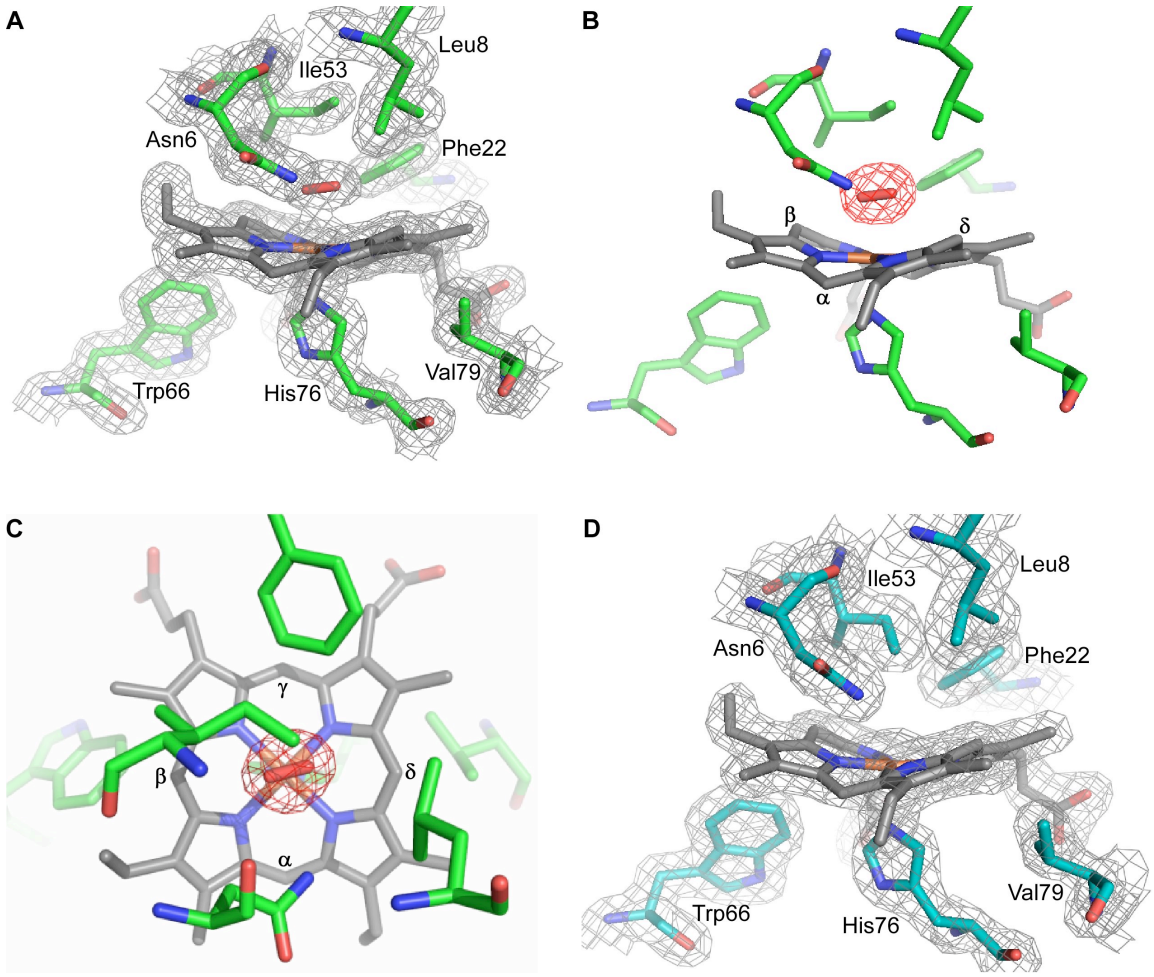

Figure 12. Crystal structure of the active site of IsdI-heme. The structure of IsdI (green) bound to heme (gray) reveals density on the distal side modeled as a dioxygen species (red) liganded to the heme-iron. **A.** *2Fo - Fc* map contoured at 1σ. **B.** *Fo - Fc* omit map for oxygen is contoured at 3σ. The heme α-, β-, and δ-*meso* carbons are labeled. The γ-*meso* carbon is buried in the protein. **C.** The same figure as in *b*, but looking down perpendicular to the heme from the distal side. The heme α-, β-, γ-, and δ-*meso* carbons are labeled. **D.** Crystals of IsdI (cyan) bound to heme (gray) were reduced for 10 minutes in 50 mM (excess) dithionite. The *2Fo - Fc* map (light gray) is contoured at 1σ. Heme and selected amino acids are depicted in sticks and are labeled. Nitrogen, oxygen and iron atoms are colored blue, red, and orange, respectively.

Purification of the IsdG- and IsdI-catalyzed heme degradation products

As previous attempts to crystallize the product-bound enzymes were unsuccessful, we sought to isolate the product of IsdG-mediated heme degradation for structural studies. *In vitro* heme degradation reactions were performed with purified recombinant IsdG and IsdI using ascorbate as the electron donor and catalase to prevent coupled oxidation (see Methods). Purification of the products of IsdG- and IsdI-catalyzed heme degradation results in a red-orange solid that becomes yellow when dissolved in dimethyl sulfoxide (DMSO) or water:acetonitrile (1:1). This is in stark contrast to the blue-green color of the canonical heme degradation product biliverdin (Figure 13A-C, insets). HPLC-separation of the IsdG and IsdI reaction products results in two distinct peaks which elute earlier than both biliverdin and bilirubin, indicating a higher degree of polarity (Figure 13A-C). Product peaks from both IsdG- and IsdI-mediated degradation exhibit similar optical spectra with one maximum at ~390 nm and one at ~460 nm. The peak maxima of biliverdin are 365 and 663 nm and the peak maximum of bilirubin is 446 nm (Figure 13D-F). Together, these data suggest that the IsdG-family of oxygenases catabolize heme to a unique chromophore that is more polar than biliverdin and bilirubin.

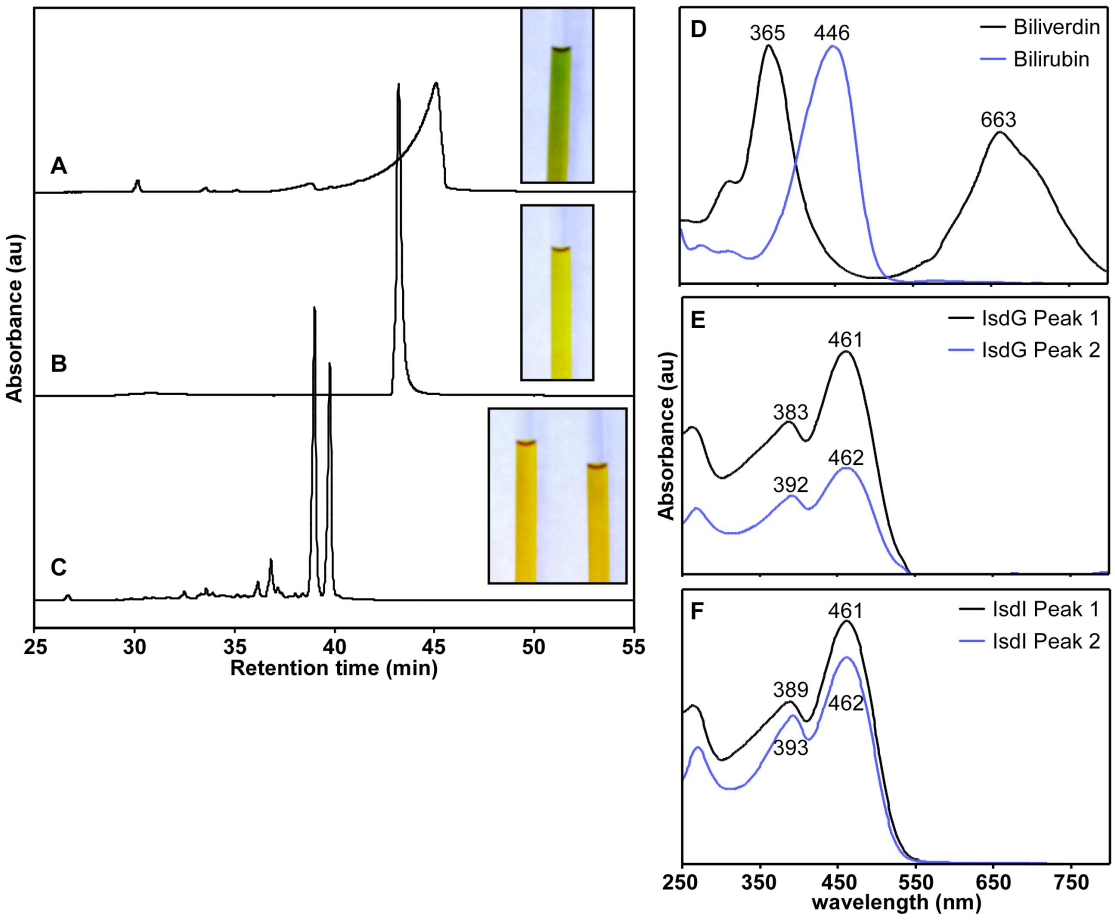

Figure 13. Purification and optical spectra of heme degradation products. HPLC tracings of heme degradation products separated on a linear acetonitrile gradient. Insets are images of products dissolved in DMSO in 3 mm NMR tubes. The contrast of the photos was adjusted to present the clearest image. **A.** Biliverdin purification monitored at 405 nm. **B.** Bilirubin purification monitored at 405 nm. **C.** The product of IsdI-catalyzed heme degradation monitored at 465 nm. The two prominent peaks were collected separately. IsdG- and IsdI-catalyzed heme degradation products have overlapping spectra so only that of IsdI is shown for simplicity. **D-F.** Optical spectra of each fraction as measured by the photodiode array detector upon elution.

IsdG and IsdI degrade heme to staphylobilin

To determine the molecular composition of the products of IsdG- and IsdI-mediated heme degradation, the HPLC-purified samples were subjected to high resolution electrospray ionization mass spectrometry (HRESIMS). Each of the eluting product peaks gave a mass of 598.25 Da (*m/z* 599.2605 [M + H], Δ = 3.0 - 4.2 ppm), corresponding to a molecular formula of $C_{33}H_{34}N_4O_7$ (data not shown). As biliverdin and bilirubin have molecular masses of 582.6 and 584.7 Da, respectively, these data conclusively demonstrate that heme degradation catalyzed by IsdG and IsdI does not produce biliverdin or bilirubin.

This hypothesis is supported by analysis of ^{1}H NMR spectra of the purified fractions acquired in d_6-DMSO. Inspection of the downfield region indicates that both eluting fractions possess two pyrrol amide (δ 10.4 – 10.5) and two pyrrol amine (δ 11.0 – 11.3) resonances; however notable chemical shift differences in this region were evident between the two fractions (Figure 14). Furthermore, both products of IsdG- and IsdI-mediated heme degradation have distinct ^{1}H NMR spectra in comparison to bilirubin (Figure 14A) (46). The most significant dissimilarity is again in the NH region in which the pyrrol amines of the IsdG and IsdI products are shifted as much as 0.8 ppm in comparison to reported hemes (Figure 14). Chemical shift values in this range are also observed in 10-oxo-mesobilirubin which was chemically synthesized by Chen *et al*. in order to investigate possible oxidative pathways of bilirubin elimination *in vivo* (10). Due to the addition of a carbonyl group at the γ-*meso* carbon of bilirubin, 10-oxo-mesobilirubin is more stable than the parent molecule and the pyrrole NHs are considerably more deshielded than the corresponding NHs of bilirubin (10). These similarities further suggest that the products of IsdG-mediated heme degradation may be oxidized forms of bilirubin.

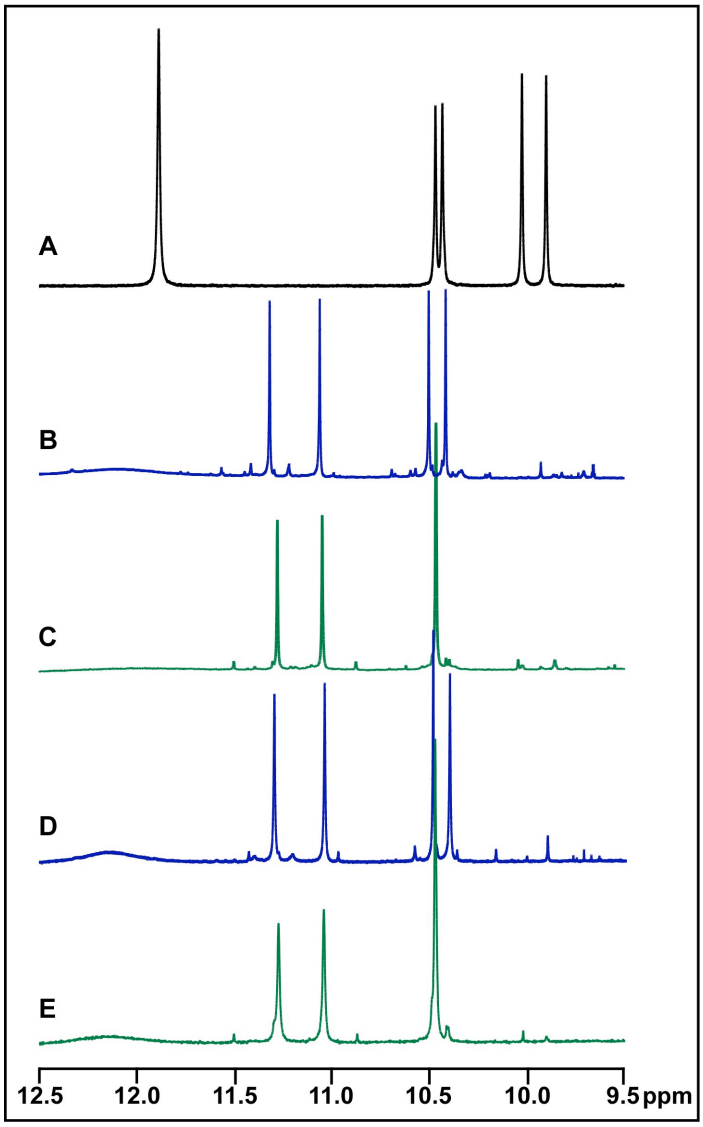

Figure 14. ^{1}H NMR spectra comparing downfield regions of heme degradation products. Comparison of the downfield regions of bilirubin (**A**), IsdG peak 1 (**B**), IsdG peak 2 (**C**), IsdI peak 1 (**D**), and IsdI peak 2 (**E)**.

The ^{1}H NMR spectra also establish several regions of biliverdin and bilirubin that are conserved in the IsdG-family products. All side-chain resonances present comparable chemical shifts and coupling values to canonical hemes (Tables 2 and 3), indicating that the vinyl side chains and the α- and β-CH2 positions of the propionate group chains are intact and that the methyl substituents are unmodified. Side-chain functional groups are readily positioned in their corresponding pyrrol rings using two-dimensional NMR data (Figure 15A). The observed nuclear Overhauser effect (NOE) interactions between C20-CH and C3-CH_3 and also C18-CH= indicate that the α-bridge is intact, and correlations between C10-CH and α,α'-CH_2, β,β'-CH_2 indicate that the γ-bridge is intact (Figure 15A). These spectral data allow us to assemble two partial structures, one hemisphere containing the intact α-bridge and the other encompassing the intact γ-bridge (Figure 15B). Therefore, although the IsdG-family heme degradation products share structural similarities with bilirubin, these products are not cleaved at the α-*meso* carbon.

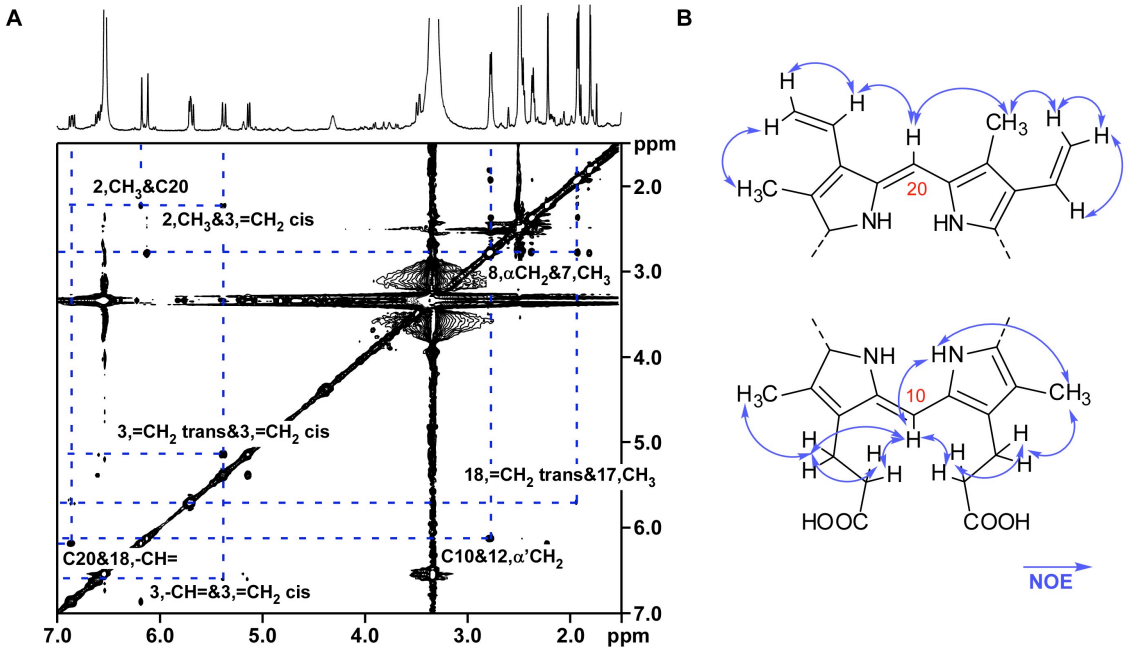

Figure 15. NOESY correlations of IsdG product peak 1. A. NOESY spectrum (in d_6-DMSO) of the first eluting product focused on key regions that demonstrate correlations between the α- and γ-bridge CHs and neighboring protons. The second eluting product from the IsdG-catalyzed reaction and the IsdI-catalyzed products have similar NOESY spectra. **B.** Two fragments of a bilirubin-like molecule with NOE correlations (arrows). Carbon 10 and 20 are labeled according to standard bilirubin nomenclature in which C10 corresponds to the γ-*meso* carbon and C20 corresponds to the α-*meso* carbon of the porphyrin ring.

From the molecular formula obtained by HRESIMS and the NMR data described above, we have been able to propose structures of the products of IsdG- and IsdI-mediated heme degradation. In accordance with the 10-oxo-mesobilirubin nomenclature (10), we have named these unprecedented molecules 5-oxo-δ-bilirubin (elution peak 1) and 15-oxo-β-bilirubin (elution peak 2) (Figure 16). Collectively, we refer to these molecules as staphylobilins. The β- and δ-*meso* carbon cleavage is in agreement with the alignment of molecular oxygen in two orientations along the β,δ-heme axis in the crystal structure of heme-bound IsdI (Figure 12C). Alternatively, the heme molecule may bind in either orientation about the α,γ-axis in the active site, resulting in either the β- or δ-isomer of oxo-bilirubin, as reported previously for the CoPPIX and inactive IsdG variant (53). Similarly, in human HO-1, heme is orientationally disordered about the α,γ-axis, although in that case α-cleavage occurs with either heme seating (91).

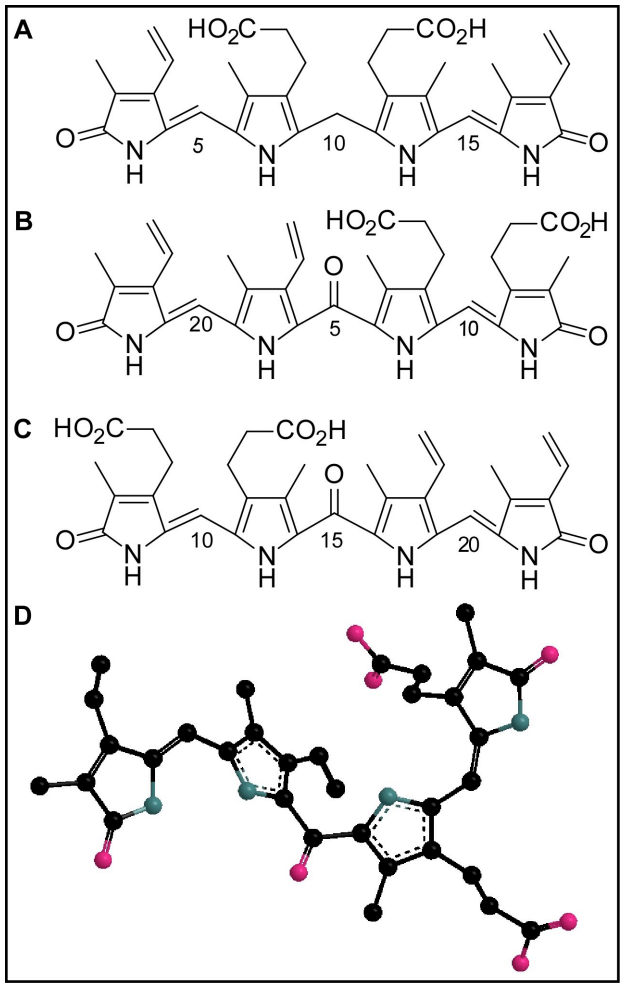

Figure 16. Structures of heme degradation products. A. Bilirubin. **B.** 5-oxo-δ-bilirubin, the first eluting product. **C.** 15-oxo-β-bilirubin, the second product to elute upon HPLC purification. The bilirubin carbon numbering scheme was used for the IsdG and IsdI products for simplicity. **D.** Three-dimensional representation of 5-oxo-δ-bilirubin. The carbons, nitrogens, and oxygens have been colored black, teal, and pink, respectively. The structure was adjusted to minimize the cumulative potential energy for the model.

Table 2. ^{1}H and ^{13}C data of 5-oxo-δ-bilirubin

Position[a]	^{1}H, m (J in Hz)	^{13}C (ppm)	COSY	HMBC	NOESY
13, CH_3	1.80, s	7.9	-	126.7, 144.3, 172.0	2.79
7, CH_3	1.92, s	9.1	-	125.3, 131.7	2.76, 11.30
17, CH_3	1.93, s	9.1	-	140.3, 171.6	5.71
2, CH_3	2.22, s	10.8	-	-	5.37, 6.18
8, α CH_2	2.36, t (7.1)	34.4	2.76	126.7, 173.4	2.76, 6.12
12, α' CH_2	2.46, t (7.5)	33.5	2.79	144.3, 173.1	2.79, 6.12
8, β CH_2	2.76, d (7.0)	18.5	2.36	-	1.92, 2.36
12, β' CH_2	2.79, d (7.0)	18.5	2.46	144.3, 173.1	1.80, 2.46
3, =CH_2 cis	5.13, dd (1.6, 11.7)	115.2	6.60	125.1	5.37, 6.60
3, =CH_2 trans	5.37, dd (1.7, 18.0)	115.2	6.60	125.1	2.22, 5.13
18, =CH_2 trans	5.68, dd (1.4, 13.5)	122.7	6.86	140.3	1.93
18, =CH_2 cis	5.71, dd (1.5, 7.4)	122.7	6.86	140.3	6.86
5	-	174.7	-	-	-
10	6.12, s	95.9	-	126.7, 144.3	2.36, 2.46, 2.79, 11.30
20	6.18, s	96.8		121.4, 140.3	2.22, 6.86
3, -CH=	6.60, dd (11.7, 18.0)	128.2	5.13, 5.37	121.4	5.13
18, -CH=	6.86, dd (11.6, 17.6)	126.5	5.68, 5.71	125.8	5.71, 6.18
23 NH	10.40, s	-	-	126.7, 132.5, 144.3	11.04, 11.30
24 NH	10.48, s	-	-	125.8, 131.7, 140.3	11.04, 11.30
21 NH	11.04, s	-	-	125.1, 127.6, 131.6	10.40, 10.48
22 NH	11.30, s	-	-	120.4, 125.3	1.92, 6.12, 10.48, 10.40
8, COOH	12.09, bs	173.4	-	-	-
12, COOH	12.09, bs	173.1	-	-	-

a. Position based on numbering scheme in Figure 16

Table 3. ^{1}H and ^{13}C data of 15-oxo-β-bilirubin

Position[a]	^{1}H, m (J in Hz)	^{13}C (ppm)	COSY	HMBC	NOESY
7, CH_3	1.81, s	7.8	-	126.6, 144.3, 172.0	2.79
13, CH_3	1.99, s	9.5	-	124.8, 127.5, 131.3	2.79
17, CH_3	2.05, s	11.0	-	122.9, 132.5	-
2, CH_3	2.18, s	8.8	-	124.2, 133.6, 142.1	-
12, α CH_2	2.37, m (1.8)	34.3	2.79	18.4, 173.3	2.79
8, α' CH_2	2.46, d (7.6)	33.4	2.79	18.6, 172.9	-
8, β CH_2	2.79, q (7.2, 12.0)	18.4, 18.6	2.37, 2.46	33.4, 126.6, 144.3, 173.3	1.81, 1.99, 2.37
12, β' CH_2					
18, $=CH_2$ cis	5.35, dd (1.5, 11.6)	115.8	6.87	124.8	-
3, $=CH_2$ cis	5.38, d (2.3)	118.6	6.60	124.2	6.24
18, $=CH_2$ trans	5.41, dd (1.6, 17.6)	115.8	6.87	-	6.24, 6.87
10	6.12, s	95.8	-	126.6, 144.3	2.79
15	-	174.9	-	-	-
20	6.24, s	97.1	-	124.2, 142.1	2.18, 5.38, 6.87
3, $=CH_2$ trans	6.25, dd (2.4, 17.5)	118.6	6.60	124.2	2.18, 5.38
3, -CH=	6.60, dd (11.6, 17.6)	126.2	5.38	-	-
18, -CH=	6.87, dd (11.6, 17.8)	128.3	5.35, 5.41	-	5.41, 6.24
21 NH	10.47, s	-	-	124.2, 132.4, 142.1	11.05, 11.28
22 NH	10.47, s	-	-	124.2, 132.4, 142.1	11.05, 11.28
23 NH	11.05, s	-	-	126.6	10.47, 11.28
24 NH	11.28, s	-	-	122.9, 124.8	10.47, 11.05
8, COOH	12.09, bs	172.9	-	-	-
12, COOH	12.09, bs	173.3	-	-	-

a. Position based on numbering scheme in Figure 16

The position of the remaining oxygen atom in the proposed structures of β- and δ-oxo-bilirubins was confirmed by tandem ESI-MS analyses and two-dimensional NMR (Figures 17 and 18). Fragmentation generated by collision-induced dissociation results in cleavage on either side of the proposed dipyrryl ketone and is diagnostic for the presence of the 5- and 15-oxo-bridges in these structures. Fragmentation at these positions results in the formation of ion pairs consisting of an oxonium ion (*m/z* 359, 267 [M+]) and pyrrolium ion (*m/z* 241, 333 [M'+H]). Pyrrolium ions M' correspond to ions resulting from intramolecular proton transfer reactions, possibly facilitated by propionate groups which are proximal in the ridge-tile conformation (10). Beta-fragmentation of the β-propionic acid side chains is also evident (*m/z* 539.2), as has been noted in the mass spectral analysis of analogous mesobiliverdin (17). Lastly, we observe cleavage at the C-10 methine bridge (*m/z* 418.2), similar to that observed in mesobiliverdin (17). The 5- and 15-oxo-bridges in these structures were further confirmed by observation of a fifth carbonyl resonance in 5-oxo-bilirubin at 175.1 ppm via cryogenic ^{13}C-NMR (Tables 2 and 3), consistent with the reported shift of the oxo-bridge in 10-oxo-bilirubin at 176 ppm (10).

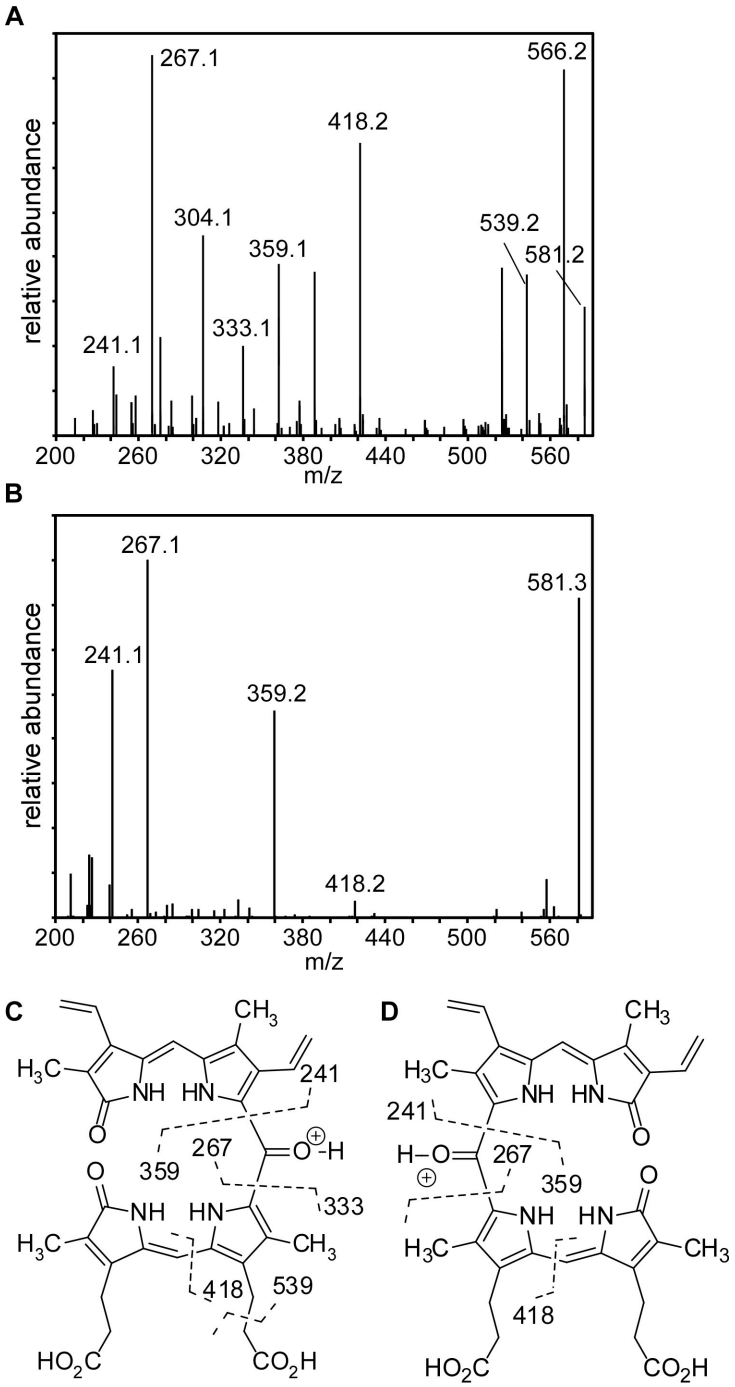

Figure 17. Tandem LC-HRESIMS of staphylobilin. A. ESI-MS/MS spectrum of fragment ions selecting for 599.3 *m/z* for 5-oxo-δ-bilirubin. **B.** ESI-MS/MS spectrum of fragment ions selecting for 599.3 *m/z* for 15-oxo-β-bilirubin. **C,D.** Fragmentation scheme corresponding to the masses and molecular formulas obtained in *A* and *B* respectively. ESI-MS/MS spectra for IsdI-catalyzed products are similar.

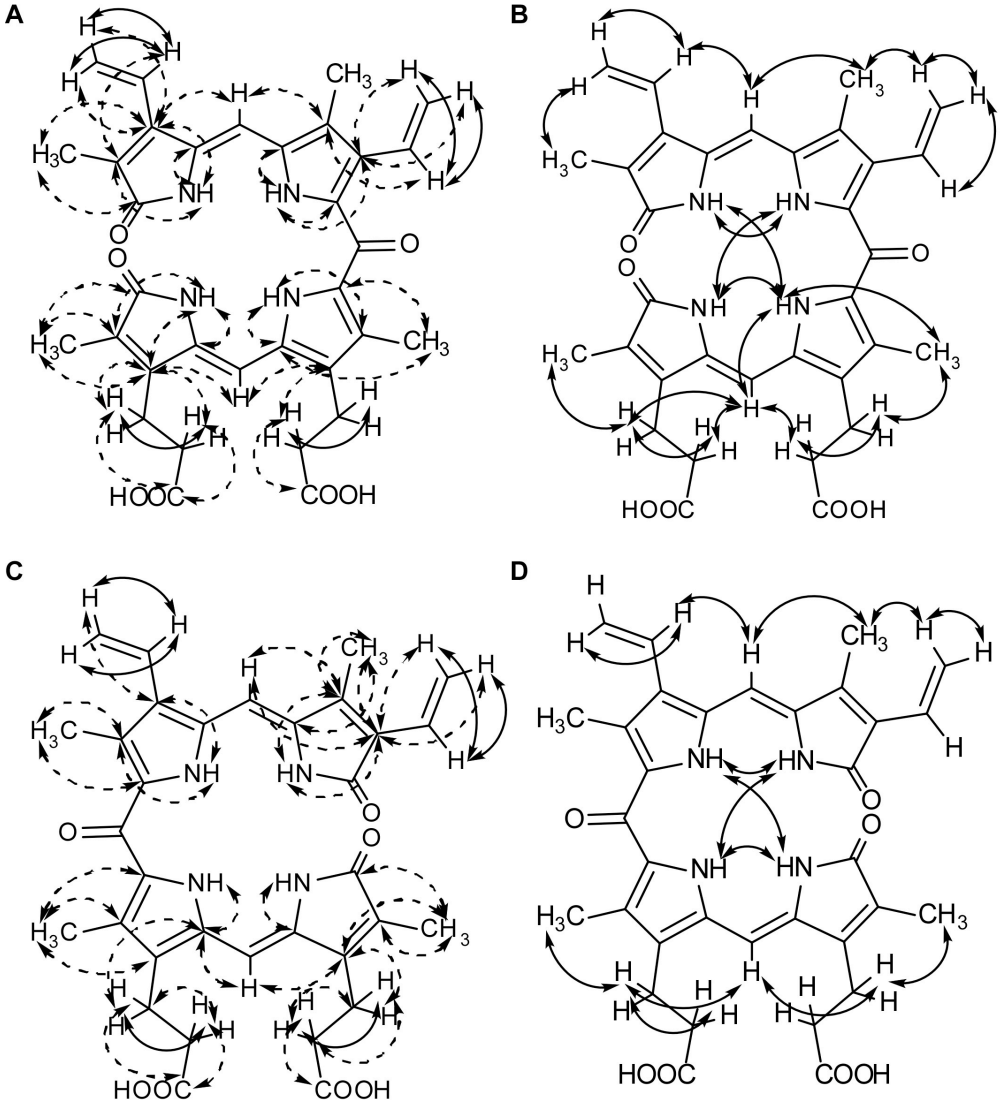

Figure 18. Two-dimensional NMR correlations of IsdG products. A. 5-oxo-δ-bilirubin COSY correlations (solid lines) and HMBC correlations (dashed lines). **B.** 5-oxo-δ-bilirubin NOESY correlations. **C.** 15-oxo-β-bilirubin COSY correlations (solid lines) and HMBC correlations (dashed lines). **D.** 15-oxo-β-bilirubin NOESY correlations. IsdI products have similar 2D NMR spectra.

Discussion

In this study we presented the crystal structure of native IsdI bound to heme and described HRESIMS and NMR studies on the products of IsdG- and IsdI-catalyzed heme degradation. Combined, these data demonstrate that IsdG and IsdI degrade heme to release a mixture of β- and δ- isomers of oxo-bilirubin. To the best of our knowledge, these oxo-bilirubin isomers have not been previously observed or characterized.

It has been reported that IsdG-mediated heme degradation results in the formation of biliverdin based on similar HPLC elution profiles between these molecules (96). However, the prior study utilized standard methods for isolating biliverdin, which includes a chloroform extraction. In these studies we have found that staphylobilin is not very soluble in chloroform, and therefore, the previously published chromatograms are not representative of purified staphylobilin. Moreover, the previous chromatographic method used a methanol:water mobile phase and monitored absorbance at 380 nm. In the current study we have used an acetonitrile:water mobile phase and 465 nm, which better distinguishes the two products. We believe it is for these reasons that the product of IsdG-mediated heme degradation was previously misassigned as biliverdin.

The HRESIMS data provide conclusive evidence that heme degradation catalyzed by IsdG-family enzymes does not result in the canonical heme degradation product biliverdin or the eukaryotic metabolite bilirubin. The UV/VIS and downfield regions of the ^{1}H NMR spectra demonstrate that the IsdG-family products share similarities with 10-oxo-mesobilirubin (Figures 13 and 14) (10). Moreover, the hetero-nuclear multiple bond coherence (HMBC) and NOESY spectra demonstrate an intact correlation network between the α-*meso* carbon proton and the vinyl protons at C18 and methyl protons at C2. The γ-*meso* proton also displays correlations with the propionate side chain protons of rings B and C (Figure 15 and 18). These data provide strong

evidence that the α- and γ-*meso* carbons of the porphyrin ring are intact, accounting for all but 28 Daltons of the isolated heme degradation products. ESI-MS/MS data and ^{13}C NMR spectra demonstrate that the remaining mass comprises a bridging carbonyl (C=O) between the α/γ positions in the two isomers (data not shown).

The mechanism of the HO-1 family of enzymes has been studied extensively, although surprisingly, many details remain unclear (Figure 19) (111, 120). After the enzyme binds ferric-heme, one electron is donated by the reducing substrate, converting heme-iron to the ferrous state. Molecular oxygen then binds the reduced pentacoordinate heme to form a meta-stable oxy complex. From there, a one electron reduction and protonation yields a ferric-hydroperoxo complex. This complex then self-hydroxylates at the α-*meso* carbon, although it is unknown how the protonation activates the hydroperoxo intermediate to promote *meso*-hydroxylation. Ferric α-*meso*-hydroxyheme is then converted to biliverdin through multiple oxidoreductive steps and a verdoheme intermediate (58, 91, 111). The conversion of verdoheme to biliverdin is incompletely understood, although it is known to be the rate-limiting step of the reaction *in vivo* (111). However, *in vitro* the rate-limiting step is biliverdin release. In mammals this step is accelerated by biliverdin reductase, which removes biliverdin from the active site and reduces it to bilirubin. All characterized bacterial heme oxygenases catalyze single-turnover reactions *in vitro*, suggesting that another protein is required to remove the heme degradation product from bacterial heme oxygenases *in vivo* (76, 121).

Both IsdG-like and HO-1-like enzymes produce biliverdin derivatives suggesting that both reactions may proceed similarly up to formation of a hydroperoxo intermediate. However, in the case of IsdG-like enzymes the complex would self-hydroxylate at the β- or δ-*meso* carbon, rather than the α-*meso* carbon. Importantly, HO-1-like enzymes contain an ordered set of water molecules in the binding pocket that funnel protons to the catalytic site and stabilize the hydroperoxy intermediate (33, 51). This water network

is absolutely required for catalysis in all HO-1 enzymes (58, 91, 92, 103); however, a similar water network is not present in IsdG-family enzymes (53). Therefore, it is currently unclear how intermediates are activated and stabilized during IsdG-mediated catalysis.

It is possible that the *meso*-hydroxyheme intermediate may then go through a verdoheme intermediate that is hydroxylated and then degraded to staphylobilin, or through formation of a β,δ-dihydroxyheme intermediate that is subsequently degraded to staphylobilin (Figure 19). Addition of biliverdin to purified IsdG and ascorbate does not lead to the formation of staphylobilin (data not shown), indicating that α-biliverdin is not an intermediate in the pathway. However, more experiments are necessary to elucidate the mechanism of staphylobilin formation.

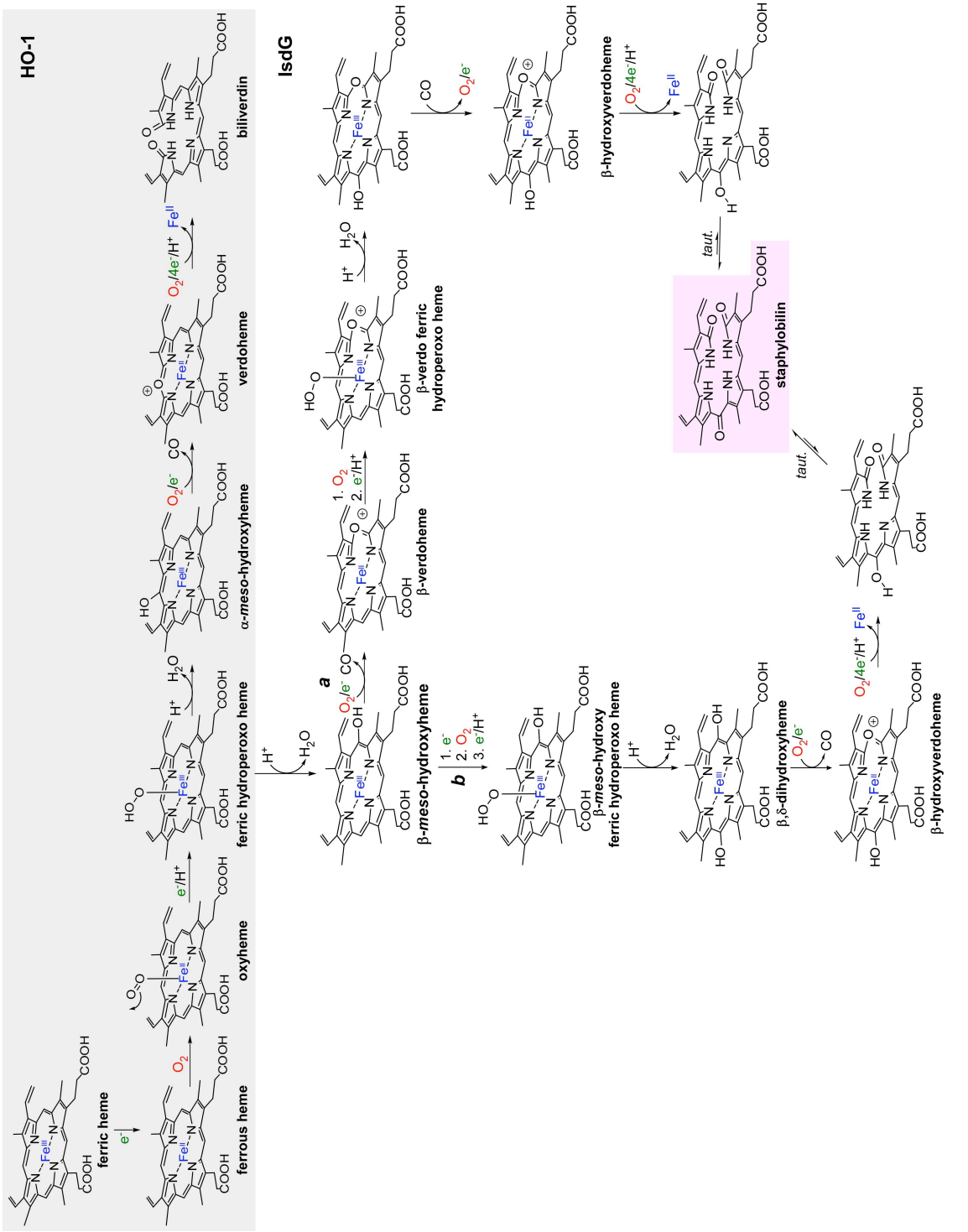

Figure 19. Mechanisms of heme oxygenases. The mechanism of the HO-1 family of heme oxygenases is highlighted in gray. The proposed IsdG-family mechanism follows the same pathway up to the ferric hydroperoxo heme intermediate. From there, β-meso-hydroxyheme may be formed, which could then follow one of two pathways, ultimately resulting in production of staphylobilin.

In the active site of IsdI there are several amino acids that are completely conserved among members of the IsdG-family of enzymes, including Asn6. We hypothesize that the conserved asparagine has two roles in heme catalysis. The asparagine amide is observed to form an H-bond to the bound oxygen species and potentially stabilizes intermediate(s) in the pathway. Asn6 along with Phe22 may also sterically direct the sites of hydroxylation, as they are only 3.5 Å from the α- and γ-*meso* carbons, respectively (Figure 12). Phe22 is conserved in all IsdG members with the exception of HmuD and HmuQ from *B. japonicum*, which encode for tryptophan at that site. Though the precise nature of the oxygen species observed in the crystal structure remains to be characterized, the steric constraints imposed by Asn6 and Phe22 are likely to be structurally conserved leaving only the β- and δ-*meso* carbons accessible for hydroxylation. Indeed, Phe22 is one of the residues implicated in directing heme ruffling such that the β- or δ-*meso* carbons are tilted towards the oxygen species (53). Considering that the pathway of heme degradation has not been experimentally determined, identification of the reaction products of IsdG-family enzymes raises many mechanistic questions to be investigated in future studies.

Interestingly, we noted that 67.5 ± 1.9% of the IsdG-catalyzed product elutes in the first peak as the δ-isomer, whereas only 56.2 ± 1.6% of the IsdI-catalyzed product elutes as the δ-isomer. This may indicate that the heme-binding pocket of IsdG is more constricted than that of IsdI, and therefore preferentially allows for one heme seating over another. The ramifications for this regiospecificity *in vivo* and the fate and function of staphylobilin inside the cell are currently under investigation.

Bilirubin, the terminal product of heme degradation in mammals, is one of the most potent antioxidants in the serum (101). The other products of vertebrate heme catabolism, biliverdin and carbon monoxide, also have beneficial antioxidative and anti-inflammatory properties (47). In fact, only one instance of an HO-1 deficient human has

been reported, indicating that HO-1 deficiency is most likely lethal *in utero* (63). In contrast, the role of bacterial heme degradation products *in vivo* has yet to be uncovered. Considering the important roles of biliverdin and bilirubin within vertebrate cells, it is tempting to speculate that staphylobilins may have important functions within bacterial pathogens. This is particularly intriguing considering that IsdG and IsdI are differentially regulated in response to environmental changes experienced by the bacterium (80). It is possible that the different isomers of staphylobilin are required under different environmental conditions. Moreover, the significant difference in protein structure and mechanism between human HO-1 and the IsdG-family of enzymes, combined with the known requirement for IsdG-mediated heme degradation during bacterial pathogenesis (80, 95), suggests that inhibiting this class of bacterial HOs is an attractive therapeutic strategy.

CHAPTER V

THE INTRACELLULAR FATE OF NON-DEGRADED METALLOPORPHYRINS

Introduction

In iron-restricted environments *Staphylococcus aureus* can degrade exogenously acquired heme for use as a nutrient iron source. However, heme is also valuable to *S. aureus* in its intact form (81). This supposition is based on the requirement for heme as a cofactor in numerous bacterial proteins. The majority of heme-binding proteins are cytochromes located within the plasma membrane (106). When iron is not limiting bacteria may utilize exogenous heme as an enzyme cofactor, as it is thermodynamically favorable to import host heme rather than synthesize the porphyrin ring *de novo*. In fact, it has been shown that when radiolabeled heme is added to cultures of *Bacillus subtilis,* heme is taken up and incorporated into four distinct cytochromes (84). Moreover, some pathogens, such as *Enterococcus faecalis* and Group B Streptococcus*,* rely solely on exogenously acquired heme for respiration (123, 126).

A role for exogenously acquired heme in staphylococcal hemoproteins is supported by the observation that heme-iron is preferentially acquired and segregated intact to the plasma membrane when other iron sources are simultaneously available (97). The molecular mechanisms required for trafficking heme to the membrane of Gram positive bacteria are not fully understood. Moreover, the cytochrome profile of *S. aureus* has not been studied in detail. Based on the requirement for heme in staphylococcal pathogenesis, determining the fate of intact heme in the membrane may lead to the discovery of novel therapeutic targets. We hypothesize that the subcellular fate of heme is dependent upon the environmental conditions experienced by the bacterium.

Methods

Bacterial strains and growth conditions. S. aureus clinical isolate Newman was used in all experiments (24). Bacteria were grown in TSB at 37°C with shaking at 180 rpm unless otherwise stated.

Electron microscopy (EM). S. aureus was grown overnight in iron-rich TSB, iron-deplete TSB containing 1 mM dip, or iron-deplete TSB supplemented with heme (10 μM). The cultures were pelleted and washed several times with fixative buffer. Finally, fixative buffer was added to the samples, which were then submitted for sectioning and staining at the Vanderbilt EM Core.

Degradation of Metalloporphyrin. IsdG and IsdI were expressed in *Escherichia coli* BL21 (DE3) and purified as previously described (96). Metalloporphyrins (Frontier Scientific) were dissolved in 0.1 N NaOH (10 mM) and spectra were obtained with a Varian Cary 50-BIO UV-visible spectrophotometer from 300 to 700 nm. For degradation studies purified protein (10 μM) was combined with dissolved metalloporphyrin (10 μM) in TBS and allowed to bind for 1 hour at 4°C. Initial spectra were obtained, followed by addition of ascorbic acid (1 mM) as an electron donor. Spectra were obtained every 5 minutes for 90 minutes. For spectra of metalloporphyrins alone, the same procedure was used without the addition of purified protein.

Inductively-coupled plasma mass spectrometry (ICP-MS) tracking. All Teflon tubes were incubated in 6 N HCl for 2 weeks and then washed at least 5 times with deionized water to remove all metals. Overnight cultures of *S. aureus* grown in iron-replete TSB or iron-deplete TSB (1 mM dip) media were washed and normalized by optical density (OD). Bacteria were then subcultured into iron-replete or iron-deplete media containing Ga-PPIX (2.0 μg/mL) and were incubated at 37°C for 4 hours. The cultures were then

normalized and pelleted. The supernatants were removed and concentrated at room temperature in Teflon tubes. The pellets were then washed three times in TBS and transferred to flat-bottom Teflon tubes. The cell wall was removed by lysostaphin (0.1 mg) treatment in TSM, followed by pelleting. The cell wall fraction (supernatant) was transferred to Teflon tubes while the pellets were resuspended in TBS and sonicated, followed by ultracentrifugation (100,000 x g) for 1 hour. The cytoplasmic fractions (supernatant) were transferred to clean Teflon tubes and the membrane fractions (pellets) were resuspended in TBS. Nitric acid (1 mL, Optima) and hydrogen peroxide (100 μL) were added to each Teflon tube and samples were boiled at 130°C until dry. Dried samples were sent for analysis by ICP-MS.

Growth analysis and lactate production. Overnight cultures of *S. aureus* were subcultured in triplicate (1:100) into TSB supplemented with Ga-PPIX (0, 0.1, 1, 10 μM). For aerobic growth, cultures were inoculated into 50 mL TSB in 250 mL flasks. For anaerobic growth, bacteria were inoculated into 5 mL TSB in 6–well plates and incubated with Anaero*Gen* (Oxoid Ltd, England) compact atmosphere generating pouches. Growth was measured after 24 hours by optical density (OD) at 600 nm using a Cary 50 MPR microplate reader coupled to the Varian Cary 50-BIO UV-visible spectrophotometer. Following incubation, the cultures were pelleted and supernatants were collected. Lactate was measured using the Lactate Assay Kit (University at Buffalo) according to manufacturer's instructions. Cultures exposed to 10 μM heme did not grow well enough to analyze the lactate concentration of the supernatants.

Results

Exogenously acquired heme can be visualized by electron microscopy.

In an attempt to visually track the subcellular localization of exogenously acquired heme, I grew *S. aureus* to stationary phase and then prepared samples for sectioning and staining at the Vanderbilt Electron Microscopy (EM) core. *S. aureus* grown in iron-rich medium appear normal with electron-dense regions near the center of the cells, likely representing nucleoid material (data not shown). However, *S. aureus* grown in iron-deplete medium supplemented with heme exhibit striking electron-dense foci near the periphery of the cells (Figure 20). The foci are not due to the iron chelator, as cells grown in iron-deplete medium alone appear identical to bacteria grown in iron-rich conditions (data not shown). Based on these observations, we conclude that these are heme-dependent foci localized near the plasma membrane. We hypothesize that these foci represent an accumulation of exogenously acquired heme that is specifically trafficked to membrane-localized proteins.

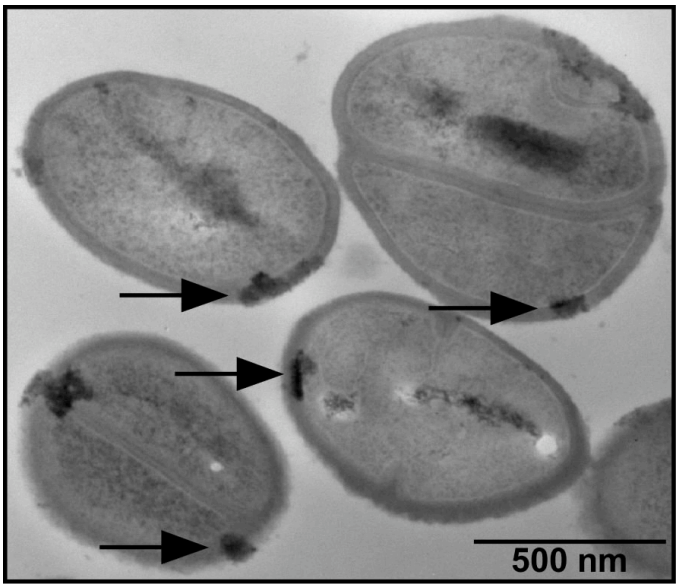

Figure 20. Transmission electron microscopy of *S. aureus* grown in the presence of heme. Wild type *S. aureus* was grown overnight in iron-deplete media containing heme. Arrows point to electron-dense foci that are specific to bacteria grown in heme.

Non-iron metalloporphyrins remain intact in *S. aureus*

Non-iron metalloporphyrins are comprised of the same tetrapyrrole as heme, with a substitution for the central coordinated metal. A seminal paper by Igor Stojiljkovic and colleagues demonstrated a potent antibacterial effect of non-iron metalloporphyrins against pathogenic bacteria, including several multi-drug resistant clinical isolates of *S. aureus* (102). It was hypothesized that these heme-like molecules act as ‘‘molecular Trojan horses’’ that enter bacteria through heme transport systems where they then exert their antibacterial effect in the cytoplasm or membrane (102). The potent antibacterial effect of metalloporphyrins suggests that these molecules target vital cellular processes inside the bacteria, which may represent novel therapeutic targets against *S. aureus* infection. Additionally, due to their similarity to heme, we hypothesized that metalloporphyrins may be useful as surrogates for heme trafficking. To this end, we first sought to determine if these heme-like molecules can be degraded inside the cell by the heme oxygenases IsdG and IsdI.

In vitro metalloporphyrin binding experiments were performed with equimolar concentrations of heme oxygenase and metalloporphyrin. We tested several toxic metalloporphyrins, including gallium protoporphyrin IX (Ga-PPIX), manganese protoporphyrin IX (Mn-PPIX), and zinc protoporphyrin IX (Zn-PPIX), as well as the non-toxic compound cobalt protoporphyrin IX (Co-PPIX) (102). As previously reported, we found that purified recombinant IsdG and IsdI rapidly degrade heme (Fe-PPIX) in the presence of electron donor (Figure 21A). In contrast, neither enzyme was able to degrade any of the non-iron metalloporphyrins tested (Figure 21B-E). This lack of activity was despite the fact that all of these metalloporphyrins are bound by IsdG and IsdI as evidenced by alterations in the visible absorption spectra upon co-incubation of enzyme with metalloporphyrin. Notably, Co-PPIX, Ga-PPIX, and Zn-PPIX undergo spectral changes upon exposure to ascorbate, and these changes are inhibited by complex

formation with IsdG or IsdI. Taken together, these results demonstrate that despite the fact that IsdG and IsdI complex non-iron metalloporphyrins *in vitro*, the catabolic activity of IsdG and IsdI is specific for Fe-PPIX. Therefore, the antibacterial effect of non-iron metalloporphyrins is not due to the released metal ion upon tetrapyrrole cleavage, but rather, due to an effect of the intact metalloporphyrin.

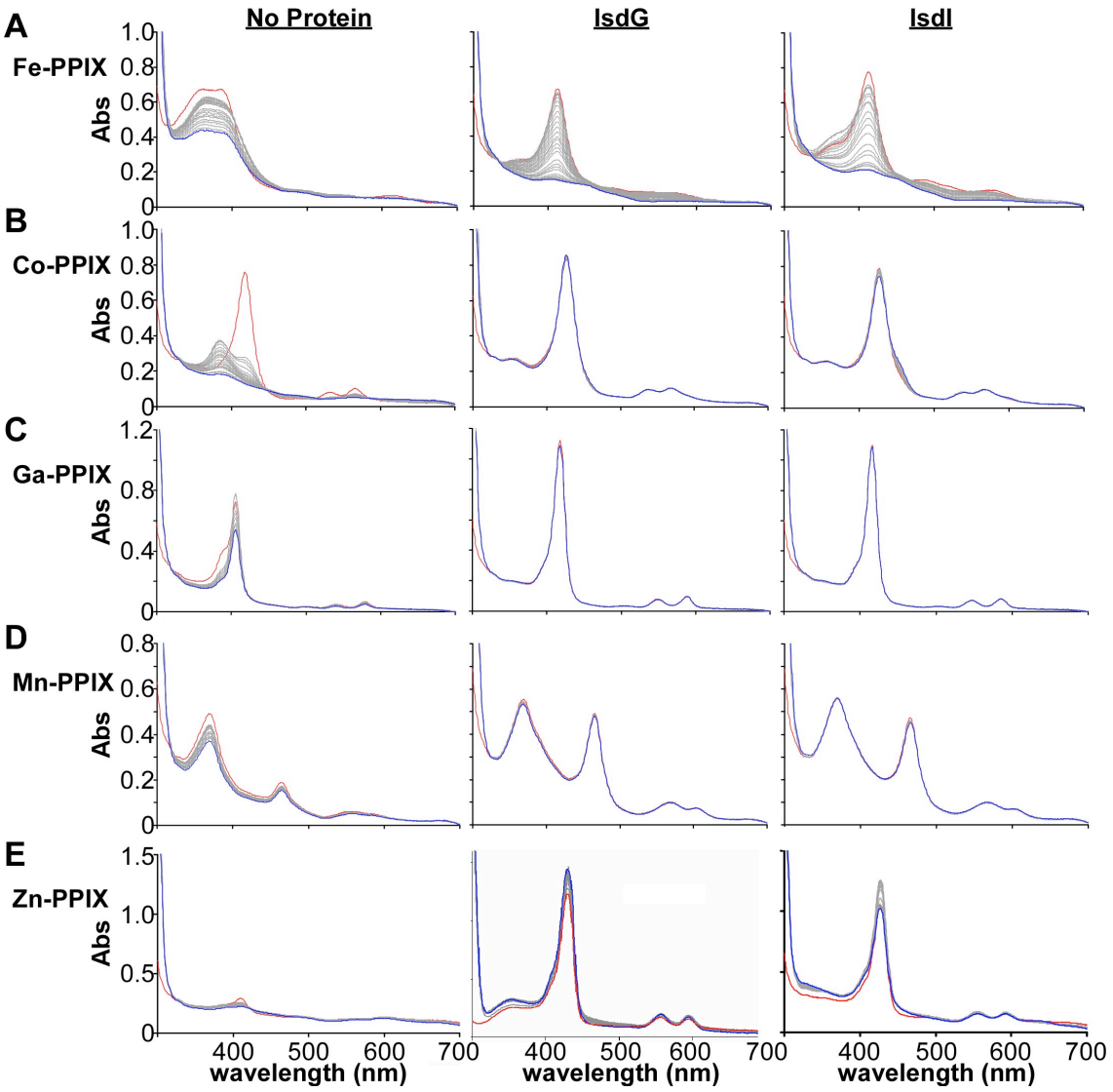

Figure 21. Binding of non-iron metalloporphyrins by IsdG and IsdI. *In vitro* enzymatic degradation of several metalloporphyrins was analyzed via UV-visible spectrophotometry. IsdG- and IsdI-mediated degradation of Fe-PPIX (**A**), Co-PPIX (**B**), Ga-PPIX (**C**), Mn-PPIX (**D**), and Zn-PPIX (**E**) was analyzed after addition of ascorbate as an electron donor. Red lines indicate absorbance (Abs) before addition of electron donor. Blue lines indicate absorbance after 90 minutes in the presence of ascorbate. Adapted from Lee et al. 2008 (53).

Ga-PPIX is specifically trafficked to the plasma membrane.

The metalloporphyrin degradation assay suggests that non-iron metalloporphyrins may be useful as surrogate molecules for tracking the subcellular localization of intact heme. We chose Ga-PPIX for this analysis because, unlike iron, cobalt, manganese, and zinc, gallium is not found in nature at detectable levels, making the background of our experiment minimal.

We have previously shown that heme is specifically segregated to the membrane when *S. aureus* is grown under iron-replete conditions (97). To determine if Ga-PPIX trafficking mimics that of heme, we utilized inductively-coupled plasma mass spectrometry (ICP-MS) to track the gallium atom of the non-iron metalloporphyrin Ga-PPIX. ICP-MS is a highly sensitive technique that is capable of quantifying atoms in a complex mixture at concentrations as low as one part per trillion. Specifically, *S. aureus* was grown in iron-restricted media supplemented with either Ga-PPIX or gallium salt $Ga(NO_3)_3$. Cells were divided into cell wall, membrane, and cytoplasmic fractions and were analyzed by ICP-MS in order to determine the quantity of gallium in each fraction. We found significantly more gallium in whole cell *S. aureus* grown in Ga-PPIX than in bacteria grown in gallium salt (15.9% versus 4.5% of the media gallium content), although quantities of gallium added to the media prior to bacterial growth are similar (Figure 22A). This supports the hypothesis that *S. aureus* actively imports the non-iron metalloporphyrin similarly to heme under iron-restricted conditions. Furthermore, the majority of the gallium from Ga-PPIX localizes to the membrane fraction (52%), whereas the majority of gallium from the salt localizes to the cell wall (Figure 22B). From these results we conclude that Ga-PPIX is actively acquired and preferentially sorted to the plasma membrane.

A

Sample	Total Ga (ng) [Ga Atoms/CFU]
Media	34.8
Media + Ga-PPIX	1080
Media + $Ga(NO_3)_3$	881
S. aureus	12.7
S. aureus + Ga-PPIX	171.5 [619,664]
S. aureus + $Ga(NO_3)_3$	39.8 [35,936]

B

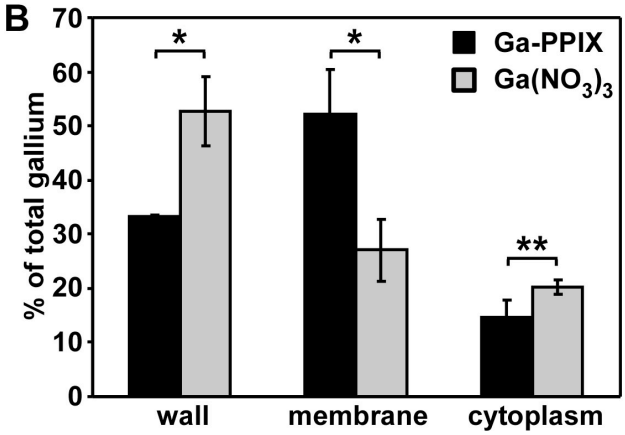

Figure 22. ICP-MS tracking of Ga-PPIX. A. Quantification of gallium atoms in media and whole cell *S. aureus*, as determined by ICP-MS analysis. **B.** Percentage of total gallium in each fraction. Error bars represent the standard deviation of three independent samples. Asterisks represent statistically significant differences between Ga-PPIX and $Ga(NO_3)_3$ localization, as determined by Student's *t* test (* $p < 0.02$, ** $p < 0.05$).

Ga-PPIX toxicity is dependent on aerobicity.

The antibacterial activity of several metalloporphyrins has been established, although the mechanism of toxicity is not yet understood (102). In an effort to determine the mechanism of Ga-PPIX toxicity, I analyzed the growth of *S. aureus* in iron-deplete medium supplemented with various concentrations of Ga-PPIX. As expected, Ga-PPIX inhibits *S. aureus* growth in a dose-dependent manner (data not shown). It was previously demonstrated that anaerobically grown *E. coli* are resistant to non-iron metalloporphyrins, suggesting that these compounds are only toxic to actively respiring bacteria (102). To test the susceptibility of anaerobic *S. aureus* to Ga-PPIX, bacteria were grown in iron-deplete medium supplemented with Ga-PPIX in well-aerated flasks or anaerobic cultures. Ga-PPIX inhibits *S. aureus* growth in aerobic conditions significantly more than when grown anaerobically (Figure 23A). However, unlike *E. coli*, anaerobic *S. aureus* is not fully resistant to Ga-PPIX, suggesting that the mechanism of Ga-PPIX toxicity may be different between the two bacteria.

Ga-PPIX is preferentially sorted to the plasma membrane and exerts greater toxicity when *S. aureus* is actively respiring. Therefore we hypothesized that Ga-PPIX is incorporated into membrane-localized cytochromes in place of heme. Gallium lacks the redox potential of iron, consequently the incorporation of Ga-PPIX would be expected to disrupt electron transport during respiration. The disruption of respiration may lead to an accumulation of reactive oxygen species and the observed toxicity. To circumvent this, *S. aureus* is capable of switching to fermentative metabolism. Fermentation leads to the accumulation of lactate and minor amounts of pyruvate, acetate, and acetoin (105). To test the hypothesis that Ga-PPIX inhibits respiration, I measured the lactate produced from overnight cultures of *S. aureus* grown aerobically or anaerobically in the presence of Ga-PPIX. As expected, *S. aureus* produces significantly more lactate when grown in an anaerobic environment as compared to bacteria grown aerobically (Figure 23B). In

support of our hypothesis, I observed that *S. aureus* grown in an aerobic environment increases lactate production in a dose-dependent manner when exposed to Ga-PPIX (Figure 23B). These results indicate that Ga-PPIX induces *S. aureus* to undergo fermentative metabolism, suggesting that the antibacterial effect of Ga-PPIX may be due to inhibition of respiration.

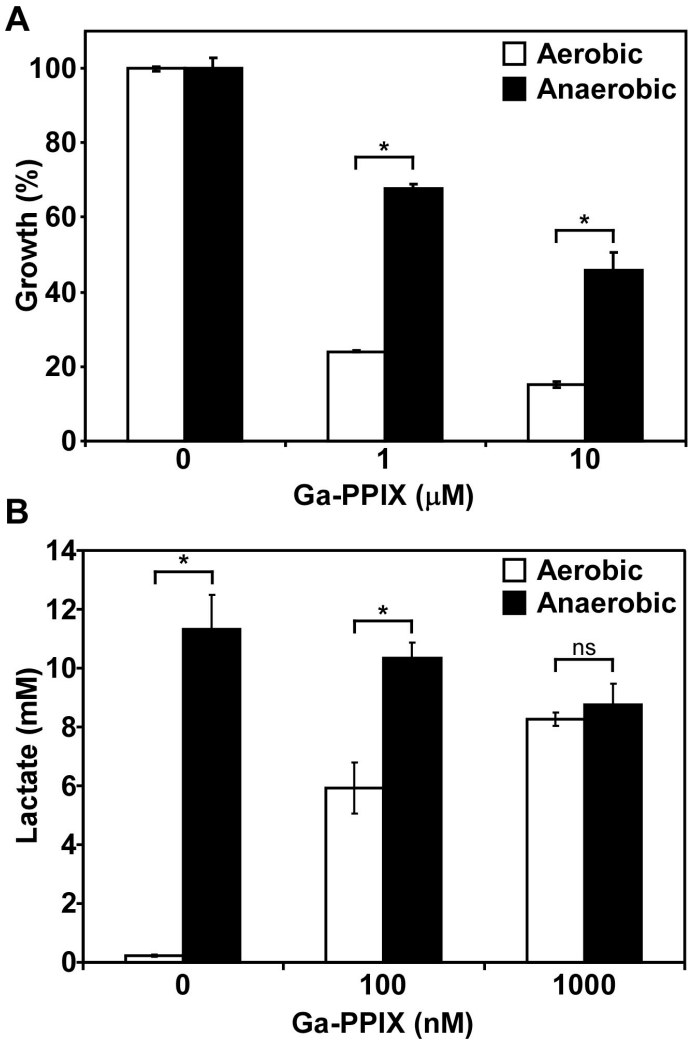

Figure 23. Ga-PPIX toxicity is dependent on aerobicity. A. *S. aureus* growth in Ga-PPIX is graphed as a percentage of growth in the absence of Ga-PPIX. **B.** The lactate concentration of supernatants from overnight cultures of *S. aureus* was measured. Asterisks indicate statistically significant differences between aerobic and anaerobic conditions, as measured by Student's *t* test (*$p < 0.01$; ns, $p > 0.3$).

Discussion

It is now established that many bacterial pathogens, including *S. aureus*, import and degrade host heme for use as a nutrient iron source (29, 98). Data is now beginning to emerge indicating that the fate of heme inside the cell is multifaceted, although the mechanisms of intracellular heme trafficking are poorly understood. Endogenous heme synthesis, intracellular heme degradation, and non-heme iron stores make tracking exogenously acquired heme inside the cell technically difficult. To this end, I have demonstrated that the non-iron metalloporphyrin Ga-PPIX is a viable surrogate molecule for heme tracking. Moreover, IsdG and IsdI are incapable of degrading non-iron metalloporphyrins such as Ga-PPIX, enabling us to specifically localize the intact porphyrin (Figure 21).

S. aureus is known to segregate exogenously acquired heme to the plasma membrane (97). I have demonstrated that under similar conditions the heme analogue Ga-PPIX is actively imported and sorted to the plasma membrane. This is in contrast to $Ga(NO_3)_3$ which enters the cell passively, as evidenced by the low amount of intracellular gallium and its localization to the cell wall (Figure 22). These results establish Ga-PPIX as a valuable laboratory tool for investigating the intracellular fate of intact heme.

In addition to the laboratory setting, it has been shown that metalloporphyrins may have utility in the clinic. In a mouse model of burn wound infection, topical application of a heme-deuterophorphyrin mixture reduced bacterial loads by over 99.9% in only one application (68). Moreover, Stojiljkovic and colleagues demonstrated that the viability of human primary fibroblasts was unaffected when exposed to Ga-PPIX at concentrations up to 50-times the MIC of *S. aureus* (102). Combined, these results indicate that metalloporphyrins may be viable therapeutics. However, the mechanism of

their antibacterial activity is not yet understood. In order to develop metalloporphyrins for the clinic it is imperative that we understand their mode of action inside the cell. To this end I have shown that *S. aureus* grown anaerobically is more resistant to Ga-PPIX than aerobically respiring cultures (Figure 23A), indicating that Ga-PPIX may be poisoning a component of aerobic respiration. Considering the structural similarity to heme, we hypothesized that Ga-PPIX may be erroneously incorporated into heme-binding proteins, such as cytochromes. Exposure to Ga-PPIX increases lactate production in aerobically respiring cultures, indicating that Ga-PPIX induces *S. aureus* to switch to fermentative metabolism (Figure 23B). Combined, these data suggest that Ga-PPIX is incorporated into membrane-associated cytochromes in the place of heme. Unlike iron, which commonly exists in the +2 or +3 oxidation states, gallium has one valence state and only exists as Ga^{+3}. Therefore, Ga-PPIX does not have the same oxidation potential as heme, which could inhibit cytochrome-mediated electron transport, resulting in the over-production of oxidative radicals and observed toxicity. However, *S. aureus* is not fully resistant to Ga-PPIX when grown anaerobically (Figure 23B), suggesting that the mechanism of Ga-PPIX toxicity is more complicated than simply blocking aerobic respiration through cytochrome inactivation. Further research is needed to investigate the mechanism of Ga-PPIX toxicity in bacteria.

Herein I have defined the subcellular localization of the non-iron metalloporphyrin Ga-PPIX and demonstrated its value as a surrogate for heme trafficking. Additionally, I have demonstrated that exogenously acquired heme can be visualized by EM. Combined, these techniques are valuable tools to further elucidate the localization of exogenously acquired heme inside *S. aureus*. Considering the requirement for heme during staphylococcal pathogenesis, understanding the fate of intact heme may lead to the development of novel therapeutics.

CHAPTER VI

CONCLUSIONS

Summary

Most bacterial pathogens require iron to be infectious and *Staphylococcus aureus* is no exception (74). However, the neutral pH found within a vertebrate host renders iron insoluble (8). Moreover, host iron-binding proteins such as hemoproteins, lactoferrin, transferrin, and ferritin are present in sufficient quantities to bind virtually all available iron (117). In order to acquire iron during infection bacteria must overcome these host sequestration techniques known as nutritional immunity (117). The majority (80%) of iron in the human body is found as a component of the tetrapyrrolic molecule heme (8). Heme is a cofactor in many proteins, the most abundant of which is the oxygen transport protein hemoglobin, found within circulating erythrocytes. *S. aureus* is capable of utilizing hemoglobin as an iron source, a process which is dependent upon expression of proteins of the iron-regulated surface determinant (Isd) system (108). It is modeled that upon erythrocyte lysis by staphylococcal hemolysins, hemoglobin is released at the site of infection. The *S. aureus* Isd machinery then binds hemoglobin, removes the heme cofactor, and traffics heme into the cytoplasm (98). In order to utilize heme as an iron source the porphyrin ring must be cleaved to release nutrient iron. To this end, the cytoplasmic proteins of the Isd system, IsdG and IsdI, catalytically degrade heme, releasing free iron (96).

Although heme-iron acquisition is vital for staphylococcal pathogenesis (97, 108), the intracellular components of this process have not been examined. More specifically, the requirement for two heme-degrading enzymes has not been investigated and the

role of heme degradation in pathogenesis remains undefined. I have demonstrated that IsdG and IsdI are each required for *S. aureus* growth on heme as a sole iron source (Chapter II). The observation that both single heme oxygenase mutants are impaired for growth on heme indicates that IsdG and IsdI are not functionally redundant enzymes. In fact, I have established that IsdG and IsdI are differentially regulated depending upon the microenvironment encountered by the bacterium. In low iron environments Fur-mediated repression is released and both *isdG* and *isdI* are transcribed. IsdG is additionally regulated post-transcriptionally by heme. Therefore, IsdI is most abundantly expressed in iron-deplete environments, while IsdG levels are maximal in low iron conditions containing heme. These observations provide insight into the basis for two paralogous enzymes in *S. aureus* with seemingly identical functions (Chapter II). We hypothesize that this differential regulation allows *S. aureus* to rapidly adapt to the microenvironment it encounters during infection.

Accordingly, we have demonstrated that IsdG and IsdI are each required for full staphylococcal pathogenesis during systemic infection. While both *isdG* and *isdI* mutants are impaired for colonization of the hearts of infected animals, only the *isdG* mutant is defective at colonizing the kidneys. This organ-specific phenotype is not yet understood; however, we hypothesize that the variability in iron and heme concentrations in each organ may dictate the differential requirement for IsdG and IsdI during infection. The observed decrease in the virulence of staphylococcal strains lacking IsdG and IsdI suggests that these enzymes are expressed and functional during a wild type infection. To this end, I have utilized a luminescent transcriptional reporter system (IVIS) to demonstrate that *isdI* is expressed *in vivo* during staphylococcal pathogenesis (Chapter II). Moreover, the co-localization of luminescence with sites of abscess formation in the livers and kidneys of infected animals indicates that abscesses are iron-starved microenvironments. Although *isdG* and *isdI* mutants are not impaired at colonizing the

liver of infected animals, IVIS data indicate that the hepatic abscesses are iron-starved environments. The liver is the iron storage organ in vertebrates; therefore, we hypothesize that non-heme iron sources can be readily obtained, rendering heme oxygenase activity dispensable for colonization of the liver. According to the model proposed above, hepatic abscesses may be an example of an iron-deplete environment in which Fur-mediated transcriptional repression is released and *isdG* and *isdI* are transcribed. However due to the lack of heme, IsdG is not required and is therefore degraded. Notably, these experiments are the first to demonstrate a requirement for bacterial heme oxygenases in pathogenesis and establish the staphylococcal abscess as an iron-starved microenvironment.

Our results reveal that IsdG and IsdI are required for staphylococcal pathogenesis and suggest that the differential regulation of these enzymes is important during infection. The regulated synthesis of proteins is widely accepted as a mechanism by which bacteria can adapt to their surroundings; however, targeted proteolysis is only beginning to be recognized as an equally important adaptive strategy (42). Although seemingly a drastic solution, the targeted destruction of proteins allows the bacterium to adapt rapidly to the changing environment (37). The mechanism by which staphylococcal proteases specifically recognize and degrade cellular proteins is not well understood.

To more precisely define the role for heme oxygenase activity *in vivo*, we sought to elucidate the mechanism of IsdG degradation (Chapter III). I have demonstrated that ATP is required for IsdG degradation, indicating a role for ATP-dependent proteases in the regulation of IsdG. Moreover, the flexible loop region encompassing amino acids 82-88 is required for IsdG degradation. These results suggest that the flexible loop may be recognized by cellular proteases that specifically degrade IsdG in the absence of heme. Alternatively, a distinct motif of IsdG may be recognized by proteolytic machinery, which

cleaves IsdG at the flexible loop. Further research is needed to determine how IsdG is targeted and degraded. Importantly, the high degree of structural and sequence similarity between IsdG and IsdI provides an amenable system for analysis of proteolytic substrate specificity in *S. aureus*.

Heme oxygenases are ubiquitous enzymes in nature and are highly conserved from humans to plants and bacteria. All previously identified bacterial heme oxygenases are structurally similar to human heme oxygenase 1 (HO-1) (29, 120). Heme catabolism by the HO-1 family has been studied extensively in both bacteria and vertebrates and the mechanism of heme degradation proceeds similarly across all heme oxygenases, resulting in the production of α-biliverdin (110). IsdG and IsdI represent the founding members of the novel IsdG-family of heme oxygenases (81, 125). Due to the unique three-dimensional structure and mode of heme binding by IsdG-like enzymes, it has been hypothesized that this new family of heme oxygenases degrades heme by a distinct mechanism. Here, we demonstrate that IsdG and IsdI degrade heme to a mixture of β- and δ-oxo-bilirubin isomers, which we have collectively named staphylobilins (Chapter IV).

Staphylobilin is a novel heme catabolite that has not been previously observed or characterized. Staphylobilin differs from the canonical heme degradation product biliverdin in several ways. First, the vast majority of HO-1-like exclusively cleave the tetrapyrrole ring at the α-*meso* carbon. The single exception in bacteria is PigA from *Pseudomonas aeruginosa*, which produces a mixture of biliverdin isomers (79). Unlike the HO-1 family, IsdG and IsdI cleave the porphyrin ring at the β- or δ-*meso* carbon, presumably dependent upon the orientation of molecular oxygen in the active site. Moreover, all HO-1-like enzymes produce biliverdin, which is then converted to bilirubin in mammals by biliverdin reductase. The IsdG-family degrades heme directly to a

bilirubin-like molecule with the addition of a carbonyl group at the β- or δ-bridge. Considering the important roles of biliverdin and bilirubin within vertebrate cells, it is likely that staphylobilins may have important functions within bacterial pathogens, such as *S. aureus*. This is particularly intriguing considering the varying production of β- and δ-isomers by IsdG and IsdI. It is possible that each isomer of staphylobilin is utilized under distinct environmental conditions, a requirement mediated by the differential regulation of IsdG and IsdI.

In addition to its value as an iron source, heme is potentially valuable to *S. aureus* in its intact form. This is due to the requirement for heme as a cofactor in many bacterial proteins and the thermodynamic advantage of importing host heme, rather than synthesizing heme *de novo*. Accordingly, it has been established that exogenously acquired heme is preferentially acquired and segregated to the plasma membrane (97); however, the intracellular fate of intact heme is unknown. To this end I have established Ga-PPIX as a useful tool for tracking subcellular heme localization (Chapter V). Non-iron metalloporphyrins, including Ga-PPIX, are not degraded by the heme oxygenases IsdG and IsdI. Therefore, these molecules are viable surrogates for intact heme. Similarly to heme, Ga-PPIX is preferentially sorted to the staphylococcal membrane. Our current model predicts that Ga-PPIX exerts its antibacterial effect at the membrane by binding to cytochromes in place of heme and disrupting electron transport. Although anaerobically grown *S. aureus* is not entirely resistant to Ga-PPIX, indicating that the mechanism of toxicity may be more complex than simply inhibiting respiration. Further research is necessary to elucidate the mechanism of Ga-PPIX toxicity in this bacterium.

Future Directions

Determine the impact of IsdG degradation on pathogenesis.

IsdG and IsdI are differentially regulated depending upon the microenvironment encountered by *S. aureus*. Accordingly, mutants lacking either *isdG* or *isdI* display distinct virulence defects, demonstrating that they are differentially required during pathogenesis. Specifically, the *isdG*-deficient strain exhibits a more pronounced defect in the hearts and kidneys of infected animals. Therefore, we hypothesize that the heme-dependent stability of IsdG may be required for efficient staphylococcal pathogenesis.

To test this hypothesis, the flexible loop sequence of IsdG will be mutated in the chromosome to that of the IsdI loop sequence ($IsdG_{loop*}$). I have demonstrated that the flexible loop is required for IsdG degradation in the absence of heme (Chapter III). Therefore, it is expected that IsdG will be stable in this mutant, independently of heme. This mutation may render *S. aureus* less virulent, as it will not be able to fine-tune the abundance of IsdG in order to quickly adapt to its environment. Moreover, I have shown that non-degraded heme is preferentially sorted to the plasma membrane where it is likely incorporated into bacterial cytochromes (Chapter V). The $IsdG_{loop*}$ mutant will presumably have less non-degraded heme in the cytoplasm due to the over-abundance of heme oxygenase activity, and may therefore have altered cytochrome function. Alternatively, the $IsdG_{loop*}$ mutant may not exhibit a virulence defect. The vertebrate host is an iron-starved environment rich in heme and a mutation that renders *S. aureus* more efficient at heme degradation may give the bacterium a pathogenic advantage. However, this benefit would be expected to come at the cost of maximal growth in low-heme environments. Results from this experiment will provide further insight into the role of heme degradation in pathogenesis and the requirement for two heme oxygenases in *S. aureus*.

Identify the minimum region necessary to target a protein for degradation.

The regulated degradation of intracellular proteins is a critical component of the bacterial life cycle. In order to remove damaged, misfolded, or unnecessary proteins the bacterium must have a means of identifying these potentially toxic proteins. Several recognition sequences are known in *E. coli* and these are assumed to be consistent in other bacteria; however, few have been tested in *S. aureus*. I have demonstrated that the flexible loop sequence is required for IsdG degradation but is not sufficient to target a protein for degradation. I hypothesize that the flexible loop is the site of proteolytic cleavage, but the recognition motif that targets IsdG for degradation is located at a distinct site on the protein.

In order to identify the region of IsdG that is recognized for degradation, I have made a panel of chimeric proteins that contain regions of both IsdG and IsdI sequence (Figure 24). All chimeras have been expressed and purified from *E. coli* and the heme binding and degradation were found to be similar to wild type IsdG and IsdI. Pulse-chase analyses will be performed and the chimera(s) with heme-dependent stability will be identified. It is expected that chimeras containing the flexible loop sequence of IsdG will exhibit heme-dependent stability if they also contain the recognition motif. From these experiments we will be able to further define the mechanism by which IsdG is targeted for degradation and may be able to utilize the recognition motif to identify other protease substrates.

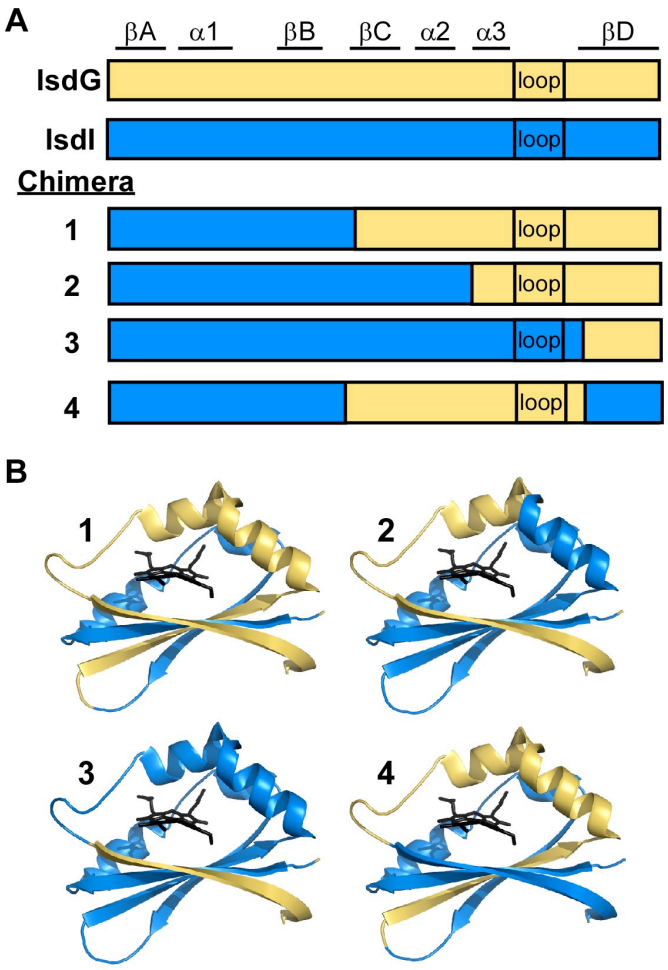

Figure 24. IsdG and IsdI chimeras. A. Schematic of IsdG, IsdI, and chimeric proteins. Secondary structural elements are indicated. **B.** Three-dimensional crystal structures of IsdG bound to heme (black), color-coded to indicate the portions of each chimera corresponding to IsdG (yellow) or IsdI (blue) sequence.

Identify the protease(s) responsible for IsdG degradation.

IsdG degradation is ATP- and heme-dependent, suggesting that under specific conditions IsdG is targeted for degradation by an ATP-dependent intracellular protease (Chapter IIII). To date, the majority of work on bacterial intracellular proteases has focused on the model Gram negative bacterium *E. coli*, which expresses four classes of cytoplasmic proteases: serine proteases ClpP, HslV and Lon, and the metalloprotease FtsH (36). Of these, *S. aureus* expresses proteins with homology to ClpP, HslV, and FtsH; no staphylococcal Lon homologue has been identified (Table 4) (31, 32, 55).

The Clp (caseinolytic protease) family of serine proteases is ubiquitous in bacteria and is the best characterized intracellular protease family. ClpP and HslV (also named ClpQ) are peptidase subunits that associate with ATPase subunits to form holo-proteolytic complexes. Staphylococcal ClpP can associate with ClpC or ClpX while HslV only complexes with HslU (30, 32). It is not yet known if the Clp ATPases ClpB and ClpL can interact with ClpP (30). Although Clp ATPases are ubiquitous in bacteria, the number and type vary, suggesting some degree of functional redundancy. *S. aureus* mutants lacking *clpP* or an ATPase component exhibit defects in stress tolerance, biofilm formation, and defective regulation of virulence factors (30, 31). Conversely, a *S. aureus hslUV* mutant is only impaired for growth at very high temperatures, but is fully capable of adapting to other stressors (32). The mechanism by which these serine proteases mediate these effects is not well understood.

FtsH (named for its filamentous temperature-sensitive phenotype in *E. coli*) is a membrane-bound ATP- and Zn^{2+}-dependent metalloprotease that contains both an ATPase domain and a proteolytic domain. FtsH is known to degrade both cytoplasmic and integral membrane proteins (43). A *S. aureus ftsH* mutant exhibits reduced viability under starvation conditions, slower growth, and increased sensitivity to multiple

stressors (55). However, no staphylococcal FtsH substrates have been identified and the biochemical properties of this protease have not been examined.

In order to identify the protease(s) responsible for IsdG degradation I have constructed deletion strains of *hslUV* and *ftsH*. The *clpP* deletion strain in the Newman background was a gift from Hanne Ingmer at the University of Copenhagen (Table 4). I plan to test the stability of IsdG in each of these protease-deficient strains by pulse-chase analysis. ATPase subunits recognize, unfold, and translocate substrates into the active site of the proteolytic subunit. If the *clpP* mutant is unable to degrade IsdG similarly to wild type, I plan to test IsdG stability in strains lacking individual ATPases to determine which ATPase subunit is involved in recognizing IsdG. To this end, I am currently generating deletion strains of *clpB*, *clpC*, *clpL,* and *clpX* (Table 4). As ClpB and ClpL are functionally redundant, I also plan to generate strains lacking a combination of ATPases (30). These strains will be valuable for elucidating the mechanism of IsdG degradation in the absence of heme. Additionally, these strains will advance our understanding of regulated proteolysis in *S. aureus*. To date, studies on staphylococcal intracellular proteases have focused only on stress-induced pleiotropic effects and the regulation of a subset of virulence factors (30, 32, 55). These protease- and ATPase-deficient strains can be utilized for proteomic and transcriptional analyses to elucidate the molecular mechanism of protease regulation, substrate recognition, and degradation.

Table 4. ATP-dependent intracellular proteases in *S. aureus*

Gene	Name	Function	Deletion strain
NWMN_0473	*ftsH*	ATP- and Zn^{2+}-dependent metalloprotease	confirmed
NWMN_0487	*clpC*	ATP-binding subunit, associates with ClpP	in process
NWMN_0736	*clpP*	Proteolytic subunit, associates with ClpC and ClpX	received (31)
NWMN_0845	*clpB*	ATP-binding subunit	in process
NWMN_1163	*hslV*	Proteolytic subunit, associates with HslU	confirmed
NWMN_1164	*hslU*	ATP-binding subunit, associates with HslV	confirmed
NWMN_1568	*clpX*	ATP-binding subunit, associates with ClpP	in process
NWMN_2448	*clpL*	ATP-binding subunit	in process

According to our model, heme binds IsdG, altering its conformation such that it is no longer recognized as a substrate for proteolysis. However, it is also possible that exogenously acquired heme induces a general stress response in the cell which recruits cellular proteases to other substrates, resulting in increased IsdG stability (129). In this scenario, the recognition sequence that targets IsdG for degradation is unchanged but the cellular environment is altered, rendering IsdG more stable. Exhaustive attempts at creating IsdG point mutants that are incapable of binding heme have been unsuccessful. Therefore, I cannot directly test the effect of exogenous heme on IsdG stability when IsdG is not able to bind heme. To test the possibility that IsdG stabilization is a side-effect of heme toxicity, I plan to analyze the effect of the non-toxic heme analogue Co-PPIX on IsdG stability. This metalloporphyrin binds IsdG but does not induce toxicity, enabling us to separate the conformational change induced by porphyrin binding and the potential cellular stress caused by heme. Results from these experiments will further elucidate the mechanism of heme-dependent IsdG stability.

Determine the fate and function of staphylobilin

The products of mammalian heme degradation, iron, biliverdin, and carbon monoxide, have many important functions, some of which include immunomodulation and cytoprotection (47). Additionally, biliverdin is converted to bilirubin, the most potent antioxidant in the plasma (101). However no homologue of biliverdin reductase has been found in bacteria and the function of biliverdin in the cell is unknown. Although the mechanism of the IsdG-family of enzymes is not yet known, the reaction is thought to require nine electrons, two electrons more than canonical heme degradation that produces biliverdin. The extra energy required to produce staphylobilin indicates that it may have important functions in the cell. Unlike bilirubin, however, staphylobilin is not expected to have antioxidant properties due to the substitution of a carbonyl in place of

the hydrogen at the γ-bridge of bilirubin. Thus, the function of staphylobilin inside *S. aureus* is unknown.

In addition to the function of biliverdin and staphylobilin, there are many other aspects of bacterial heme degradation that are not well understood. *In vitro* experiments indicate that an additional factor is necessary *in vivo* to remove biliverdin or staphylobilin from the heme oxygenase active site. However, the identity and function of this hypothetical factor have not been uncovered. Moreover, unlike other bacterial heme oxygenases, recombinant IsdG and IsdI are purified from *E. coli* as apo-proteins. There are several possible reasons for this discrepancy: (i) the IsdG-family requires heme to be delivered to the heme oxygenase and the factor(s) that perform this task *in vivo* are not expressed in *E. coli*; (ii) the IsdG-family of heme oxygenases requires a different reducing environment to effectively bind heme than is found in the *E. coli* cytoplasm; (iii) the IsdG-family is capable of degrading heme in *E. coli* and the staphylobilin that is bound to the purified protein has not been detected. To answer these questions we plan to perform a bacterial-two-hybrid experiment to screen for proteins in the cell that interact with IsdG and/or IsdI. This experiment may identify proteins involved in transporting heme to the heme oxygenase, similarly to PhuS in *Pseudomonas aeruginosa*, which delivers heme to the heme oxygenase PigA (52). It may also identify factors involved in trafficking staphylobilin away from IsdG or IsdI. It is also possible that the bacterial-two-hybrid system will identify protease components or chaperone proteins that recognize IsdG in the absence of heme.

An alternative approach is to directly select for proteins that bind staphylobilin in the cell. To this end I plan to add ^{14}C-heme to *S. aureus* p*isdG* (*isdG* over-expression) or Δ*isdGI* and separate proteins of the cell wall, membrane, and cytoplasmic fractions by electrophoresis. Radiolabeled proteins will be visualized using a phosphorimager and can be identified by tryptic digest and mass spectrometry of identical non-radiolabeled

samples. By comparing the bands found in samples from *S. aureus* p*isdG* but not in Δ*isdGI,* we may be able to identify proteins specifically bound to staphylobilin rather than intact heme. Further, I plan to purify staphylobilin in large quantities and add it to *S. aureus* Δ*isdGI* grown in various stress-inducing conditions to identify an environment in which staphylobilin production may benefit the cell. Results from these experiments have the potential to identify proteins that bind staphylobilin and discover growth conditions under which *S. aureus* requires staphylobilin. Combined, these studies will begin to elucidate the function of staphylobilin in the cell.

LIST OF PUBLICATIONS

Reniere ML, Torres VJ, and Skaar EP. 2007. Intracellular metalloporphyrin metabolism in *Staphylococcus aureus*. *Biometals* **20**(3-4): 333-345.

Palazzolo-Ballance AM, Reniere ML, Braughton KR, Sturdevant DE, Otto M, Kreiswirth BN, Skaar EP, and DeLeo FR. 2008. Neutrophil microbicides induce a pathogen survival response in community-associated methicillin-resistant *Staphylococcus aureus*. *J Immunol* **180**(1): 500-509.

Reniere ML and Skaar EP. 2008. *Staphylococcus aureus* haem oxygenases are differentially regulated by iron and haem. *Mol Microbiol* **69**(5): 1304-1315.

Lee WC, Reniere ML, Skaar EP, and Murphy ME. 2008. Ruffling of metalloporphyrins bound to IsdG and IsdI, two heme-degrading enzymes in *Staphylococcus aureus*. *J Biol Chem* **283**(45): 30957-30963.

Reniere ML, Pishchany G, and Skaar EP. 2010. Iron uptake in Staphylococci. *In* Iron Uptake and Homeostasis in Microorganisms. Caister Academic Press.

Reniere ML, Ukpabi GN, Harry SR, Stec DF, Krull R, Wright DW, Bachmann BO, Murphy ME, and Skaar EP. 2010. The IsdG-family of heme oxygenases degrades heme to a novel chromophore. *Mol Microbiol*. **In Press**.

BIBLIOGRAPHY

1. **Aguila, A., A. G. Herrera, D. Morrison, B. Cosgrove, A. Perojo, I. Montesinos, J. Perez, G. Sierra, C. G. Gemmell, and J. H. Brock.** 2001. Bacteriostatic activity of human lactoferrin against *Staphylococcus aureus* is a function of its iron-binding properties and is not influenced by antibiotic resistance. FEMS Immunol Med Microbiol **31:**145-52.

2. **Bachmair, A., D. Finley, and A. Varshavsky.** 1986. *In vivo* half-life of a protein is a function of its amino-terminal residue. Science **234:**179-86.

3. **Bae, T., and O. Schneewind.** 2006. Allelic replacement in *Staphylococcus aureus* with inducible counter-selection. Plasmid **55:**58-63.

4. **Barton Pai, A., M. P. Pai, J. Depczynski, C. R. McQuade, and R. C. Mercier.** 2006. Non-transferrin-bound iron is associated with enhanced *Staphylococcus aureus* growth in hemodialysis patients receiving intravenous iron sucrose. Am J Nephrol **26:**304-9.

5. **Bibb, L. A., C. A. Kunkle, and M. P. Schmitt.** 2007. The ChrA-ChrS and HrrA-HrrS signal transduction systems are required for activation of the *hmuO* promoter and repression of the *hemA* promoter in *Corynebacterium diphtheriae.* Infect Immun **75:**2421-31.

6. **Brotz-Oesterhelt, H., D. Beyer, H. P. Kroll, R. Endermann, C. Ladel, W. Schroeder, B. Hinzen, S. Raddatz, H. Paulsen, K. Henninger, J. E. Bandow, H. G. Sahl, and H. Labischinski.** 2005. Dysregulation of bacterial proteolytic machinery by a new class of antibiotics. Nat Med **11:**1082-7.

7. **Bubeck Wardenburg, J., W. A. Williams, and D. Missiakas.** 2006. Host defenses against *Staphylococcus aureus* infection require recognition of bacterial lipoproteins. Proc Natl Acad Sci U S A **103:**13831-6.

8. **Bullen, J., Griffiths, E. .** 1999. Iron and infection. Molecular, physiological and clinical aspects. John Wiley and Sons, New York.

9. **CDC.** 2007. HIV/AIDS Surveillance Report. **17**.

10. **Chen, Q., Huggins, M.T., Lightner, D.A., Norona, W., McDonagh, A.F.** 1999. Synthesis of a 10-oxo-bilirubin: Effects of the oxo group on conformation, transhepatic transport, and glucuronidation. Journal of the American Chemical Society **121:**9253-9264.

11. **Chen, X., W. C. Solomon, Y. Kang, F. Cerda-Maira, K. H. Darwin, and K. J. Walters.** 2009. Prokaryotic ubiquitin-like protein pup is intrinsically disordered. J Mol Biol **392:**208-17.

12. **Cheng, A. G., H. K. Kim, M. L. Burts, T. Krausz, O. Schneewind, and D. M. Missiakas.** 2009. Genetic requirements for *Staphylococcus aureus* abscess formation and persistence in host tissues. FASEB J **23:**3393-404.

13. **Chim, N., A. Iniguez, T. Q. Nguyen, and C. W. Goulding.** 2009. Unusual Diheme Conformation of the Heme-Degrading Protein from *Mycobacterium tuberculosis*. J Mol Biol.

14. **Chung, S. W., S. R. Hall, and M. A. Perrella.** 2009. Role of haem oxygenase-1 in microbial host defence. Cell Microbiol **11:**199-207.

15. **Clarke, S. R., and S. J. Foster.** 2008. IsdA protects *Staphylococcus aureus* against the bactericidal protease activity of apolactoferrin. Infect Immun **76:**1518-26.

16. **Clarke, S. R., M. D. Wiltshire, and S. J. Foster.** 2004. IsdA of *Staphylococcus aureus* is a broad spectrum, iron-regulated adhesin. Mol Microbiol **51:**1509-19.

17. **Cole, W. J., D. J. Chapman, and H. W. Siegelman.** 1968. The structure and properties of phycocyanobilin and related bilatrienes. Biochemistry **7:**2929-35.

18. **Coombs, G. S., R. C. Bergstrom, E. L. Madison, and D. R. Corey.** 1998. Directing sequence-specific proteolysis to new targets. The influence of loop size and target sequence on selective proteolysis by tissue-type plasminogen activator and urokinase-type plasminogen activator. J Biol Chem **273:**4323-8.

19. **Crichton, R.** 2001. Inorganic Biochemistry of Iron Metabolism: From Molecular Mechanisms to Clinical Consequences, vol. 2. John Wiley & Sons, Ltd., West Sussex, England.

20. **Darwin, K. H., S. Ehrt, J. C. Gutierrez-Ramos, N. Weich, and C. F. Nathan.** 2003. The proteasome of *Mycobacterium tuberculosis* is required for resistance to nitric oxide. Science **302:**1963-6.

21. **Drabkin, D.** 1951. Metabolism of the Hemin Chromoproteins. Physiological Reviews **31:**345-431.

22. **Dryla, A., B. Hoffmann, D. Gelbmann, C. Giefing, M. Hanner, A. Meinke, A. S. Anderson, W. Koppensteiner, R. Konrat, A. von Gabain, and E. Nagy.** 2007. High-affinity binding of the staphylococcal HarA protein to haptoglobin and hemoglobin involves a domain with an antiparallel eight-stranded beta-barrel fold. J Bacteriol **189:**254-64.

23. **Dunman, P. M., E. Murphy, S. Haney, D. Palacios, G. Tucker-Kellogg, S. Wu, E. L. Brown, R. J. Zagursky, D. Shlaes, and S. J. Projan.** 2001. Transcription profiling-based identification of *Staphylococcus aureus* genes regulated by the *agr* and/or *sarA* loci. J Bacteriol **183:**7341-53.

24. **Duthie, E. S., and L. L. Lorenz.** 1952. Staphylococcal coagulase; mode of action and antigenicity. J Gen Microbiol **6:**95-107.

25. **Escolar, L., J. Perez-Martin, and V. de Lorenzo.** 1999. Opening the iron box: transcriptional metalloregulation by the Fur protein. J Bacteriol **181:**6223-9.

26. **Evans, P.** 2006. Scaling and assessment of data quality. Acta Crystallographica Section D **62:**72-82.

27. **Foster, T. J.** 2005. Immune evasion by staphylococci. Nat Rev Microbiol **3:**948-58.

28. **Francis, K. P., D. Joh, C. Bellinger-Kawahara, M. J. Hawkinson, T. F. Purchio, and P. R. Contag.** 2000. Monitoring bioluminescent *Staphylococcus aureus* infections in living mice using a novel *luxABCDE* construct. Infect Immun **68:**3594-600.

29. **Frankenberg-Dinkel, N.** 2004. Bacterial heme oxygenases. Antioxid Redox Signal **6:**825-34.

30. **Frees, D., A. Chastanet, S. Qazi, K. Sorensen, P. Hill, T. Msadek, and H. Ingmer.** 2004. Clp ATPases are required for stress tolerance, intracellular replication and biofilm formation in *Staphylococcus aureus*. Mol Microbiol **54:**1445-62.

31. **Frees, D., S. N. Qazi, P. J. Hill, and H. Ingmer.** 2003. Alternative roles of ClpX and ClpP in *Staphylococcus aureus* stress tolerance and virulence. Mol Microbiol **48:**1565-78.

32. **Frees, D., L. E. Thomsen, and H. Ingmer.** 2005. *Staphylococcus aureus* ClpYQ plays a minor role in stress survival. Arch Microbiol **183:**286-91.

33. **Friedman, J., L. Lad, R. Deshmukh, H. Li, A. Wilks, and T. L. Poulos.** 2003. Crystal structures of the NO- and CO-bound heme oxygenase from *Neisseriae meningitidis*. Implications for O2 activation. J Biol Chem **278:**34654-9.

34. **Ganz, T.** 2003. Hepcidin, a key regulator of iron metabolism and mediator of anemia of inflammation. Blood **102:**783-8.

35. **Ganz, T.** 2009. Iron in innate immunity: starve the invaders. Curr Opin Immunol **21:**63-7.

36. **Gottesman, S.** 1996. Proteases and their targets in *Escherichia coli.* Annu Rev Genet **30:**465-506.

37. **Gottesman, S., and M. R. Maurizi.** 1992. Regulation by proteolysis: energy-dependent proteases and their targets. Microbiol Rev **56:**592-621.

38. **Grigg, J. C., C. L. Vermeiren, D. E. Heinrichs, and M. E. Murphy.** 2007. Heme coordination by *Staphylococcus aureus* IsdE. J Biol Chem **282:**28815-22.

39. **Guo, Y., G. Guo, X. Mao, W. Zhang, J. Xiao, W. Tong, T. Liu, B. Xiao, X. Liu, Y. Feng, and Q. Zou.** 2008. Functional identification of HugZ, a heme oxygenase from *Helicobacter pylori.* BMC Microbiol **8:**226.

40. **Haeusser, D. P., A. H. Lee, R. B. Weart, and P. A. Levin.** 2009. ClpX inhibits FtsZ assembly in a manner that does not require its ATP hydrolysis-dependent chaperone activity. J Bacteriol **191:**1986-91.

41. **Herron-Olson, L., J. R. Fitzgerald, J. M. Musser, and V. Kapur.** 2007. Molecular Correlates of Host Specialization in *Staphylococcus aureus.* PLoS ONE **2:**e1120.

42. **Ingmer, H., and L. Brondsted.** 2009. Proteases in bacterial pathogenesis. Res Microbiol **160:**704-10.

43. **Ito, K., and Y. Akiyama.** 2005. Cellular functions, mechanism of action, and regulation of FtsH protease. Annu Rev Microbiol **59:**211-31.

44. **Ji, G., R. C. Beavis, and R. P. Novick.** 1995. Cell density control of staphylococcal virulence mediated by an octapeptide pheromone. Proc Natl Acad Sci U S A **92:**12055-9.

45. **Jurado, R. L.** 1997. Iron, infections, and anemia of inflammation. Clin Infect Dis **25:**888-95.

46. **Kaplan, D., Navon, G.** 1982. Nuclear magnetic resonance studies of the conformatin of bilirubin and its derivatives in solution. J.C.S. Perkin II **10:**1374-1383.

47. **Kirkby, K. A., and C. A. Adin.** 2006. Products of heme oxygenase and their potential therapeutic applications. Am J Physiol Renal Physiol **290:**F563-71.

48. **Klevens, R. M., M. A. Morrison, J. Nadle, S. Petit, K. Gershman, S. Ray, L. H. Harrison, R. Lynfield, G. Dumyati, J. M. Townes, A. S. Craig, E. R. Zell, G. E. Fosheim, L. K. McDougal, R. B. Carey, and S. K. Fridkin.** 2007. Invasive methicillin-resistant *Staphylococcus aureus* infections in the United States. JAMA **298:**1763-71.

49. **Kloos, W.** 1997. Taxonomy and systematic of staphylococci indigenous to humans. Churchill Livingstone, New York.

50. **Kuehnert, M. J., D. Kruszon-Moran, H. A. Hill, G. McQuillan, S. K. McAllister, G. Fosheim, L. K. McDougal, J. Chaitram, B. Jensen, S. K. Fridkin, G. Killgore, and F. C. Tenover.** 2006. Prevalence of *Staphylococcus aureus* nasal colonization in the United States, 2001-2002. J Infect Dis **193:**172-9.

51. **Lad, L., J. Wang, H. Li, J. Friedman, B. Bhaskar, P. R. Ortiz de Montellano, and T. L. Poulos.** 2003. Crystal structures of the ferric, ferrous, and ferrous-NO forms of the Asp140Ala mutant of human heme oxygenase-1: catalytic implications. J Mol Biol **330:**527-38.

52. **Lansky, I. B., G. S. Lukat-Rodgers, D. Block, K. R. Rodgers, M. Ratliff, and A. Wilks.** 2006. The cytoplasmic heme-binding protein (PhuS) from the heme uptake system of *Pseudomonas aeruginosa* is an intracellular heme-trafficking protein to the delta-regioselective heme oxygenase. J Biol Chem **281:**13652-62.

53. **Lee, W. C., M. L. Reniere, E. P. Skaar, and M. E. Murphy.** 2008. Ruffling of metalloporphyrins bound to IsdG and IsdI, two heme-degrading enzymes in *Staphylococcus aureus*. J Biol Chem **283:**30957-63.

54. **Lies, M., and M. R. Maurizi.** 2008. Turnover of endogenous SsrA-tagged proteins mediated by ATP-dependent proteases in *Escherichia coli*. J Biol Chem **283:**22918-29.

55. **Lithgow, J. K., E. Ingham, and S. J. Foster.** 2004. Role of the *hprT-ftsH* locus in *Staphylococcus aureus*. Microbiology **150:**373-81.

56. **Marcelis, J. H., H. J. den Daas-Slagt, and J. A. Hoogkamp-Korstanje.** 1978. Iron requirement and chelator production of staphylococci, *Streptococcus faecalis* and enterobacteriaceae. Antonie Van Leeuwenhoek **44:**257-67.

57. **Marraffini, L. A., and O. Schneewind.** 2005. Anchor structure of staphylococcal surface proteins. V. Anchor structure of the sortase B substrate IsdC. J Biol Chem **280:**16263-71.

58. **Matsui, T., M. Furukawa, M. Unno, T. Tomita, and M. Ikeda-Saito.** 2005. Roles of distal Asp in heme oxygenase from *Corynebacterium diphtheriae*, HmuO: A water-driven oxygen activation mechanism. J Biol Chem **280:**2981-9.

59. **Mazmanian, S. K., E. P. Skaar, A. H. Gaspar, M. Humayun, P. Gornicki, J. Jelenska, A. Joachmiak, D. M. Missiakas, and O. Schneewind.** 2003. Passage of heme-iron across the envelope of *Staphylococcus aureus*. Science **299:**906-9.

60. **Menestrina, G., M. Dalla Serra, M. Comai, M. Coraiola, G. Viero, S. Werner, D. A. Colin, H. Monteil, and G. Prevost.** 2003. Ion channels and bacterial infection: the case of beta-barrel pore-forming protein toxins of *Staphylococcus aureus*. FEBS Lett **552:**54-60.

61. **Mense, S. M., and L. Zhang.** 2006. Heme: a versatile signaling molecule controlling the activities of diverse regulators ranging from transcription factors to MAP kinases. Cell Res **16:**681-92.

62. **Mogk, A., R. Schmidt, and B. Bukau.** 2007. The N-end rule pathway for regulated proteolysis: prokaryotic and eukaryotic strategies. Trends Cell Biol **17:**165-72.

63. **Morse, D., and A. M. Choi.** 2005. Heme oxygenase-1: from bench to bedside. Am J Respir Crit Care Med **172:**660-70.

64. **Murray, G. L., K. M. Ellis, M. Lo, and B. Adler.** 2008. *Leptospira interrogans* requires a functional heme oxygenase to scavenge iron from hemoglobin. Microbes Infect **10:**791-7.

65. **Muryoi, N., M. T. Tiedemann, M. Pluym, J. Cheung, D. E. Heinrichs, and M. J. Stillman.** 2008. Demonstration of the iron-regulated surface determinant (Isd) heme transfer pathway in *Staphylococcus aureus*. J Biol Chem **283:**28125-36.

66. **Narberhaus, F., M. Obrist, F. Fuhrer, and S. Langklotz.** 2009. Degradation of cytoplasmic substrates by FtsH, a membrane-anchored protease with many talents. Res Microbiol **160:**652-9.

67. **Ochsner, U. A., and M. L. Vasil.** 1996. Gene repression by the ferric uptake regulator in *Pseudomonas aeruginosa*: cycle selection of iron-regulated genes. Proc Natl Acad Sci U S A **93:**4409-14.

68. **Orenstein, A., D. Klein, J. Kopolovic, E. Winkler, Z. Malik, N. Keller, and Y. Nitzan.** 1997. The use of porphyrins for eradication of *Staphylococcus aureus* in burn wound infections. FEMS Immunol Med Microbiol **19:**307-14.

69. **Paiva-Silva, G. O., C. Cruz-Oliveira, E. S. Nakayasu, C. M. Maya-Monteiro, B. C. Dunkov, H. Masuda, I. C. Almeida, and P. L. Oliveira.** 2006. A heme-degradation pathway in a blood-sucking insect. Proc Natl Acad Sci U S A **103:**8030-5.

70. **Park, R. Y., H. Y. Sun, M. H. Choi, Y. H. Bai, and S. H. Shin.** 2005. *Staphylococcus aureus* siderophore-mediated iron-acquisition system plays a dominant and essential role in the utilization of transferrin-bound iron. J Microbiol **43:**183-90.

71. **Pearce, M. J., J. Mintseris, J. Ferreyra, S. P. Gygi, and K. H. Darwin.** 2008. Ubiquitin-like protein involved in the proteasome pathway of *Mycobacterium tuberculosis*. Science **322:**1104-7.

72. **Perkins-Balding, D., M. Ratliff-Griffin, and I. Stojiljkovic.** 2004. Iron transport systems in *Neisseria meningitidis*. Microbiol Mol Biol Rev **68:**154-71.

73. **Pilpa, R. M., S. A. Robson, V. A. Villareal, M. L. Wong, M. Phillips, and R. T. Clubb.** 2009. Functionally distinct NEAT (NEAr Transporter) domains within the *Staphylococcus aureus* IsdH/HarA protein extract heme from methemoglobin. J Biol Chem **284:**1166-76.

74. **Posey, J. E., and F. C. Gherardini.** 2000. Lack of a role for iron in the Lyme disease pathogen. Science **288:**1651-3.

75. **Potterton, E., P. Briggs, M. Turkenburg, and E. Dodson.** 2003. A graphical user interface to the CCP4 program suite. Acta Crystallogr D Biol Crystallogr **59:**1131-7.

76. **Puri, S., and M. R. O'Brian.** 2006. The *hmuQ* and *hmuD* genes from *Bradyrhizobium japonicum* encode heme-degrading enzymes. J Bacteriol **188:**6476-82.

77. **Qi, Z., I. Hamza, and M. R. O'Brian.** 1999. Heme is an effector molecule for iron-dependent degradation of the bacterial iron response regulator (Irr) protein. Proc Natl Acad Sci U S A **96:**13056-61.

78. **Ratliff, M., W. Zhu, R. Deshmukh, A. Wilks, and I. Stojiljkovic.** 2001. Homologues of neisserial heme oxygenase in gram-negative bacteria: degradation of heme by the product of the *pigA* gene of *Pseudomonas aeruginosa*. J. Bacteriol. **183:**6394-403.

79. **Ratliff, M., W. Zhu, R. Deshmukh, A. Wilks, and I. Stojiljkovic.** 2001. Homologues of neisserial heme oxygenase in gram-negative bacteria: degradation of heme by the product of the *pigA* gene of *Pseudomonas aeruginosa*. J Bacteriol **183:**6394-403.

80. **Reniere, M. L., and E. P. Skaar.** 2008. *Staphylococcus aureus* haem oxygenases are differentially regulated by iron and haem. Mol Microbiol **69:**1304-15.

81. **Reniere, M. L., V. J. Torres, and E. P. Skaar.** 2007. Intracellular metalloporphyrin metabolism in *Staphylococcus aureus*. Biometals **20:**333-45.

82. **Ridley, K. A., J. D. Rock, Y. Li, and J. M. Ketley.** 2006. Heme utilization in *Campylobacter jejuni*. J Bacteriol **188:**7862-75.

83. **Rooijakkers, S. H., M. Ruyken, A. Roos, M. R. Daha, J. S. Presanis, R. B. Sim, W. J. van Wamel, K. P. van Kessel, and J. A. van Strijp.** 2005. Immune evasion by a staphylococcal complement inhibitor that acts on C3 convertases. Nat Immunol **6:**920-7.

84. **Schiott, T., M. Throne-Holst, and L. Hederstedt.** 1997. *Bacillus subtilis* CcdA-defective mutants are blocked in a late step of cytochrome c biogenesis. J Bacteriol **179:**4523-9.

85. **Schmitt, M. P.** 1997. Transcription of the *Corynebacterium diphtheriae hmuO* gene is regulated by iron and heme. Infect Immun **65:**4634-41.

86. **Schmitt, M. P.** 1997. Utilization of host iron sources by *Corynebacterium diphtheriae*: identification of a gene whose product is homologous to eukaryotic heme oxygenases and is required for acquisition of iron from heme and hemoglobin. J. Bacteriol. **179:**838-45.

87. **Schmitt, M. P.** 1997. Utilization of host iron sources by *Corynebacterium diphtheriae*: identification of a gene whose product is homologous to eukaryotic heme oxygenases and is required for acquisition of iron from heme and hemoglobin. J Bacteriol **179:**838-45.

88. **Schneewind, O., P. Model, and V. A. Fischetti.** 1992. Sorting of protein A to the staphylococcal cell wall. Cell **70:**267-81.

89. **Schrader, E. K., K. G. Harstad, and A. Matouschek.** 2009. Targeting proteins for degradation. Nat Chem Biol **5:**815-22.

90. **Schuller, D. J., A. Wilks, P. Ortiz de Montellano, and T. L. Poulos.** 1998. Crystallization of recombinant human heme oxygenase-1. Protein Sci **7:**1836-8.

91. **Schuller, D. J., A. Wilks, P. R. Ortiz de Montellano, and T. L. Poulos.** 1999. Crystal structure of human heme oxygenase-1. Nat Struct Biol **6:**860-7.

92. **Schuller, D. J., W. Zhu, I. Stojiljkovic, A. Wilks, and T. L. Poulos.** 2001. Crystal structure of heme oxygenase from the gram-negative pathogen *Neisseria meningitidis* and a comparison with mammalian heme oxygenase-1. Biochemistry **40:**11552-8.

93. **Sebastian, S., S. Agarwal, J. R. Murphy, and C. A. Genco.** 2002. The gonococcal fur regulon: identification of additional genes involved in major catabolic, recombination, and secretory pathways. J Bacteriol **184:**3965-74.

94. **Sharp, K. H., S. Schneider, A. Cockayne, and M. Paoli.** 2007. Crystal structure of the heme-IsdC complex, the central conduit of the Isd iron/heme uptake system in *Staphylococcus aureus*. J Biol Chem **282:**10625-31.

95. **Skaar, E. P., A. H. Gaspar, and O. Schneewind.** 2006. *Bacillus anthracis* IsdG, a heme-degrading monooxygenase. J Bacteriol **188:**1071-80.

96. **Skaar, E. P., A. H. Gaspar, and O. Schneewind.** 2004. IsdG and IsdI, heme-degrading enzymes in the cytoplasm of *Staphylococcus aureus.* J Biol Chem **279:**436-43.

97. **Skaar, E. P., M. Humayun, T. Bae, K. L. DeBord, and O. Schneewind.** 2004. Iron-source preference of *Staphylococcus aureus* infections. Science **305:**1626-8.

98. **Skaar, E. P., and O. Schneewind.** 2004. Iron-regulated surface determinants (Isd) of *Staphylococcus aureus*: stealing iron from heme. Microbes Infect **6:**390-7.

99. **Smeltzer MS, L. C., Harik N, Hart ME.** 2009. Molecular basis of pathogenicity. *In* J. K. Crossley KB, Archer GL, Fowler VG (ed.), Staphylococci in human disease, 2nd ed. Blackwell Publishing Ltd, West Sussex, UK.

100. **Stauff, D. L., V. J. Torres, and E. P. Skaar.** 2007. Signaling and DNA-binding activities of the *Staphylococcus aureus* HssR-HssS two-component system required for heme sensing. J Biol Chem **282:**26111-21.

101. **Stocker, R., Y. Yamamoto, A. F. McDonagh, A. N. Glazer, and B. N. Ames.** 1987. Bilirubin is an antioxidant of possible physiological importance. Science **235:**1043-6.

102. **Stojiljkovic, I., V. Kumar, and N. Srinivasan.** 1999. Non-iron metalloporphyrins: potent antibacterial compounds that exploit haem/Hb uptake systems of pathogenic bacteria. Mol Microbiol **31:**429-42.

103. **Sugishima, M., Y. Omata, Y. Kakuta, H. Sakamoto, M. Noguchi, and K. Fukuyama.** 2000. Crystal structure of rat heme oxygenase-1 in complex with heme. FEBS Lett **471:**61-6.

104. **Suits, M. D., G. P. Pal, K. Nakatsu, A. Matte, M. Cygler, and Z. Jia.** 2005. Identification of an *Escherichia coli* O157:H7 heme oxygenase with tandem functional repeats. Proc Natl Acad Sci U S A **102:**16955-60.

105. **Theodore, T. S., and A. L. Schade.** 1965. Carbohydrate metabolism of iron-rich and iron-poor *Staphylococcus aureus*. J Gen Microbiol **40:**385-95.

106. **Thony-Meyer, L.** 1997. Biogenesis of respiratory cytochromes in bacteria. Microbiol Mol Biol Rev **61:**337-76.

107. **Timmer, J. C., W. Zhu, C. Pop, T. Regan, S. J. Snipas, A. M. Eroshkin, S. J. Riedl, and G. S. Salvesen.** 2009. Structural and kinetic determinants of protease substrates. Nat Struct Mol Biol **16:**1101-8.

108. **Torres, V. J., G. Pishchany, M. Humayun, O. Schneewind, and E. P. Skaar.** 2006. *Staphylococcus aureus* IsdB is a hemoglobin receptor required for heme iron utilization. J Bacteriol **188:**8421-9.

109. **Unno, M., T. Matsui, G. C. Chu, M. Couture, T. Yoshida, D. L. Rousseau, J. S. Olson, and M. Ikeda-Saito.** 2004. Crystal structure of the dioxygen-bound heme oxygenase from *Corynebacterium diphtheriae:* implications for heme oxygenase function. J Biol Chem **279:**21055-61.

110. **Unno, M., T. Matsui, G. C. Chu, M. Couture, T. Yoshida, D. L. Rousseau, J. S. Olson, and M. Ikeda-Saito.** 2004. Crystal structure of the dioxygen-bound heme oxygenase from *Corynebacterium diphtheriae*: Implications for heme oxygenase function. J Biol Chem.

111. **Unno, M., T. Matsui, and M. Ikeda-Saito.** 2007. Structure and catalytic mechanism of heme oxygenase. Nat Prod Rep **24:**553-70.

112. **Vermeiren, C. L., M. Pluym, J. Mack, D. E. Heinrichs, and M. J. Stillman.** 2006. Characterization of the heme binding properties of *Staphylococcus aureus* IsdA. Biochemistry **45:**12867-75.

113. **Visai, L., N. Yanagisawa, E. Josefsson, A. Tarkowski, I. Pezzali, S. H. Rooijakkers, T. J. Foster, and P. Speziale.** 2009. Immune evasion by *Staphylococcus aureus* conferred by iron-regulated surface determinant protein IsdH. Microbiology **155:**667-79.

114. **von Eiff, C., R. A. Proctor, and G. Peters.** 2000. *Staphylococcus aureus* small colony variants: formation and clinical impact. Int J Clin Pract Suppl**:**44-9.

115. **Wegele, R., R. Tasler, Y. Zeng, M. Rivera, and N. Frankenberg-Dinkel.** 2004. The heme oxygenase(s)-phytochrome system of *Pseudomonas aeruginosa*. J Biol Chem **279:**45791-802.

116. **Weinberg, E. D.** 2004. Exposing the hidden dangers of iron. Cumberland House, Nashville, TN.

117. **Weinberg, E. D.** 1974. Iron and susceptibility to infectious disease. Science **184:**952-6.

118. **Weiner, M. P., G. L. Costa, W. Schoettlin, J. Cline, E. Mathur, and J. C. Bauer.** 1994. Site-directed mutagenesis of double-stranded DNA by the polymerase chain reaction. Gene **151:**119-23.

119. **Wickner, S., M. R. Maurizi, and S. Gottesman.** 1999. Posttranslational quality control: folding, refolding, and degrading proteins. Science **286:**1888-93.

120. **Wilks, A.** 2002. Heme oxygenase: evolution, structure, and mechanism. Antioxid Redox Signal **4:**603-14.

121. **Wilks, A., and M. P. Schmitt.** 1998. Expression and characterization of a heme oxygenase (Hmu O) from *Corynebacterium diphtheriae*. Iron acquisition requires oxidative cleavage of the heme macrocycle. J Biol Chem **273:**837-41.

122. **Wilks, A., and M. P. Schmitt.** 1998. Expression and characterization of a heme oxygenase (Hmu O) from *Corynebacterium diphtheriae.* Iron acquisition requires oxidative cleavage of the heme macrocycle. J. Biol. Chem. **273:**837-41.

123. **Winstedt, L., L. Frankenberg, L. Hederstedt, and C. von Wachenfeldt.** 2000. *Enterococcus faecalis* V583 contains a cytochrome bd-type respiratory oxidase. J Bacteriol **182:**3863-6.

124. **Wright, A. C., L. M. Simpson, and J. D. Oliver.** 1981. Role of iron in the pathogenesis of *Vibrio vulnificus* infections. Infect Immun **34:**503-7.

125. **Wu, R., E. P. Skaar, R. Zhang, G. Joachimiak, P. Gornicki, O. Schneewind, and A. Joachimiak.** 2005. *Staphylococcus aureus* IsdG and IsdI, heme-degrading enzymes with structural similarity to monooxygenases. J Biol Chem **280:**2840-6.

126. **Yamamoto, Y., C. Poyart, P. Trieu-Cuot, G. Lamberet, A. Gruss, and P. Gaudu.** 2006. Roles of environmental heme, and menaquinone, in *Streptococcus agalactiae*. Biometals **19:**205-10.

127. **Zarychanski, R., and D. S. Houston.** 2008. Anemia of chronic disease: a harmful disorder or an adaptive, beneficial response? CMAJ **179:**333-7.

128. **Zhu, H., G. Xie, M. Liu, J. S. Olson, M. Fabian, D. M. Dooley, and B. Lei.** 2008. Pathway for heme uptake from human methemoglobin by the iron-regulated surface determinants system of *Staphylococcus aureus*. J Biol Chem **283:**18450-60.

129. **Zhu, J., and S. C. Winans.** 2001. The quorum-sensing transcriptional regulator TraR requires its cognate signaling ligand for protein folding, protease resistance, and dimerization. Proc Natl Acad Sci U S A **98:**1507-12.

130. **Zhu, W., A. Wilks, and I. Stojiljkovic.** 2000. Degradation of heme in gram-negative bacteria: the product of the *hemO* gene of *Neisseriae* is a heme oxygenase. J. Bacteriol. **182:**6783-6790.

131. **Zhu, W., A. Wilks, and I. Stojiljkovic.** 2000. Degradation of heme in gram-negative bacteria: the product of the *hemO* gene of Neisseriae is a heme oxygenase. J Bacteriol **182:**6783-90.